Control of Neurotransmitter Release Properties by Presynaptic Calcium

Control of Neurotransmitter Release Properties by Presynaptic Calcium

A dissertation presented

by

Monica Shishir Thanawala

to

The Division of Medical Sciences

in partial fulfillment of the requirements

for the degree of

Doctor of Philosophy

in the subject of

Neurobiology

Harvard University

Cambridge, Massachusetts

May 2014

Dissertation Advisor: Professor Wade Regehr **Monica Shishir Thanawala**

Control of Neurotransmitter Release Properties by Presynaptic Calcium

Abstract

Presynaptic terminals of neurons are optimized for neurotransmitter release, which is tightly controlled by presynaptic calcium. Here, we evaluate the role of calcium influx through voltage-gated calcium channels (VGCCs) in regulating the initial vesicular release probability (*p*) and the number of vesicles available for release by action potentials (effective RRP) at the calyx of Held synapse in mice. Two established methods of estimating effective RRP size and *p* reveal that both are calcium dependent. Reducing calcium influx by blocking R-type (VGCCs) or P/Q-type VGCCs also reduces EPSC amplitude via *p* and effective RRP size. Furthermore, activation of γ-aminobutryic acid class B ($GABA_B$) receptors, which reduces presynaptic calcium by regulating VGCCs without other significant effects on release, also reduces the effective RRP size and *p*. These findings suggest that the calcium dependence of RRP size may influence the manner in which certain neuromodulators affect neurotransmitter release.

In the second chapter, we extend the previous work to develop a simple model of synaptic transmission at the calyx of Held. We validate the model by comparing its estimates of *p* and effective RRP to well-established methods and use it to explore the consequences of changing the properties of synaptic transmission on estimated *p* and RRP. High stimulus frequency, low rates of RRP replenishment, and high *p* are crucial for obtaining accurate estimates of *p* and RRP by established methods.

The final chapter addresses regulation of synaptic transmission by tonic activation of presynaptic G protein-coupled receptors (GPCRs) at the parallel fiber to Purkinje cell (PF-PC) synapse in the rat cerebellum. Presynaptic inhibition is known to occur through four $G_{i/o}$ coupled receptors at this synapse: adenosine A1 receptors, cannabinoid type 1 (CB1) receptors, $GABA_B$ receptors, and type 4 metabotropic glutamate (mGlu4) receptors. Inhibition of A1Rs, CB1Rs, or $GABA_B$Rs leads to small or moderate increases in the strength of synaptic transmission and presynaptic calcium influx. However, simultaneous inhibition of A1Rs, CB1Rs, and $GABA_B$Rs more than doubles synaptic strength and significantly increases presynaptic calcium influx. We conclude that tonic activation of multiple types of presynaptic GPCRs powerfully regulates neurotransmitter release, likely by regulating presynaptic calcium.

Table of Contents

Acknowledgments

I would like to thank my advisor, Wade Regehr, for the extraordinary opportunity to be his advisee for the last five years. His scientific rigor and rich appreciation for presynaptic processes has been inspiring. I hope that I can graduate from the lab having picked up some of his attention to detail and no-nonsense approach to scientific questions. I am also very thankful to all of the members of the lab for help in formulating ideas, learning new techniques, and critical analysis of my work, and for generally being wonderful people to work alongside. In particular, I would like to thank Drs. Michael Myoga and Diasynou Fioravante for their incredible generosity in helping me learn, particularly when I was new in the lab, and also Kimberly McDaniels for her technical expertise.

I am also very thankful to Drs. Bruce Bean, Bernardo Sabatini, and Rachel Wilson for serving on my Preliminary Qualifying Examination Committee and Dissertation Advisory Committee. It is a privilege to meet with them to share my ideas and research with them and to receive their feedback. They have all also helped me outside their duties as committee members, helping me feel more comfortable and rooted in the department.

Thanks to Karen Harmin, the administrator of the Program in Neuroscience and to Drs. Rachel Wilson and Rick Born, faculty advisors to the program.

Also, thanks to my friends inside and outside of the department for the pep talks and useful distractions from research. Thanks to Jonathan Sellon for the emotional support (and proofreading of this thesis!), and to my parents, Rati and Shishir, and to my sister, Nina Thanawala, for their patience and love.

This work was supported by NIH 5 F31 NS073252 to M.S.T.

Chapter 1

Introduction

One of the most remarkable features of cells in the nervous system is their ability to simultaneously perform a multitude of functions: detection of activity in other cells, signal integration, intracellular computations, production of an action potential, and release of neurotransmitter. These discrete tasks are enabled by intricate chemical and electrical compartmentalization in individual neurons. Presynaptic terminals are one such compartment particularly specialized for the release of secretory vesicles containing neurotransmitter. They are characterized by many components, most of which collaborate in the release of neurotransmitter to excite, inhibit, or modulate downstream target neurons.

Components of the presynaptic terminal

One of the most striking features of presynaptic terminals evident in electron micrographs is the sheer number of secretory vesicles they enclose. Even small, conventional presynaptic terminals like those of cultured hippocampal neurons contain several hundred vesicles, while large synapses like the frog neuromuscular junction or calyx of Held house hundreds of thousands of vesicles (Rizzoli and Betz, 2005). Typically these vesicles are considered to belong to one of three pools: the readily-releasable pool (RRP), recycling pool, and reserve pool.

The readily-releasable pool (RRP). The RRP is the smallest pool, consisting of 0.1-5% of all vesicles (Rizzoli and Betz, 2005). Generally, this pool is defined as the population of vesicles that is docked at the plasma membrane of the presynaptic terminal and is poised to fuse with the membrane in response to neuronal activity. Small, conventional synapses tend to have three to eight vesicles docked at an active zone (Xu-Friedman et al., 2001), while larger synapses like the climbing fiber synapse and calyx of Held synapse have similar numbers of vesicles docked at each active zone, which can amount to thousands of vesicles per terminal (Sheng et al., 2012; Taschenberger et al., 2002; Xu-Friedman et al., 2001). At the calyx of Held synapse, it has been suggested that the RRP can be further subdivided into two pools, a fast-releasing pool (FRP) and slow-releasing pool (SRP).

The recycling pool. The recycling pool is slightly larger, typically 5-20% of all vesicles (Rizzoli and Betz, 2005). Instead of being localized to the active zone, recycling vesicles can be scattered through the presynaptic terminal. At many synapses (Cole et al., 2014; Richards et al., 2004; Sakaba and Neher, 2003) but not all (Holt et al., 2003; Job, 1998), actin has been shown to be involved in transport of these vesicles to the presynaptic membrane to replace vesicles from the RRP that have been released. Movement of vesicles from the recycling pool to the RRP is facilitated by intraterminal calcium (Dittman and Regehr, 1998; Hosoi et al., 2007; Wang and Kaczmarek, 1998) and mediated by the calcium-binding messenger protein calmodulin (Sakaba and Neher, 2001a).

The reserve pool. This pool is consistently the largest, amounting to 80-90% of all vesicles, and supplies the recycling pool with vesicles. The refilling of the recycling pool from the reserve pool is relatively slow, with mobililization of reserve pool vesicles only observed

during prolonged periods of intense stimulation (Rizzoli and Betz, 2005) or if trafficking of vesicles from the recycling pool to the RRP is artificially inhibited (Kuromi and Kidokoro, 1998). Other reports indicate that reserve pool vesicles may rarely or never be recruited in vivo (Denker et al., 2011a). Interestingly, it has been shown at the mouse NMJ that reserve vesicles may instead serve as a storage area for proteins involved in synaptic transmission (Denker et al., 2011b), suggesting a reason that neurons would maintain such a large, rarely-utilized supply of vesicles, but this has yet to be shown at other synapses.

Each vesicle is filled with a fairly consistent concentration of neurotransmitter and contains only one neurotransmitter. The vesicle is composed of a lipid bilayer with a composition similar to that of the plasma membrane of the cell, with the exception that important proteins required for vesicular fusion are also present on the vesicle membrane.

Voltage-gated calcium channels

Invasion of an AP into a presynaptic terminal causes depolarization of the compartment, activating voltage-gated calcium channels (VGCCs). All VGCCs in neurons consist of a primary α1 subunit and auxiliary β and α2δ subunits, and possibly a γ subunit. The α1 subunit is the most central to channel function, and contains the ion permeation pore, voltage sensors, and gating mechanism. The auxiliary subunits play important roles in ensuring cell-surface expression of the calcium channel and regulate channel kinetics and voltage properties (Catterall et al., 2013). In neurons, there are two major classes of VGCCs—high-voltage activated (HVA) and low-voltage activated (LVA) channels.

The Ca_v2 calcium channels, which are HVA channels, will be most important in this dissertation for the prominent role they play in synaptic transmission (Catterall et al., 2013). Multiple channels are present near active zones and are thought to collaboratively cause vesicular fusion by raising the local calcium concentration near docked vesicles (Borst and Sakmann, 1996; Catterall et al., 2013; Mintz et al., 1995; Sheng et al., 2012; Wu et al., 1999).

Calcium-dependent fusion of synaptic vesicles

Calcium influx through VGCCs triggers synchronous neurotransmitter release by binding the calcium sensor synaptotagmin (Brose et al., 1992; Fernández-Chacón et al., 2001; Geppert et al., 1994). Synaptotagmin isoforms 1 and 2 have been implicated in synchronous release at most CNS synapses. Synaptotagmin is present as an integral membrane protein embedded in the vesicle membrane, and contains cytoplasmic C2A and C2B domains that bind multiple calcium ions each (Shao et al., 1996; Südhof, 2013; Sudhof and Rizo, 1996). The cooperative binding of multiple calcium ions to synaptotagmin is thought to give rise to the power law of neurotransmitter release,

$$\text{Release} \propto [Ca]^n \tag{1.1}$$

in which the Hill coefficient *n* equals 3-6 for synchronous release (Dodge and Rahamimoff, 1967). Asynchronous release also exhibits a power-law calcium dependence, albeit a much shallower dependence, with *n*=1-2 (Burgalossi et al., 2010; Sun et al., 2007). Synaptotagmin 7

has been proposed as the molecular sensor for this mode of neurotransmitter release (Bacaj et al., 2013).

Coupling of calcium channels to synaptic vesicles

The organization of synaptic vesicles in relation to presynaptic calcium channels has been the subject of intense study for decades. However, because coupling distances are often shorter the resolution of light microscropy and therefore impossible to directly visualize in live tissue, the picture is still incomplete. At the calyx of Held, different calcium channel types exhibit different efficacies of triggering vesicular release; P/Q-type channels exhibit the steepest dependence (m=3.9), while N-type channels have a more modest ability at effecting release, with a calcium dependence of m= 1.3 (Wu et al., 1999), where:

$$\text{Release} \propto [\text{Ca}]^m . \tag{1.2}$$

These results are explained as reflecting differential distributions of N, P/Q, and R-type calcium channels in the calyx of Held, with a larger fraction of N-type and R-type localized far from release sites.

Calcium buffers and presynaptic calcium dynamics

Another crucial factor that regulates the extent of calcium spread due to VGCC opening is the presence of calcium binding proteins in neurons. Any protein that binds calcium is a buffer of free calcium ions, because the binding of free calcium ions to a protein regulates the free

concentration of ions in the terminal. The most common cytosolic calcium buffers expressed at high concentrations in neurons are parvalbumin, calbindin, and calretinin (Berridge et al., 2003; Schwaller et al., 2002) with calmodulin also considered a significant calcium buffer at some synapses (Vyleta and Jonas, 2014). Parvalbumin exhibits the highest calcium affinity of the three most common endogenous buffers, with a dissociation constant (K_d) of 4-9 nM, and an apparent K_d in the presence of physiological magnesium levels of approximately 50 nM. Calbindin and calretinin both have lower affinities for calcium with K_d values reported in the range of hundreds of nanomolar. Calbindin and calretinin are less affected by magnesium than parvalbumin due to their relative selectivity for calcium ions over magnesium ions. Despite its higher affinity for calcium, parvalbumin binds calcium much more slowly than do calbindin and calretinin. The complement of calcium buffers present in a cell can have profound implications for the extent of neurotransmitter release, affecting the probability of release, short-term plasticity, and even the functional size of the RRP (Caillard et al., 2000; Chard et al., 1995; Müller et al., 2007; Vyleta and Jonas, 2014).

Different classes of neurons are known to express one or more of these buffers (Schwaller et al., 2002). In the juvenile calyx of Held, parvalbumin is the predominant presynaptic calcium buffer and is crucial for determining the fast decay of calcium in presynaptic terminals (Müller et al., 2007). The young calyx of Held has been reported to have a relatively low buffer capacity of approximately 40 bound calcium ions per free ion (Helmchen et al., 1997). In addition to cytosolic buffers, cells can contain fixed calcium buffers, which are molecules that bind calcium that are associated with the plasma membrane or cytoskeletal structures (Wagner and Keizer, 1994; Zhou and Neher, 1993). Although fixed buffers have

received relatively little experimental attention, in some neurons fixed buffers provide a large fraction of the total buffer capacity of the cell (Matthews et al., 2013).

Calcium domains

The ability of calcium buffers to regulate neurotransmitter release is a function of the distance between calcium channels and vesicles in the RRP; slow buffers such as parvalbumin can only disrupt release if the coupling distance is sufficiently long. Many mature synapses exhibit nanodomain coupling (Eggermann et al., 2012), with vesicles positioned within tens of nanometers of presynaptic calcium channels. In contrast, many developing synapses (Eggermann et al., 2012) and at least one mature synapse (Vyleta and Jonas, 2014) exhibit loose coupling of calcium channels and vesicles, with loose coupling defined as a distance of at least 80-100 nm. At the young calyx of Held, modeling approaches indicate considerable heterogeneity of calcium channel coupling, with clusters of calcium channels positioned 30-300 nm away from release-ready vesicles, (Meinrenken et al., 2002). This is supported by experimental results in which the slow synthetic calcium buffer EGTA more significantly attenuates, but does not abolish, neurotransmitter release in pre-hearing calyces of Held as compared to the negligible effect observed in mature, post-hearing calyces (Fedchyshyn and Wang, 2005).

Presynaptic inhibition by GPCRs

Presynaptic inhibition of vesicular release by activation of presynaptic G protein-coupled receptors (GPCRs) is a well-established way to regulate neurotransmitter release. Typically,

these receptors are coupled to $G_{i/o}$ proteins (Offermanns, 2003). Presynaptic inhibition is mediated by many types of GPCRs and occurs at a variety of synapses (Stephens, 2009; Tedford and Zamponi, 2006). Most studies test the extent of presynaptic inhibition by applying agonists that activate specific GPCRs to determine their effect on *p*. In certain cases, GPCR-mediated presynaptic inhibition is an effective way to reduce *p* (Mann-Metzer and Yarom, 2002; Mapelli et al., 2009; Oliet et al., 2007; Yum et al., 2008), but in many others, the inhibitory effect of a single receptor is small enough to be considered insignificant. In almost all of these studies, a single type of presynaptic GPCR is studied in isolation. However, it is known that multiple types of $G_{i/o}$ protein-coupled receptors are often present at single presynaptic boutons (Dittman and Regehr, 1996; Hoffman et al., 2010; Zhang and Linden, 2009). This raises the possibility that multiple presynaptic GPCRs may be simultaneously activated to synergistically produce a significant reduction in *p*, perhaps by modulation of calcium channels or by various presynaptic signaling mechanisms.

Chapter 2

Presynaptic Calcium Influx Controls Neurotransmitter Release in Part by Regulating the Effective Size of the Readily-Releasable Pool

Journal of Neuroscience (2013) Mar 13; 33(11):4625– 4633.

Author contributions: M.S.T. and W.G.R. designed research; M.S.T. performed research; M.S.T. and W.G.R. analyzed data; M.S.T. and W.G.R. wrote the paper.

Abstract

The steep calcium dependence of synaptic strength that has been observed at a wide variety of synapses is thought to reflect a calcium dependence of the probability of vesicular exocytosis (*p*), with the cooperativity of three to six corresponding to the multiple calcium ion binding sites on the calcium sensor responsible for exocytosis. Here we test the hypothesis that the calcium dependence of the effective size of the readily-releasable pool (RRP) also contributes to the calcium dependence of release. Using two established methods of quantifying neurotransmitter release evoked by action potentials (effective RRP), we find that when calcium influx is changed by altering the external calcium concentration, the calcium cooperativity of *p* is insufficient to account for the full calcium dependence of EPSC size; the calcium-dependence of the RRP size also contributed. Reducing calcium influx by blocking R-type voltage-gated calcium channels (VGCCs) with Ni^{2+}, or by blocking P/Q-type VGCCs with ω-agatoxin IVA also changes EPSC amplitude by reducing both *p* and the effective RRP size. This suggests that the effective RRP size is dependent on calcium influx through VGCCs. Furthermore, activation of GABAB receptors, which reduces presynaptic calcium through VGCCs without other significant effects on release, also reduces the effective RRP size in addition to reducing *p*. These findings indicate that calcium influx regulates the size of the RRP along with *p*, this contributes to the calcium dependence of synaptic strength, and it influences the manner in which presynaptic modulation of presynaptic calcium channels affects neurotransmitter release.

Introduction

Fundamental to our understanding of synaptic transmission is the calcium dependence of neurotransmitter release. First seen at the frog neuromuscular junction (Dodge and Rahamimoff, 1967; Jenkinson, 1957), a steep dependence on calcium (n=3-6) has subsequently been observed at many synapses for postsynaptic currents evoked by action potentials, local application of Ca^{2+} or photolysis of caged calcium, and presynaptic voltage steps (Borst and Sakmann, 1996; Mintz et al., 1995; Schneggenburger and Neher, 2000; Smith et al., 1985; Wu and Saggau, 1994). The calcium cooperativity of release is widely appreciated as arising from cooperative binding of calcium to the calcium sensor responsible for vesicular fusion, which increases the probability of release (p) (Augustine, 2001).

But do changes in calcium influx affect synaptic transmission exclusively through p, or does another calcium-dependent process also play a role? It is also possible that changes in the size of the readily-releasable pool (RRP), defined as the number of synaptic vesicles accessible for release by an action potential (Rizzoli and Betz, 2005), could contribute. Previous studies have used high-frequency stimulus trains to deplete the RRP and observed an increase in the cumulative EPSC in elevated external calcium (Ca_e) (Lou et al., 2008; Schneggenburger et al., 1999). They attributed these observations to incomplete depletion in standard Ca_e, because the size of the RRP determined by a prolonged voltage step is not Ca_e dependent. These findings did, however, suggest that the size of the effective RRP, which we will define as the vesicles liberated by high-frequency stimulation, is Ca_e dependent.

Here, we argue that changes in the effective RRP size are significant, and that the extent of presynaptic calcium influx may be crucial to determine the size of the effective RRP. Unlike

presynaptic voltage steps and photolysis of caged calcium, action potentials provide a very brief, local increase in free calcium ions. It is possible that action potentials cannot access the entirety of the RRP, and that the concept of an effective RRP is important in studies of synaptic transmission. If the size of the effective RRP is calcium dependent, then changes in *p* would not fully explain changes in synaptic strength. In addition to being important for a mechanistic understanding of synaptic transmission, the relative contributions of *p* and RRP have functional implications: changes in *p* affect short-term plasticity but do not alter total vesicle fusion evoked by a train, whereas changes in RRP do not affect short-term plasticity but do alter total release.

In this study, we characterize the calcium dependence of EPSC amplitude, *p*, and the effective RRP at the calyx of Held synapse. We find that the calcium dependence of *p* is insufficient to account for the calcium dependence of the EPSC size, and that the effective RRP size is calcium-dependent. Our experiments indicate that neuromodulators that regulate presynaptic voltage-gated calcium channels (VGCCs) regulate both *p* and effective RRP size. These results can have important implications for understanding how synaptic transmission is regulated, especially in response to high-frequency activity as typically occurs at this synapse.

Methods

Animals and Preparation of Brain Slices

All animals used were wildtype mice (BL6C57/6J, Jackson Laboratories) postnatal day P11–14 of either sex. All animal handling and procedures abided by the guidelines of the Harvard Medical Area Standing Committee on Animals. Mice were deeply anesthetized with

isoflurane and killed by decapitation. Transverse 200-mm-thick slices were cut from the brainstem containing the medial nucleus of the trapezoid body (MNTB) with a vibratome slicer. Brains were dissected and sliced at 4°C in a solution consisting of the following (in mM): 125 NaCl, 25 $NaHCO_3$, 1.25 NaH_2PO_4, 2.5 KCl, 0.1 $CaCl_2$, 3 $MgCl_2$, 25 glucose, 3 myo-inositol, 2 Na-pyruvate, 0.4 ascorbic acid, continuously bubbled with 95% O_2/5% CO_2 (pH 7.4). Slices were incubated at 32°C for 20 min in a bicarbonate-buffered solution composed of the following (in mM): 125 NaCl, 25 $NaHCO_3$, 1.25 NaH_2PO_4, 2.5 KCl, 2 $CaCl_2$, 1 $MgCl_2$, 25 glucose, 3 myo-inositol, 2 Na-pyruvate, 0.4 ascorbic acid, continuously bubbled with 95% O_2/5% CO_2 (pH 7.4). For experiments conducted in an external calcium concentration other than 2 mM, slices were incubated in a solution similar to that above but with varying $CaCl_2$ and $MgCl_2$ to accommodate future experiments. The concentration of $CaCl_2$ plus that of $MgCl_2$ was always equal to 3 mM when $Ca_e \leq 2$ mM. For experiments with $Ca_e = 3$ mM and 4 mM , $[Mg^{2+}]$=0.1 mM.

Electrophysiology

Slices were transferred to a recording chamber at 21–24°C. During recordings, the standard perfusion solution consisted of the bicarbonate-buffered solution (see above) with 1 mM strychnine and 25 mM bicuculline to block inhibitory synaptic transmission. 1 mM kynurenic acid and 0.1 mM cyclothiazide (Tocris Bioscience/R&D Systems, Minneapolis, MN) were also added to block AMPA receptor saturation and desensitization, respectively. Slices were superfused at 1–3 ml/min with this external solution. Whole-cell postsynaptic patch-clamp recordings were made from visually identified cells in the MNTB region using glass pipettes of 2–3 MΩ resistance, filled with an internal recording solution of the following (in mM): 110

CsCl, 35 CsF, 10 EGTA, 10 HEPES, 2 QX-314, pH: 7.2, 315–320 mOsm. Series resistance (R_s) was compensated by up to 60% and the membrane potential was held at -60 mV. Excitatory postsynaptic potentials (EPSCs) were evoked by stimulating presynaptic axons with a bipolar stimulating electrode placed midway between the medial border of the MNTB and the midline of the brainstem. A Multiclamp 700A (Axon Instruments/Molecular Devices, Union City, CA) amplifier was used. Recordings were digitized at 20 KHz with an ITC-18 A/D converter (Instrutech, Port Washington, NY) using custom procedures (written by M.A. Xu-Friedman) in IgorPro (Wavemetrics, Lake Oswego, OR) and filtered at 8 kHz. Access resistance and leak current were monitored and experiments were rejected if either parameter changed significantly. Recordings were performed at room temperature (25°C) unless otherwise noted (elevated temperature experiments were conducted at 35°C).

Data Analysis

The effective size of the RRP was calculated using three techniques. To measure RRP_{train}, a measure of effective RRP size, peak EPSC amplitudes are measured and summed. A straight line was fitted to the final fifteen points of the cumulative EPSC and back-extrapolated to the y-axis. The y-intercept corresponds to RRP_{train}, and p_{train} equals $EPSC_0$ divided by $RRP_{train,}$ as previously described (Schneggenburger et al., 1999). RRP_{train}^{COR}, a corrected version of RRP_{train}, is measured by back-extrapolating to the y-axis with a curve instead of a straight line. The derivative of the curve is calculated by normalizing the peak EPSC amplitudes to the largest EPSC and subtracting each from 1. We then take the integral of this to get the summed capacity for replenishment (availability of empty sites) over the time elapsed from the beginning of the

train. The resulting curve is scaled such that the final fifteen points of the curve matches those of the cumulative EPSC. This process computes the RRP with a replenishment rate proportional to the number of empty sites available for new vesicles.$p_{\text{train}}^{\text{COR}}$ was calculated as $EPSC_0$ divided by $RRP_{\text{train}}^{\text{COR}}$.

To measure RRP_{EQ}, another measure of effective RRP size (Elmqvist and Quastel, 1965), peak EPSC amplitudes were plotted versus the cumulative EPSC. A line was fitted to the steepest range of this curve. We used four points for 100 Hz trains delivered at 25°C and three points for 300 Hz trains delivered at 35°C due to more rapid depletion. The x-intercept of this line corresponds to RRP_{EQ}. p_{EQ} equals $EPSC_0$ divided by RRP_{EQ}.

Data analysis was performed using routines written in IgorPro. Curve fitting was performed using a curve fitting application in IgorPro. Pairwise comparisons were performed with one-tailed Student's paired t tests. The level of significance was set at $p < 0.05$.

Simulations

Simple simulations were used to describe the effect of changing *p*, effective RRP, or both on the response to a 100 Hz train. In the absence of recovery from depression, EPSC amplitudes are the product of the number of vesicles remaining in the effective RRP (number of vesicles multiplied by quantal current) and *p*:

2.1 $$EPSC_n = pN_0(1-p)^n$$

When there is recovery:

2.2 $$EPSC_1 = EPSC_0(1 - p + pR)$$

where R is a constant that accounts for recovery. For n>1, if there are X_n sites occupied prior to stimulus n, and Y_n sites occupied immediately after stimulus n (Y_n and X_n are normalized to the total number of sites, N_0), then:

2.3 $$X_n = Y_{n-1} + R(1 - Y_{n-1})$$

2.4 $$X_n = Y_{n-1}(1 - R) + R$$

2.5 $$Y_n = (1 - p)X_n$$

2.6 $$X_n = (1 - p)X_{n-1} + R[1 - (1 - p)X_{n-1}]$$

2.7 $$X_n = (1 - p)(1 - R)X_{n-1} + R$$

The amplitude of the EPSC evoked by stimulus n is:

2.8 $$EPSC_n = pN_0X_n$$

2.9 $$EPSC_n = EPSC_{n-1}(1 - p)(1 - R) + pN_0R$$

The replenishment rate is proportional to the extent of depletion, which is consistent with the experimentally determined properties of recovery from depression. We achieve this in the model by assuming that the replenishment rate is proportional to the number of empty release sites available for newly-docked vesicles (assume constant replenishment per empty release site). The replenishment rate throughout the train is a fraction of the maximal rate. The fraction is equal to

the number of available sites open for replenishment. At time t=0, the RRP is assumed to be full (number of available release sites is zero).

Results

We initially studied the effect of altering calcium influx on synaptic transmission at the calyx of Held synapse by altering external calcium (Ca_e). Experiments were performed in the presence of kynurenate (1 mM) and cyclothiazide (100 μM) to block AMPA receptor saturation and desensitization, respectively. Presynaptic axons were stimulated with a bipolar electrode to evoke postsynaptic responses with pairs of pulses (interstimulus interval=10 ms) every 10 s to assess EPSC amplitude and the paired-pulse ratio. Periodically, a high-frequency train (40 stimuli at 100 Hz) was delivered to deplete the effective RRP. A 100 Hz train was used because it is within the physiological range and reliably evokes postsynaptic responses under our recording conditions.

As expected, the EPSC amplitude was strongly enhanced in 2 mM Ca_e as compared to 1.25 mM Ca_e (**Figure 2.1 A**) and there was a decrease in the paired-pulse ratio (**Figure 2.1 B**) that typically accompanies an increase in the probability of release (*p*). Trains were delivered in 1.25 mM external calcium (Ca_e) and 2 mM Ca_e and postsynaptic responses recorded (**Figure 2.1 C**). The first EPSCs were considerably larger in 2 mM Ca_e than in 1.25 mM Ca_e, but responses in both conditions decayed to a similar steady-state EPSC amplitude late in the train. An example in **Figure 2.1 D** illustrates an approach that is widely used to estimate the effective size of RRP that is released by a train. Peak EPSC amplitudes are summed and plotted versus stimulus

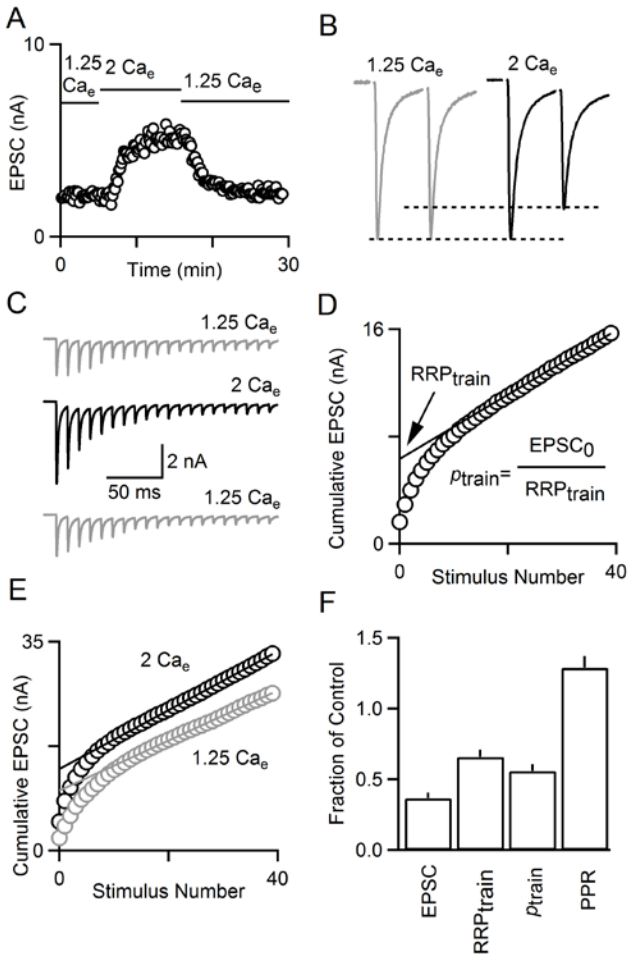

Figure 2.1. Altering presynaptic calcium influx affects synaptic transmission in part by changing effective RRP size. A Time course of EPSC amplitude during wash-in of 2 mM external calcium (Ca_e), followed by 1.25 mM Ca_e. **B** A comparison of pairs of EPSCs normalized to the amplitude of the first EPSC ($EPSC_0$) reveals that paired pulse plasticity varies with Ca_e. **C** EPSCs evoked by 100-Hz trains delivered in different Ca_e conditions. **D** Example estimation of effective RRP size (RRP_{train}) by back-extrapolation of the cumulative EPSC to the y-axis. The probability of release (p_{train}) is estimated by dividing the amplitude of the first EPSC by RRP_{train}. **E** A comparison of cumulative EPSCs reveals that RRP_{train} is larger in 2 mM Ca_e (*black arrow*) than in 1.25 mM Ca_e (*gray arrow*). **F** Summary of the effects of changing Ca_e from 2 mM to 1.25 mM on the properties of synaptic transmission (n=5).

number. The RRP is thought to be depleted early in the train, such that the steady state EPSC amplitude late in the train reflects replenishment of the RRP. The rate of replenishment is assumed to be constant and accounted for by back-extrapolating a line from the final fifteen points of the cumulative EPSC to the y-axis. The y-intercept corresponds to the number of vesicles in the RRP multiplied by the quantal size (Nq) and is called RRP_{train}. This technique was first used at the calyx of Held but has subsequently been applied at a variety of synapses (Moulder and Mennerick, 2005; Pan and Zucker, 2009; Schneggenburger et al., 1999; Stevens and Williams, 2007). The probability of release (p_{train}) can be estimated by dividing the amplitude of the first EPSC ($EPSC_0$) by RRP_{train}. This method reveals that RRP_{train} is reduced in 1.25 mM Ca_e as compared to 2 mM Ca_e (**Figure 2.1 E**). Based on the method of **Figure 2.1 D**, the reduction of EPSC amplitude in 1.25 mM Ca_e (36.7% ± 4.1% of control, $p<0.01$) is a result of reduced effective pool size (RRP_{train}; 65.9% ± 5.1% of control, $p<0.05$) and reduced release probability (p_{train}; 55.8 ± 4.7% of control, $p<0.01$). The reduction in release probability is also indicated by an increase in PPR (**Figure 2.1 F**).

The results of **Figure 2.1** suggest that alterations in calcium influx change neurotransmitter release in part by changing the effective pool size. It is, however, important to recognize that quantification of the RRP can be controversial, and each method used to quantify the RRP relies on assumptions about release. For example, the train method of **Figure 2.1** assumes that the rate of replenishment from the reserve pool to the RRP is constant during a train. We therefore decided to use an additional method to quantifying the amount of neurotransmitter released by a high-frequency train, a method described previously developed for use at the frog neuromuscular junction (Elmqvist and Quastel, 1965) and subsequently used at the calyx of Held synapse (Kushmerick et al., 2006; Taschenberger et al., 2005). This method

assumes that for a high-*p*, depressing synapse, depletion of the RRP dominates the amplitude of the synaptic responses early in a high-frequency train. In an example cell in control conditions (2 mM Ca_e), synaptic responses depress quickly during the first five to ten stimuli of a 100 Hz train, following a decaying single-exponential curve (**Figure 2.2 A**). A plot of EPSC amplitudes versus the cumulative EPSC transforms the first few responses, which serve to almost completely deplete the RRP, to follow a straight line. This line can be extrapolated to intersect the x-axis (**Figure 2.2 B**). The x-intercept corresponds to the size of the RRP (RRP_{EQ}) assuming no replenishment of the RRP during the first few stimuli. Since there will be some replenishment of the RRP during the first ~50 milliseconds of the train, RRP_{EQ} will overestimate the size of the RRP and can be considered an upper-bound estimate of RRP size. This contrasts with the RRP_{train} approach, which assumes a constant rate of replenishment equal to that of the end of the train, when in fact the rate of replenishment likely increases during the train, and therefore RRP_{train} provides a lower-bound estimate of the RRP. Thus, two entirely different methods can be used to estimate the size of the RRP for stimulus trains, each method relies on its own set of assumptions, and one method provides a lower bound for RRP while the other provides an upper bound.

We therefore compared our estimates of RRP by plotting RRP_{train} versus RRP_{EQ} for cells in different Ca_e (between 1 mM and 4 mM), and found that as expected, RRP_{EQ} was typically greater than RRP_{train} (**Figure 2.2 C**). This is apparent by comparing the fit to the data (**Figure 2.2 C**, solid line, slope (m)=0.751, y-intercept (b)=0.72 nA) with the unity line (**Figure 2.2 C**, *dashed line*). Accordingly, estimates of *p* from RRP_{EQ} (p_{EQ}) were typically smaller than p_{train} (**Figure 2.2 D**), which was again apparent by comparing the fit to the data (**Figure 2.2 D**, *solid line*, m=0.957, b=0.061) with the unity line (**Figure 2.2 D**, *dashed line*). It appears that although

Figure 2.2. Techniques to quantify neurotransmitter release in response to a stimulus train. **A** Plot of EPSC amplitude versus stimulus number for a 100 Hz train in control conditions fitted with a single-exponential curve. **B** Plot of EPSC amplitude versus cumulative EPSC amplitude for the data in (**A**). A linear fit to the steepest range of the data gives an estimate of RRP size (RRP_{EQ}) **C** Plot of RRP_{train} and RRP_{EQ} values for cells in different Ca_e (1, 1.25, 1.5, 2, 3, and 4 mM). For panels C, D, G, and H, a linear fit to the data (*black line*) and the unity line (*dashed line)* are shown. **D** Plot of p_{train} and p_{EQ} values for the same cells as in C. **E** Normalized EPSC amplitudes show recovery from depression after a single conditioning stimulus (*gray circles*) and after 40 stimuli at 100 Hz (*black circles*). Data were fit to a function of the form $(A + \mathrm{Bexp}(-t/\tau))$, with parameters {A, B, t} of {1, -0.466 ± 4.73x10^{-3}, 2.54 ± .098 s} following 1 conditioning stimulus and {1, -0.848 ± 0.011, t=2.47 ± .146 s} following a train. **F** Comparison of RRP_{train} (*dashed lines*) and corrected RRP_{train} (RRP_{train}^{COR}, *solid lines*) methods for measuring RRP. RRP_{train}^{COR} is indicated for 2 mM Ca_e (*black arrow*) and for 1.25 mM Ca_e (*gray arrow*). **G** Plot of RRP_{train}^{COR} vs. RRP_{EQ} and (**H**) corrected p_{train} (p_{train}^{COR}) vs. p_{EQ} for cells in different Ca_e.

Figure 2.2 (Continued)

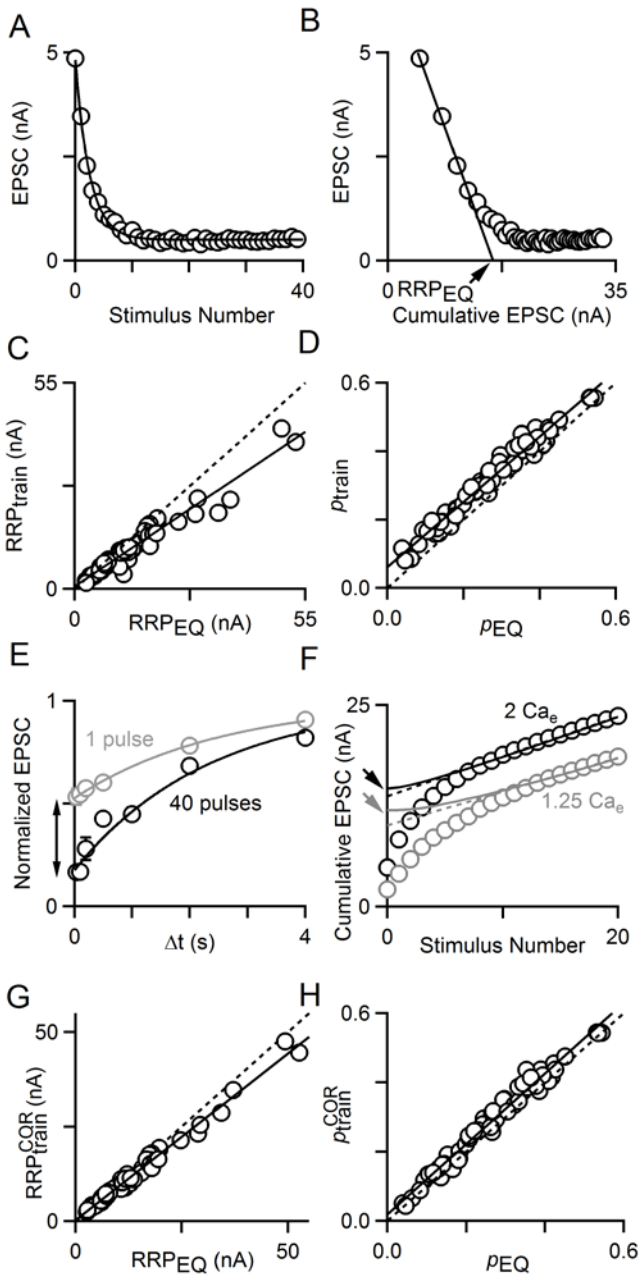

RRP_{train} is generally slightly smaller than RRP_{EQ}, these two methods provide similar estimates of RRP and do a good job of bracketing the effective RRP. To resolve the differences in pool sizes measured by these two techniques, we tested the validity of the assumption of constant recovery from depression early and late in the train. There are two potential reasons for increased recovery from depression during the train. First, the number of vesicles added to the RRP between stimuli is probably low at the beginning of the train due to the low availability of empty release sites. Late in the train, when the cumulative EPSC has reached a linear regime (constant EPSC amplitude), there should be more empty sites and replenishment should be more pronounced. A second possibility is that the time course of recovery from depression is accelerated late in the train as a result of calcium-dependent recovery from depression, which has been described at a variety of synapses (Dittman and Regehr, 1998; Stevens and Wesseling, 1998; Wang and Kaczmarek, 1998; Zucker and Regehr, 2002) and has been shown to be regulated by the calcium-binding protein calmodulin at this synapse (Sakaba and Neher, 2001a). In order to test for these two possibilities we compared recovery from depression following a single conditioning pulse with recovery from depression after a 40-pulse train at 100 Hz (**Figure 2.2 E**). We found that at the end of the train there was more depression and the magnitude of recovery was larger than that observed after a single conditioning pulse; however, the time course of recovery was about the same, with a time constant of approximately 2.5 seconds for both stimulus patterns. This suggests that it is possible to correct for differences in recovery from depression simply by taking into account the extent to which the RRP has been depleted. By performing such corrections we obtained a refined estimate of RRP_{train} that is corrected for differential recovery from depression, RRP_{train}^{COR} (**Figure 2.2 F**, *curves*, see Methods). A plot of RRP_{train}^{COR} versus RRP_{EQ} shows considerably improved agreement, (**Figure 2.2 G**, *solid line*,

m=0.881, b=0.284 nA) as does a plot of $p_{\mathrm{train}}^{\mathrm{COR}}$ versus p_{EQ} for the same cells shown in Figure 2C and 2D show (**Figure 2.2 H**, *solid line*, m=1.02, b=0.018). It should be noted that because the correction of $\mathrm{RRP}_{\mathrm{train}}$ is larger when initial *p* is smaller, the correction decreases our estimates of the size of changes in RRP. It also brings $\mathrm{RRP}_{\mathrm{train}}^{\mathrm{COR}}$ and $\mathrm{RRP}_{\mathrm{EQ}}$ into close agreement. The close agreement of the two methods suggests that they provide an excellent estimate of RRP size and *p*. We will therefore use these two methods to quantify changes in RRP and *p* in all subsequent figures.

We also went on to examine recovery from depression after a 40-pulse train in 1.25 mM Ca_e, and found that recovery from depression was approximated by an exponential with a time constant of 3.5 seconds (n=4 cells, data not shown). This is slightly longer than the time constant measured at 2 mM Ca_e.and is consistent with calcium slightly accelerating recovery from depression. It should be noted, however that the correction method we introduced in Fig. 2 provides a correction appropriate for each train that does not assume anything about the time constant of recovery from depression. Thus, small differences in recovery kinetics will be accounted for, and will not to contribute to the observed changes in $\mathrm{RRP}_{\mathrm{train}}^{\mathrm{COR}}$. Moreover, the replenishment is insufficient to account for calcium-dependent differences in $\mathrm{RRP}_{\mathrm{EQ}}$.

Having refined our methods of quantifying the RRP, we went on to determine whether the calcium dependence of effective RRP size contributes to the observed calcium dependence of the EPSC amplitude. Plots of the EPSC, RRP, and *p* normalized to the value in 2 mM Ca_e were made (**Figure 2.3 A** and **Figure 2.3 B**). Fits to the Hill equation revealed that the EPSC amplitude is steeply dependent on Ca_e (Hill coefficient (*n*)=3.6, EC_{50} ($Ca_{1/2}$)=1.78 mM), the probability of release is less steeply Ca_e dependent ($p_{\mathrm{train}}^{\mathrm{COR}}$: *n*=3.2, $Ca_{1/2}$=1.56 mM and p_{EQ}:

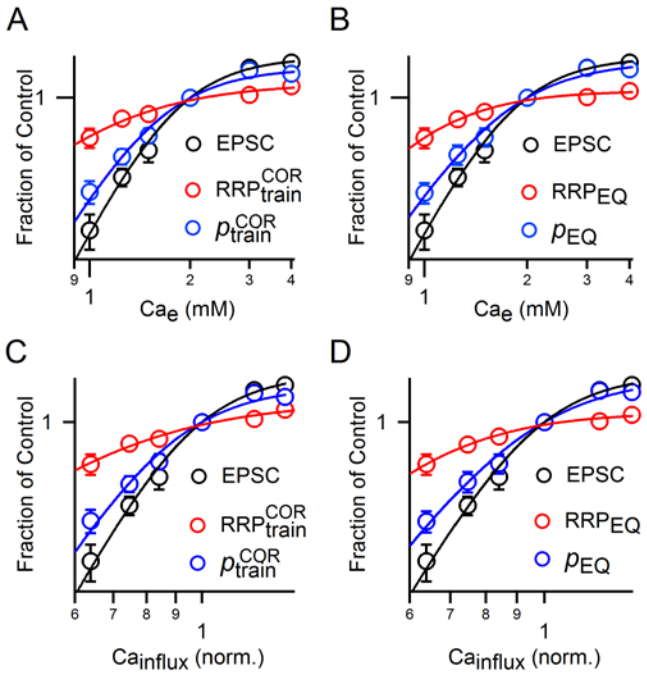

Figure 2.3. Contributions of effective RRP size to the calcium dependence of release. A Plot of EPSC size, $\mathrm{RRP}^{\mathrm{COR}}_{\mathrm{train}}$, and $p^{\mathrm{COR}}_{\mathrm{train}}$ (normalized to values in 2 mM Ca_e) vs. Ca_e. **B** Plot of EPSC, p_{EQ}, and RRP_{EQ} (normalized to values in 2 mM Ca_e) vs. Ca_e. Plots in (**C**) and (**D**) are similar to plots in (**A**) and (**B**), but values are plotted vs. calcium influx (Ca_{influx}). Relationship between Ca_e and Ca_{influx} from Schneggenburger et al., 1999. All plots show data for 1, 1.25, 1.5, 2, 3, and 4 mM Ca_e. n≥5 cells per Ca_e value.

n=3.0, $Ca_{1/2}$=1.66 mM), as is the RRP (RRP_{train}^{COR}: *n* =2.0, $Ca_{1/2}$=0.98 mM and RRP_{EQ}: *n*=2.7, $Ca_{1/2}$=0.92 mM). These findings suggest that the calcium Ca_e dependence of EPSC amplitude does not arise solely from *p*, the Ca_e dependence of the RRP also contributes. It also appears that the RRP size saturates at lower values of Ca_e than does the EPSC or *p*.

Calcium influx (Ca_{influx}) is not linearly related to Ca_e. To determine how EPSC amplitude, *p*, and RRP depend upon the Ca_{influx}, we used the previously characterized relationship between Ca_e and Ca_{influx} at this synapse (Schneggenburger et al., 1999):

2.10
$$\frac{J_{Cae,x}}{J_{Cae,2mM}} = \left(\frac{Ca_{e,x}}{Ca_{e,x}+EC_{50}}\right) \div \left(\frac{Ca_{e,2mM}}{Ca_{e,2mM}+EC_{50}}\right)$$

Here, $J_{Cae,x}$=flux of calcium ions into the presynaptic terminal at x mM Ca_e, $J_{Cae,2mM}$=flux of calcium ions into the terminal at 2 mM Ca_e, and EC_{50}=2.6 mM (Schneggenburger et al., 1999). Plots of the EPSC, RRP, and *p* normalized to 2 mM Ca_e are shown versus estimated calcium influx (Ca_{influx}) (**Figure 2.3 C-D**). Fits to the Hill equation revealed that the EPSC amplitude is very steeply dependent on Ca_{influx} (Hill coefficient (*n*)=5.6, $Ca_{1/2}$=0.96), the probability of release is less dependent on Ca_{influx} (p_{train}^{COR}: *n*=4.9, $Ca_{1/2}$=0.88 and p_{EQ}: *n*=4.4, $Ca_{1/2}$=0.93 mM), as is the RRP (RRP_{train}^{COR}: *n*=2.7, $Ca_{1/2}$=0.66 and RRP_{EQ}: *n*=3.8, $Ca_{1/2}$=0.61). Thus we find the same qualitative trends hold for the Ca_{influx} dependence of EPSC, *p* and RRP, as for the Ca_e dependence of these values, and the very steep Ca_{influx} dependence of EPSC amplitude arises in part from the Ca_{influx} dependence of the RRP.

The previous experiments suggest that the extent of action potential-evoked calcium influx through presynaptic VGCCs influences the effective size of the RRP, and therefore the

strength of synaptic transmission. We tested the role of R-type calcium channels using 100 µM Ni^{2+}, which blocks R-type calcium channels (Schneider et al., 1994; Soong et al., 1993; Zamponi et al., 1996) and reduces neurotransmitter release at the calyx of Held (Wu et al., 1998, 1999). The wash-in of Ni^{2+} reduced synaptic strength to 60.9 ± 2.6% of control ($p<0.001$), and reduced both RRP and *p* (**Figure 2.4 A-C**). Both estimates of RRP size were reduced in nickel; RRP_{train}^{COR}=81.6 ± 2.1% of control ($p<0.001$) and RRP_{EQ}=81.2 ± 2.3% of control ($p<0.01$). Estimates of *p* were reduced as well; p_{train}^{COR}= 74.8 ± 3.1% of control ($p<0.001$) and p_{EQ}= 75.3 ± 3.5% ($p<0.001$). Thus, as with alterations in external calcium, decreases in RRP contribute to decreases in EPSC amplitude.

Previous studies have shown that P-type calcium channels are the primary source of calcium that drives neurotransmitter release at the calyx of Held (Iwasaki and Takahashi, 1998). We therefore used the selective P-type calcium channel antagonist ω-agatoxin IVA (AgaIVA) to study the synaptic transmission (**Figure 2.5**). AgaIVA strongly decreased the EPSC amplitude, and once the steady-state response to AgaIVA had been attained, *p* was so low (<0.1) that it was impractical to deplete the RRP with a short train stimulus. We therefore delivered trains during the wash-in of AgaIVA, as indicated by gray arrows in **Figure 2.5 A**. The size of the first EPSC decreased as AgaIVA took effect and the number of stimuli required to deplete the train increased, as shown in a representative experiment (**Figure 2.5 B**). Plots of the cumulative EPSC revealed that RRP_{train}^{COR} (**Figure 2.5 C**) and RRP_{EQ} (**Figure 2.5 D**) had been significantly reduced in AgaIVA. Summary data shows that the reduction of EPSC amplitude was accompanied by more modest decreases in both measures of RRP size, RRP_{train}^{COR} and RRP_{EQ}, and of *p*, p_{train}^{COR} and p_{EQ} (**Figure 2.5 E** and **2.5 F**). This manipulation strongly suggests that the number of vesicles liberated by a train depends on the extent of calcium influx through presynaptic VGCCs.

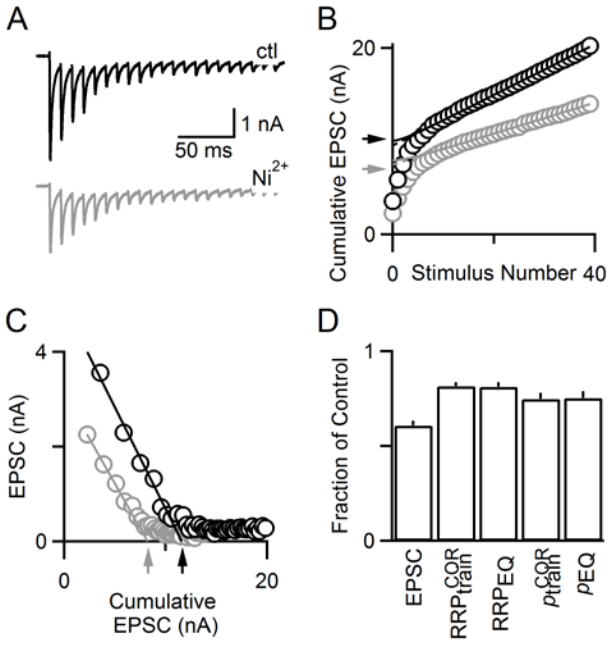

Figure 2.4. Nickel, a blocker of R-type VGCCs, reduces synaptic transmission through changes in *p* and effective RRP. A Example postsynaptic responses to 100 Hz stimulus trains in control conditions (*black*) and Ni^{2+} (*gray*). **B** A comparison of cumulative EPSCs reveals that RRP_{train}^{COR} is reduced upon application of nickel chloride. Black circles indicate control conditions, gray circles indicate Ni^{2+}. Arrows indicate RRP_{train}^{COR}. **C** Plot of EPSC amplitude versus cumulative EPSC amplitude for the same data reveals that RRP_{EQ} is also reduced in nickel chloride. Black circles indicate control conditions, gray circles indicate Ni^{2+}. Arrows indicate RRP_{EQ}. **D** Summary of the effect of Ni^{2+} on the properties of synaptic transmission (n=8).

Figure 2.5. Inhibiting calcium entry through P-type VGCCs reduces synaptic strength through changes in *p* and effective RRP. A Application of the selective P/Q-type calcium channel antagonist ω-agatoxin IVA (50 nM) potently inhibits EPSC amplitude. In this example cell, 100 Hz trains were delivered once in control conditions (*black arrow*) and three times during wash-in of ω -agatoxin IVA (AgaIVA, *gray arrows*). **B** Postsynaptic responses in an example cell to a 100 Hz train in control conditions (*black trace*) and during submaximal application (*gray traces*). Times at which trains were delivered are indicated by arrows in (A). **C** Cumulative EPSC plots for the same example cell indicate that RRP_{train}^{COR} is reduced by AgaIVA. Arrows indicate RRP_{train}^{COR}. **D** Plots of peak EPSC amplitude versus cumulative EPSC indicate that RRP_{EQ} is reduced by AgaIVA. Arrows indicate RRP_{EQ}. **E** Plots of RRP_{train}^{COR} normalized to control value (top) and p_{train}^{COR} (bottom) and **F** RRP_{EQ} normalized to control value (top) and p_{EQ} (bottom) (**F**) as a function of EPSC amplitude. Each cell has a unique marker to indicate subsequent trains.

Figure 2.5 (Continued)

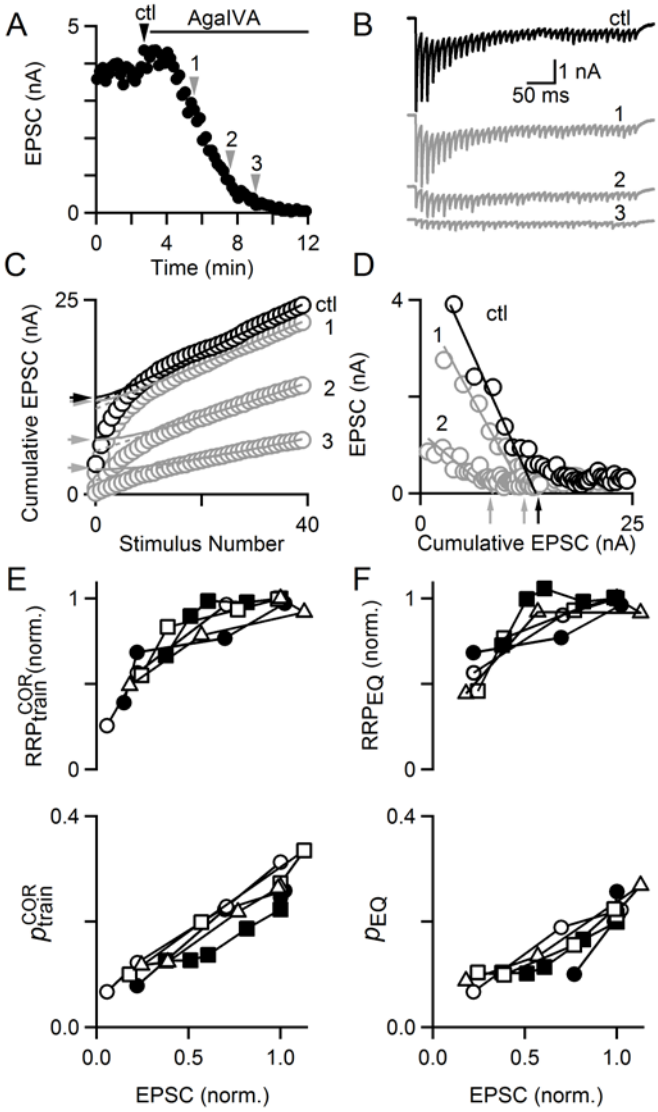

Numerous neuromodulators regulate synaptic transmission by modulating presynaptic voltage-gated calcium channels, and it has been assumed that such modulation only reflects alterations in *p* (Zucker and Regehr, 2002). However, our results suggest that changes in calcium influx can also affect the size of the RRP. We therefore tested this possibility by studying synaptic $GABA_B$ receptor-mediated synaptic inhibition at the calyx of Held synapse, which has been shown to be mediated by direct modulation of presynaptic VGCCs, with no significant downstream effects on vesicular release (Takahashi et al., 1998). We found that the $GABA_B$ receptor agonist baclofen (100 µM) strongly inhibited synaptic strength at this synapse, which was reversed with the $GABA_B$ receptor antagonist CGP 55845 (20 µM). Baclofen caused the synapse to facilitate, unlike in control conditions and in CGP 55845, and depletion of the RRP required more stimuli (**Figure 2.6 A**). In both control conditions and in baclofen, 40 stimuli were sufficient to deplete the RRP. In a representative experiment, we found that baclofen decreased both RRP_{train}^{COR} (**Figure 2.6 B**) and RRP_{EQ} (**Figure 2.6 C**). Baclofen reduced EPSC amplitudes to an average of 28.4 ± 6.9% of control ($p<0.01$), with intermediate effects on RRP_{train}^{COR} (54.8 ± 8.2% of control, $p<0.01$), RRP_{EQ} (63.9 ± 6.3% of control, $p<0.05$), p_{train}^{COR} (50.1 ± 5.7% of control, $p<0.001$), and p_{EQ} (38.8 ± 8.6% of control, $p<0.01$) (summary in **Figure 2.6 D**, n=9). This indicates that neuromodulators that act by regulating presynaptic VGCCs can affect synaptic transmission by modulating both *p* and effective RRP size.

To test whether regulation of effective RRP size might be physiologically relevant, we repeated experiments at near-physiological temperature (35°C) with higher-frequency (300 Hz) trains. We measured postsynaptic responses in control conditions and in AgaIVA (example cell, **Figure 2.7 A**). Submaximal block of P-type VGCCs reduced both RRP_{train}^{COR} (**Figure 2.7 B**) and

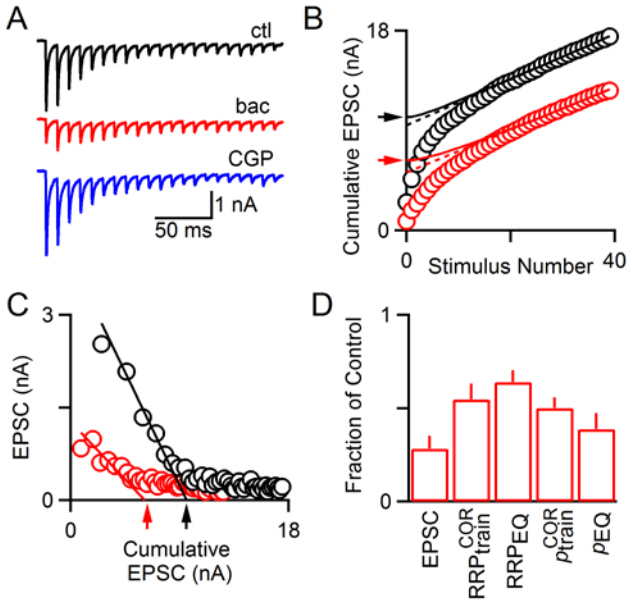

Figure 2.6. $GABA_B$ receptors modulate synaptic transmission through changes in *p* and effective RRP. A Postsynaptic responses to a 100 Hz stimulus train in control conditions (*black*), in 100 µM baclofen (bac, *red*), and in 20 µM CGP 55845 (CGP, *blue*). **B** Plot of cumulative EPSC versus stimulus number for example cell in control (*black circles*) and baclofen (*red circles*) indicates that RRP_{train}^{COR} is reduced in baclofen. RRP_{train}^{COR} is indicated by arrows. **C** Plot of EPSC amplitude versus cumulative EPSC amplitude for the same data reveals that RRP_{EQ} is also reduced in baclofen. RRP_{EQ} is indicated by arrows. **D** Summary of the effects of baclofen on properties of synaptic transmission (n=9).

Figure 2.7. The size of the effective RRP is regulated by changes in presynaptic calcium influx for 300 Hz trains at near-physiological temperature. A Postsynaptic responses of an example cell to a 300 Hz stimulus train delivered in control conditions and in AgaIVA. **B** Cumulative EPSC in an example cell in control conditions (*black circles*) and in AgaIVA (*gray circles*) for the response shown in A. The value of RRP_{train}^{COR} is reduced (*black versus gray arrows*). **C** Plot of EPSC amplitude versus cumulative EPSC for the same example cell. Agatoxin (*gray circles*) reduces RRP_{EQ} (*gray versus black arrows*). **D** Summary of changes to EPSC amplitude, RRP_{train}^{COR}, RRP_{EQ}, p_{train}^{COR}, and $p_{EQ.}$ (n=4). **E** Postsynaptic responses of an example cell to a 300 Hz stimulus train delivered in control conditions and in baclofen (100 μM). **F** Cumulative EPSC in an example cell in control conditions (black circles) and in baclofen (*gray circles*) for a 300 Hz train delivered at 35°C. The value of RRP_{train}^{COR} is reduced (*gray versus black arrows*). **G** Plot of EPSC amplitude versus cumulative EPSC for the same example cell. Baclofen (*gray circles*) reduces RRP_{EQ} (*gray versus black arrows*). **H** Summary of changes to EPSC amplitude, $RRP_{\mathrm{train}}^{\mathrm{COR}}$, RRP_{EQ}, $p_{\mathrm{train}}^{\mathrm{COR}}$, and $p_{EQ.}$ (n=5).

Figure 2.7 (Continued)

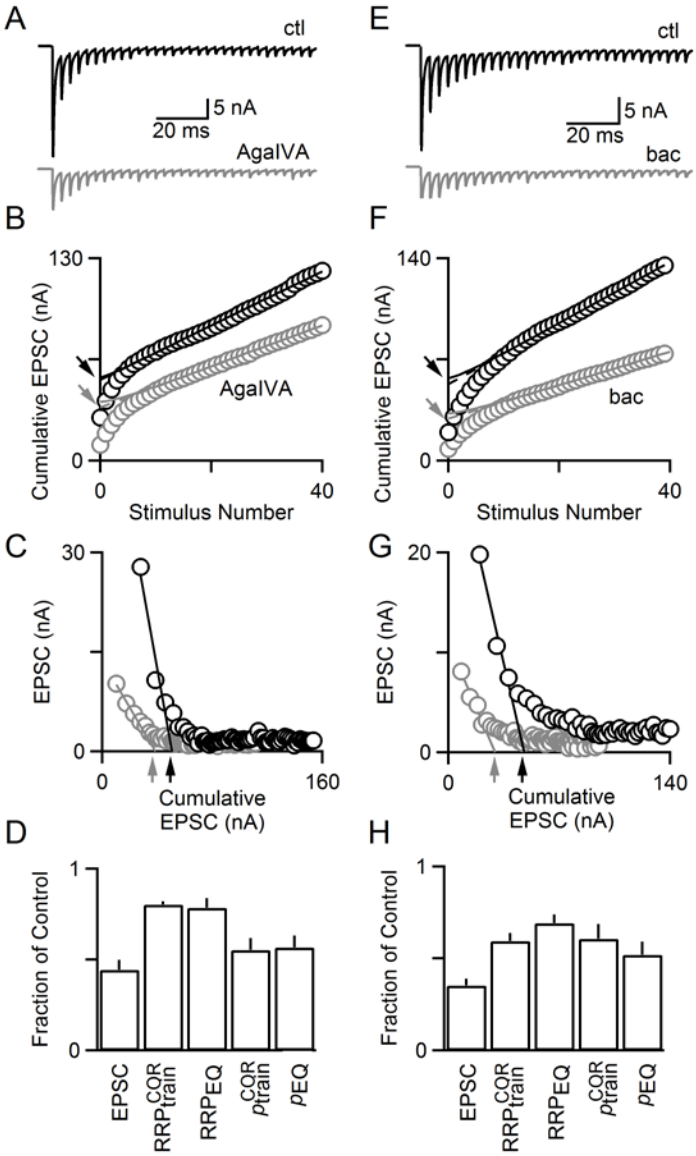

RRP_{EQ} (**Figure 2.7 C**). We restricted our analysis to trials in which the EPSC amplitude was moderately reduced (44.3 ± 5.5% of control, p<0.01, n=4 cells) and found that as for room temperature experiments the blockade of P-type calcium channels reduced both the pool size (RRP_{train}^{COR}: 80.2 ± 1.8% of control, p<0.01; RRP_{EQ}: 78.5 ± 5.4% of control, p<0.01) and *p* (p_{train}^{COR}: 55.2 ± 6.5% of control, p<0.05; p_{EQ}: 56.6 ± 6.5% of control, p<0.01). This suggests that changes in effective pool size collaborate with changes in *p* to produce the full effect of AgaIVA on synaptic transmission for higher-frequency trains at 35°C. We also testing the effect of activating presynaptic $GABA_B$ receptors (**Figure 2.7 E-H**), and found that the EPSC amplitude was reduced to 35.3 ± 3.7% of control (p<0.001, n=5 cells), with considerable effects on both measures of pool size (RRP_{train}^{COR}: 59.4 ± 4.3% of control, p<0.01; RRP_{EQ}: 69.3 ± 4.6% of control, p<0.01) and both measures of *p* (p_{train}^{COR}: 60.7 ± 8.0% of control, p<0.01; p_{EQ}: 52.1 ± 7.1% of control, p<0.01). These experiments suggest that presynaptic calcium influx regulate the effective size of the RRP under physiological temperature and firing frequencies.

A simple model (see Methods) was used to illustrate the consequences of changing synaptic strength through changes in *p* versus changes in effective RRP (**Figure 2.8 A-C**). The differences are best illustrated by considering the case where there is no replenishment of the RRP such that once the RRP is depleted no neurotransmitter release occurs (**Figure 2.8 A**). Three cases are considered that all lead to the same decrease in the initial EPSC, but one does so by decreasing *p*, another by decreasing the effective RRP, and the third by small decreases in both *p* and effective RRP. If synaptic strength is altered by reducing *p*, then it takes longer for repeated stimulation to deplete the RRP, but the total neurotransmitter release evoked by the train is unchanged (**Figure 2.8 A**, *blue line*). In contrast, reduction of the effective RRP size

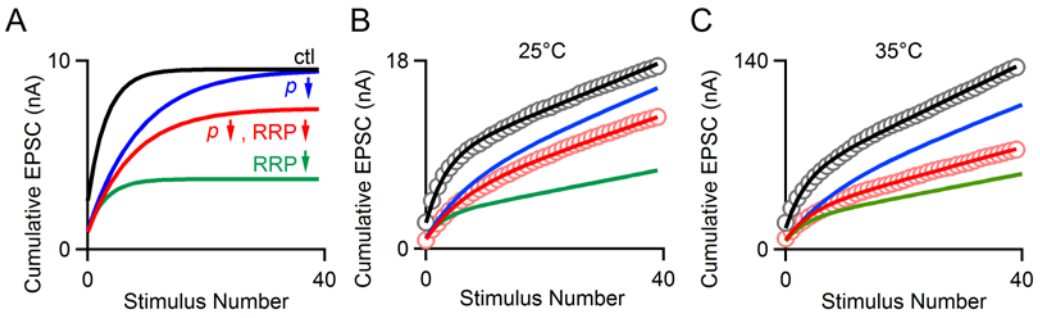

Figure 2.8. Simulations indicate that changes in the effective RRP help to explain the effect of changing presynaptic calcium influx on postsynaptic responses. These simulations are based on a model of vesicular release explained in the Methods. **A** Cumulative EPSCs are shown for control conditions (*black*), for fractional reductions in *p* (0.33 of control, *blue*), effective RRP (0.33 of control, *green*) and for both effective RRP and *p* reduced (to 0.73 and 0.46 of control, respectively, *red*). **B, C** Cumulative EPSCs are shown for two example experiments in control conditions (*gray circles*) and in the presence of baclofen (*light red circles*) for 100 Hz trains at 25°C (**B**) and for 300 Hz trains at 35°C (**C**). The black and red lines in **B** and **C** are fits to control and baclofen cumulative EPSCs, respectively, that were determined using an iterative fitting process that had 3 free parameters {effective RRP, *p*, and the replenishment rate per empty release site}. For the other lines, parameters from the control fit were used but either *p* or effective RRP was reduced. The parameters of the lines for **B** are {9.96, 0.25, 0.025, *black*}, {7.64, 0.12, 0.033, *red*}, *p* is 0.33 of control (*blue*), and effective RRP is 0.33 of control (*green*), and for **C** {65.9, 0.24, 0.036, *black*}, {37.4, 0.18, 0.037, *red*}, *p* is 0.41 of control (*blue*), and effective RRP is 0.41 of control (*green*).

without altering *p* reduces the overall neurotransmitter released by a train without altering the short-term plasticity (**Figure 2.8 A**, *green line*). If the both *p* and effective RRP are decreased, as we have found to be the case at the calyx of Held, the cumulative EPSC is both smaller in final amplitude and requires more stimuli to reach depletion (**Figure 2.8 A**, *red line*).

In the realistic case, replenishment of the RRP must also be considered. We used the same model to evaluate the effect of $GABA_B$ activation on the cumulative EPSCs for two example experiments at 25°C (**Figure 2.8 B**) and at 35°C (**Figure 2.8 C**), but in these simulations we also included replenishment of the RRP. The model takes into account the observation that replenishment is not constant but depends on the extent of depression (**Figure 2.2 E**). In the example at 25°C, for the best approximations to the experimental data, baclofen reduced RRP and *p* to 0.77 and 0.47 of control values, respectively, without decreasing the rate of replenishment (**Figure 2.8 B**, *red line*). Similarly at 35°C the best approximation was achieved by fractionally reducing the RRP and *p*, respectively, to 0.57 and 0.78 of control values, without altering replenishment (**Figure 2.8 C**, *red line*). In both cases, changes in p alone (*blue lines*) or in RRP alone (*green lines*), did not adequately describe the observed data.

The implication is that modulation of the effective RRP can change the total charge transfer in response to a train or rapid burst of presynaptic activity, which a change in only *p* would not produce. Release of a neuromodulator could therefore affect the ability of a postsynaptic cell to follow high-frequency stimuli, which would be of great importance for a high-frequency, high-fidelity synapse such as the calyx of Held.

Discussion

Our main finding is that in addition to changing *p*, alterations in presynaptic calcium influx change the effective RRP size. Thus, the calcium dependence of neurotransmitter release is determined by the combined calcium dependencies of *p* and the effective size of the RRP. These findings represent an advance in our understanding of the mechanisms controlling neurotransmitter release, and they establish that neuromodulators that change calcium entry can also change the size of the RRP, which has important functional consequences.

Multiple Approaches Indicate that Calcium Influx Regulates the RRP

Here, we study the regulation of vesicles that can be elicited by a train of action potentials. This population of vesicles is crucial to studies of synaptic transmission, and has been studied by others using electrophysiological and optical techniques (Ariel and Ryan, 2010; Moulder and Mennerick, 2005; Schneggenburger et al., 1999). We use two independent methods that rely on different assumptions to establish the calcium dependence of the effective size of the RRP. The RRP_{train} method assumes that high-frequency stimulation rapidly depletes the RRP, and that after depletion the remaining release is due to replenishment (Schneggenburger et al., 1999). By assuming replenishment is constant throughout the train the size of the RRP is determined from the cumulative EPSC amplitude. In contrast, the RRP_{EQ} method focuses on the early EPSCs in a train, in a range during which their amplitudes decay with a single exponential time course. The reasoning is that the decrement in EPSC amplitudes is a consequence of

depletion of the RRP, and they can be used to estimate the size of the RRP (Elmqvist and Quastel, 1965).

A key strength of using these two methods is that the differences in initial assumptions can allow us to draw stronger conclusions. For example, the RRP_{EQ} method assumes constant *p* during the first several EPSCs of the train, which could be problematic under low *p* conditions when facilitation occurs early in the train, or if calcium channel inactivation during the train significantly affects *p* (Cuttle et al., 1998; Forsythe et al., 1998). Conveniently, the RRP_{train}^{COR} method (and the original RRP_{train} method) does not require constant *p*. The fact that our estimates of pool size changes with both methods agree indicate that facilitation and calcium channel inactivation are unlikely to significantly affect our ability to measure the effective RRP.

These methods are expected to bracket the actual RRP, as described previously. Indeed, we found that our estimates of RRP_{train} were slightly smaller than our estimates of RRP_{EQ}. (**Figure 2.2**). However, by determining the properties of recovery from depression early and late in the train we were able to correct for decreased recovery from depression early in the train, and found a remarkable agreement between RRP_{train}^{COR} and RRP_{EQ} (**Figure 2.2 F**). This agreement strengthens our confidence in our ability to quantify the effective RRP and detect changes in the size of the RRP.

We altered calcium influx in many different ways, and in all cases changes in effective RRP size contributed to changes in EPSC amplitude. Altering Ca_e to reduce the influx per channel, blocking R-type VGCCs, and blocking a fraction of P/Q-type VGCCs all reduced *p* and effective RRP size. For all manipulations the change in *p* typically amounts to double the change

in effective RRP size, suggesting that the calcium-dependent changes of RRP size is a general feature of transmitter release at this synapse.

The results shown here have important consequences for the power law dependence of release, which is typically attributed exclusively to the calcium dependence of *p*. Our results confirm that the majority of the calcium dependence of EPSC size at the calyx of Held arises from changes in *p* (**Figure 2.3**) but that changes in the size of the effective RRP may be an important determinant of action potential-evoked release. We posit that the calcium dependence of the size of the effective RRP should be considered in future studies of synaptic transmission.

Possible Mechanisms by which Calcium Influx Regulates the RRP

The findings presented here raise the question, what determines which vesicles belong to the effective RRP, and how is this regulated by calcium influx? Measures of the RRP that have been previously used, such as hypertonic sucrose application, presynaptic voltage steps, and calcium uncaging (Rosenmund and Stevens, 1996; Sakaba and Neher, 2001b; Schneggenburger et al., 1999) do not use physiological stimuli to deplete the RRP, in contrast to our methods. Measurement of the RRP with hypertonic sucrose application has been shown to be invariant with presynaptic calcium (Rosenmund and Stevens, 1996), while our measures of effective RRP size in this study are clearly calcium-dependent. The main difference between these techniques is that action potential-evoked calcium influx is temporally and spatially constrained, such that action potentials only generate brief microdomains of high Ca^{2+} while the other stimuli either create prolonged Ca^{2+} signals or do not rely on calcium influx to cause release.

The extent of calcium microdomains cannot be measured directly, but modeling approaches suggest that single VGCCs can only affect release within about 50 nm (Fogelson and Zucker, 1985; Simon and Llinás, 1985). At the calyx of Held, clusters of VGCCs are responsible for the release of most vesicles (Borst and Sakmann, 1999) and can create calcium microdomains of a few hundred nanometers (Meinrenken et al., 2002). This raises the possibility that the distance between docked vesicles and VGCCs determines their inclusion in the effective RRP, which we define here as the vesicles that can be released by action potential stimuli. It is known that the distance between vesicles and presynaptic calcium channels varies, and this distance is crucial for determining whether action-potential induced calcium entry can cause exocytosis (Augustine, 2001; Fogelson and Zucker, 1985; Simon and Llinás, 1985; Wadel et al., 2007). Many studies have suggested that vesicle positioning within calcium microdomains can lead to heterogeneous probabilities of release for individual vesicles (Pr) at the calyx of Held synapse (Meinrenken et al., 2002; Sakaba and Neher, 2001b) and other synapses (Beaumont et al., 2005; Cooper et al., 1996; Shahrezaei and Delaney, 2004). Some vesicles may be positioned sufficiently far away from presynaptic calcium channels that they never experience sufficient calcium concentrations for release under conditions of reduced calcium influx, and therefore are excluded from the effective RRP. It is also possible that heterogeneity of the molecular sensors responsible for molecular fusion could lead to the observed calcium dependence of the size of the effective RRP; however it is unlikely to account for the majority of the effect at this synapse (Wadel et al., 2007).

Functional Implications of Changes in Calcium Influx regulating the RRP

The generalizability of this mechanism may have important physiological implications. At many different types of synapses, neuromodulators regulate presynaptic VGCCs to decrease presynaptic calcium influx. It had previously been assumed that such neuromodulation alters transmission exclusively by changing *p* (Zucker and Regehr, 2002). We find, however, that $GABA_B$ receptor activation at the calyx of Held does not reduce neurotransmitter release exclusively by regulating *p*; instead, the effective RRP size is also regulated (**Figure 2.6**). Moreover the relative contributions of changes in *p* and changes in RRP are similar to those observed when calcium entry is regulated. These effects persist at near-physiological temperature for faster trains (**Figure 2.7**).

We used a simple model to illustrate the consequences of changing synaptic strength through changes in *p* versus changes in effective RRP (**Figure 2.8 A-C**). The differences between changes in *p* and RRP are best illustrated by considering the case where there is no replenishment of the RRP, and once the RRP is depleted no neurotransmitter release occurs (**Figure 2.8 A**). If synaptic strength is altered by reducing *p*, then it takes longer for repeated stimulation to deplete the RRP, but the overall release evoked by the train is unchanged. In contrast, reduction of the effective RRP size reduces the overall neurotransmitter released by a train. The same holds true when replenishment is added into the simulation (**Figure 2.8 B, C**). The data presented in this paper suggests that both processes occur and that a change in *p* accounts for about two-thirds of the change in EPSC size and a change in effective RRP for the remaining one-third (**Figure 2.8 A-C**, *red lines*).

The implication is that modulation of the effective RRP can change the total charge transfer in response to a train or rapid burst of presynaptic activity, which a change in only *p*

would not produce. Release of a neuromodulator could therefore affect the ability of a postsynaptic cell to follow high-frequency stimuli, which would be of great importance for a high-frequency, high-fidelity synapse such as the calyx of Held.

Chapter 3

Modeling Neurotransmitter Release at the Calyx of Held Synapse

Abstract

In the previous chapter, a model to describe synaptic transmission in terms of three parameters was introduced. The three parameters are the number of vesicles in the readily-releasable pool (N), the average probability of fusion occurring for an individual vesicle in the RRP due to an AP (*p*), and the rate of replenishment of the RRP with vesicles from a recycling pool (R). In this chapter, I will explain the model and compare its assumptions to more commonly-used linear extrapolation methods for measuring RRP size and *p*. When applied to data collected at the juvenile mouse calyx of Held synapse, the model exhibits excellent qualitative agreement with the conclusions of linear extrapolation methods. Moreover, we provide evidence that it is likely to provide a more accurate estimate of RRP size, probably due to its more nuanced assumptions regarding replenishment of the RRP. Additionally, the approach we present has the advantage of providing a direct estimate of *p*, unlike existing linear extrapolation methods. We then use the model to demonstrate the advantages and disadvantages of linear extrapolation techniques and the regimes under which they can most accurately be applied. Generally, we find that high *p*, low R, and high stimulus frequency are important for accurate assessment of RRP size with linear extrapolation techniques. We also find that the apparent frequency dependence of RRP size may be due to the methods by which linear extrapolation techniques estimate RRP size, instead of actual changes in the effective RRP. In the future, we plan to characterize the time course and magnitude of facilitation at this synapse and incorporate this as an additional parameter in the model.

Introduction

Many researchers have constructed models of neurotransmitter release at a variety of synapses. These models can provide important insight that explains experimental observations, and also suggest possibilities that are difficult to directly test through experimentation. One of the earliest, simplest models of synaptic transmission comes from Liley and North (Liley and North, 1953). Their experiments at the rat neuromuscular junction revealed that a stimulus train could reduce the subsequent release effected by a stimulus train delivered shortly afterwards, and that this deficit would eventually recover over a time course of seconds. They hypothesized that either a change in the quantity of acetylcholine in nerve terminals or a change in the readiness of release of acetylcholine is responsible for the changes observed, or that:

$$Release = RRP \times f_0 \tag{3.1}$$

in which RRP corresponds to the quantity of neurotransmitter immediately available for release and f_0 corresponds to the fraction of the RRP that is liberated by a single stimulus. This quantity can be considered an estimate of release probability (p). Similar assumptions were made by others, who suggested that depletion of neurotransmitter at nerve terminals was the primary determinant of postsynaptic responses during high-frequency stimulation (Elmqvist and Quastel, 1965).

Later modeling approaches evolved to consider replenishment of the RRP and mechanisms of short-term plasticity. At the squid giant synapse, changing the external calcium concentration proved to affect the rate of recovery from depression (Kusano and Landau, 1975), providing the first hint that calcium accumulates in the presynaptic terminal and might regulate

refilling of the RRP. Later, more direct observations of calcium-dependent recovery from depression at a variety of synapses (Dittman and Regehr, 1998; Hosoi et al., 2007; Sakaba and Neher, 2001a; Wang and Kaczmarek, 1998) led to the generation of new models that account for variable replenishment of the RRP. Additionally, the appreciation that the occupancy of the RRP changes during high-frequency stimulation, and that the replenishment of the RRP should scale with the availability of empty release sites that can accept vesicles has led to more variants of the depletion model, (Wesseling and Lo, 2002) some of which also account for facilitation (Varela et al., 1997).

Models of neurotransmitter release can vary widely in their number of parameters and scope. Almost all models of release account for p. At the calyx of Held synapse and others, experimental data reveals significant heterogeneity in the release probability of individual vesicles (p_r), likely due to the wide range of coupling distances between channel clusters and vesicles (Dobrunz and Stevens, 1997; Moulder and Mennerick, 2005). Due to the complex architecture and presence of hundreds of active zones in a single calyx, it is impossible to determine the precise distribution of vesicular p_r values in a given terminal. Some experimental evidence has suggested a simplification, that the RRP can be divided into a fast-releasing pool (FRP) and slow-releasing pool (SRP) with two separate release probabilities and replenishment rates (Sakaba and Neher, 2001a). This view gained some traction, with a modeling approach devised to account for these two pools (Schneggenburger et al., 2012; Trommershäuser et al., 2003), although it has been proposed that this two-pool model is an approximate way to begin describing the heterogeneity of release sites in the calyx of Held rather than a perfectly accurate delineation of two vesicle populations (Trommershäuser et al., 2003). Importantly, the studies that report an FRP and SRP have not used AP stimuli to elicit neurotransmitter release; instead,

they used large, prolonged stimuli such as presynaptic depolarizing voltage steps or calcium uncaging to study fast and slow RRP kinetics (Sakaba and Neher, 2001a; Trommershäuser et al., 2003; Wölfel et al., 2007). This raises a very reasonable possibility that the SRP may not contribute to AP-evoked release. Another modeling study used experimental data to infer the distance between calcium channels and presynaptic vesicles, as well as the clustering arrangement of calcium channels. Here, all release-ready vesicles were assumed to be part of one RRP, with variations in p_r explained by heterogeneity in channel-vesicle coupling distances (Meinrenken et al., 2002). This approach incorporated a very thorough and nuanced appreciation for presynaptic architecture, but did not account for replenishment of the RRP and is most applicable at very short time scales.

In this chapter, I will develop and characterize a simple model of neurotransmitter release very much based on the original principles described by early depletion models with a new way of accounting for replenishment during activity. The model contains only three parameters—a single RRP of a certain size that contains release-ready vesicles (N), an average probability with which these vesicles are released by action potentials (p), and a replenishment rate per available vesicular release site (R). These will be carefully explained in the upcoming Materials and Methods and Results sections. I will first apply the model to data sets collected in **Chapter 2** as well as new data to test the validity of the model, and then use the same equations to simulate postsynaptic responses in order to shed light on current methods of estimating RRP and p.

Materials and Methods

Animals and Preparation of Brain Slices

The use of animals and procedure for preparing brain slices was the same in this chapter as for **Chapter 2**.

Electrophysiology

Electrophysiological procedures and solutions were all identical to those used in **Chapter 2**. In this chapter, all recordings were performed at room temperature (25°C).

Data Analysis

The effective size of the RRP was calculated using two techniques. RRP_{train} and RRP_{EQ}, both measures of effective RRP size. The methods for these calculations are described in **Chapter 2**. Data analysis was performed using routines written in IgorPro. Linear and exponential curve fitting was performed using a built-in least-squares curve fitting application in IgorPro. Statistical tests were performed as two-tailed paired Student's t-tests performed in IgorPro. Although sample sizes were too small to test for normality, larger data sets (data not shown) for which only one stimulus frequency was applied do have normal distributions, suggesting that this data is likely to have a normal distribution as well. The significance level was set at $p<0.05$.

Modeling and simulations

The equations introduced in the Materials and Methods of **Chapter 2** (**Equations 2.1-2.9)** were originally written for use in a curve fitting procedure custom-written in IgorPro, which receives EPSC amplitudes as a function of stimulus number as its input and returns values of N, *p*, and R as outputs. This procedure finds optimal output values using the Levenberg-Marquardt algorithm, which is a commonly used method for solving non-linear least-squares problems. The curve fitting procedure is instructed to select the optimal values of N, *p*, and R to fit the amplitudes of EPSCs resulting from a high-frequency stimulus train. N equals the initial RRP size multiplied by the quantal size, *p* equals the fraction of the RRP released per action potential, and R corresponds to the replenishment of RRP (expressed as a fraction of the RRP, i.e., R=0.01 corresponds to refilling of 1% of available release sites between stimulus *n*-1 and stimulus *n*).

To calculate the optimal values of the three output parameters, the procedure begins with initial guesses for N, *p*, and R, provided by the user. The procedure uses three one-dimensional data arrays to contain the results of a given set of N, *p*, and R values. Here, we call those data arrays RRP (containing the size of the readily releasable pool prior to stimulus number *n* multiplied by the quantal size, in units of current), Rec (containing the recovery of the readily releasable pool between stimulus *n*-1 and *n*, units of current), and EPSC (containing the size of the EPSC resulting from stimulus *n*, in units of current).

For the first stimulus, which results in $EPSC_0$,

3.2 $RRP_0=N$

3.3 $EPSC_0=pN$

3.4 $Rec_0=0$

Rec, which contains the fraction of the RRP replenished prior to stimulus *n*, is equal to zero here because the RRP is assumed to be full prior to stimulation, preventing any additional vesicles from joining the RRP.

For the second stimulus, which results in $EPSC_1$:

3.5 $RRP_1=RRP_0(1-p+pR)$

3.5 $EPSC_1=p(RRP_1)$

3.6 $Rec_1= pR(RRP_0)$

For all subsequent EPSCs (stimulus number $n>1$)

3.7 $RRP_n=RRP_{n-1}(1-p-R+pR)+(RRP_0)R$

3.8 $EPSC_n=p(RRP_n)$

3.9 $Rec_n=RRP_{n-1}(-R+pR)+_(RRP_0)R$

Different values of N, *p*, and R are implemented by the procedure until discrepancies between the experimental data and modeled EPSC wave are minimized.

The same equations shown above govern the simulated postsynaptic responses generated in this chapter. Their implementation in simulations (as compared to data-fitting) is much

simpler. In the case of a simulation, the values of N, *p*, and R are dictated by the user, and the procedure outputs three one-dimensional data arrays, as above, containing the RRP size (RRP), fractional recovery of the RRP from depression (Rec) and resulting EPSC amplitudes (EPSC) for stimulus 0 through stimulus *n*. The EPSC wave can be used to predict the amplitudes of postsynaptic responses to high-frequency stimulation according to the model proposed here.

To mimic the effects of varying frequency in our simulations, we determined the time course of recovery from depression induced by stimulation at 100 Hz. We fit this time course with a double-exponential function to estimate the amount of replenishment that would occur at between stimuli at different frequencies, which is:

3.10 $$EPSC_{norm}(\Delta t) = 1 - 0.246e^{-\left(\frac{\Delta t}{185\ ms}\right)} - 0.697e^{-\left(\frac{\Delta t}{2900\ ms}\right)}$$

in which the steady state EPSC (EPSCss) is normalized to the amplitude of the first EPSC in a stimulus train ($EPSC_0$) and Δt=the interstimulus interval for a given stimulus frequency (i.e., Δt=10 ms for a 100 Hz stimulus train). We calculate the replenishment rate R (which corresponds to the extent of replenishment between stimuli, not per unit time) for a given frequency in Hz (*f*) as:

3.11 $$R(f) = R(100\ Hz) \times \frac{EPSC_{norm}(1000/f) - EPSC_{norm}(0)}{EPSC_{norm}(1000/100\ Hz) - EPSC_{norm}(0)}$$

in which Δt=1000/*f*. Simulations are then performed with R(*f*) as the input value for replenishment rate (R).

Results

In this chapter, we present a simple model to explain neurotransmitter release in response to high-frequency activity. The calyx of Held is characterized by a relatively high average release probability (*p*) and noticeable depression of postsynaptic responses in response to a train of action potentials (Schneggenburger et al., 2002). In the presence of cyclothiazide and kynurenic acid, EPSC amplitudes can be interpreted as a linear measure of presynaptic vesicular release (Sakaba and Neher, 2001b). Here, we construct a model with the following assumptions: 1) that the RRP is a single pool of vesicles that begins with all release sites full (**Figure 3.1 A**, left), 2) that an average release probability *p* describes the fraction of vesicles released from the RRP with each AP stimulus, 3) depletion of vesicles in the RRP determines the extent of synaptic depression, and that 4) a recycling pool of vesicles (**Figure 3.1 A**) reloads emptied release sites in the RRP with a constant rate per site. In control conditions (Ca_e= 2 mM), EPSCs amplitudes are fit well by a single exponential equation, suggesting that depletion of the RRP is the predominant factor causing synaptic depression. This assumption has been applied at other high *p* synapses (Elmqvist and Quastel, 1965; Liley and North, 1953). A depiction of postsynaptic responses according to this model is shown in **Figure 3.1 B**. The amplitude of the first EPSC is equal to the size of the RRP at time t=0 (N) multiplied by *p* and by the quantal size (q). All subsequent EPSCs are the product of the size of the remaining RRP, *p*, and q. The amplitudes of EPSCs decay throughout the train due to depletion of the RRP and eventually reach a steady state amplitude. A graphical depiction of RRP occupancy is shown in **Figure 3.1 C**. One of the most significant features of this model is that RRP occupancy has an effect on the total number of vesicles re-entering the RRP; therefore, more vesicles are added to

Figure 3.1. A model of synaptic responses in response to high-frequency firing at the calyx of Held synapse. **A** Cartoon depicting the three parameters of the model. A presynaptic terminal with two pools of vesicles is shown: an RRP (consisting of N vesicles) and a pool of recycling vesicles (depicted as vesicles located far from the presynaptic membrane). For clarity, the RRP is shown as vesicles in close contact with the synaptic membrane and the recycling pool is shown as vesicles far from the membrane. *Left* Before high-frequency stimulation, the RRP is assumed to be full of neurotransmitter-containing vesicles with no unoccupied release sites. The number of vesicles in the RRP before firing is N. *Middle* After one action potential, a fraction of vesicles has been released that corresponds to the average probability of vesicular release (*p*) multipled by the initial size of the RRP (N). Replenishment of the RRP from a recycling pool occurs to refill the newly-vacated release sites in the presynaptic terminal. Replenishment occurs with a fixed rate per empty release site (R). *Right* After many action potentials, the RRP has been almost entirely depleted and has reached a steady state occupancy set by the replenishment rate (R). **B** Simulated EPSCs in response to a 100 Hz stimulus train, with N=1000 vesicles, p=0.4, and R=0.1. q equals the quantal size. **C** Plot of the number of vesicles in RRP versus time for simulated EPSCs in B. Each action potential releases a fraction of vesicles in the RRP corresponding to *p.* Vesicles enter the RRP with a rate of R per unoccupied release site per stimulus. In this example, 10% of unoccupied release sites are filled between stimuli.

Figure 3.1 (Continued)

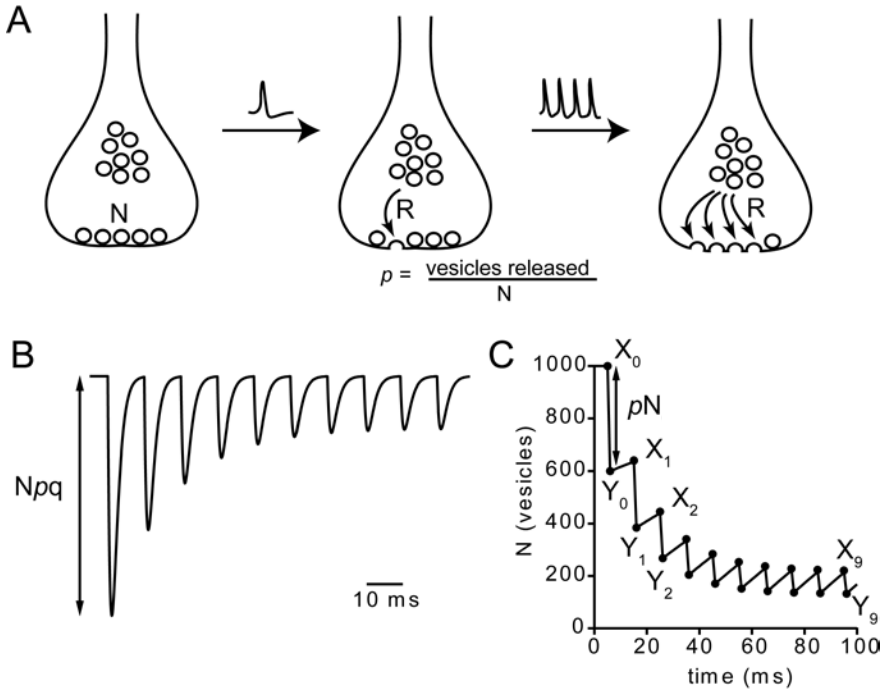

the RRP between stimuli towards the end of a stimulus train than at the beginning (**Figure 3.1 C**).

The two linear extrapolation methods I will describe here make simpler assumptions regarding replenishment than our model. One technique, which we call RRP_{train}, plots the cumulative EPSC amplitude that results from a high-frequency train (**Figure 3.2 A**). This technique was thoroughly described in **Chapter 2** and is frequently used at a variety of synapses (Liu et al., 2014; Moulder and Mennerick, 2005; Schneggenburger et al., 1999; Stevens and Williams, 2007). When the RRP is depleted, the cumulative EPSC reaches a constant slope, which corresponds to the steady-state EPSC amplitude that replenishment of the RRP can maintain. Back-extrapolation of this slope to the y-axis gives a quantity in units of current that is an estimate of the number of vesicles in the RRP multiplied by the quantal size (Schneggenburger et al., 1999). The assumption here is that the RRP is replenished at a constant rate per terminal, which means that the replenishment rate *per empty release site* in the RRP actually decreases as the RRP is depleted with a train stimulus. A second linear extrapolation technique, first described by Elmqvist and Quastel (Elmqvist and Quastel, 1965), plots EPSC amplitudes versus the cumulative EPSC and extrapolates a line to the x-axis (**Figure 3.2 B**). This quantity, also in units of current, gives an estimate of the RRP size with the assumption that replenishment of the RRP within the first few tens of milliseconds is negligible. This assumption will lead to an over-estimation of RRP size (Elmqvist and Quastel, 1965). The assumptions that characterize these methods are shown in **Table 3.1**. The most important difference between the RRP_{train} and RRP_{EQ} methods is that the RRP_{train} method overestimates replenishment, and therefore may underestimate the size of the RRP, and that RRP_{EQ} underestimates (or rather, neglects) replenishment, and therefore will overestimate the size of the RRP. Accordingly,

Figure 3.2. Linear extrapolation methods and model fits for determining RRP size and *p*. A Example estimation of effective RRP size (RRP_{train}, black arrow) by back-extrapolation of the cumulative EPSC to the y-axis. The probability of release (p_{train}) is estimated by dividing the amplitude of the first EPSC by RRP_{train}. This widely-used method is explained extensively in Chapter 2. **B** Example estimation of effective RRP size (RRP_{EQ}, black arrow) by linear extrapolation of the first four points of the EPSC amplitude versus the cumulative EPSC to the x-axis. This method, developed by Elmqvist and Quastel (1965), is explained extensively in Chapter 2. The probability of release (p_{EQ}) is estimated by dividing the amplitude of the first EPSC by RRP_{EQ}. **C** Plot of RRP_{train} and RRP_{EQ} values for cells in different Ca_e (1, 1.25, 1.5, 2, 3, and 4 mM). For panels C and D, linear fits to the data (*black line*) are shown. In C-F, the unity line (*dashed)* is shown. **D** Plot of p_{train} and p_{EQ} values for the same cells as in C. **E** Plot of RRP_{model} versus RRP_{train} (red circles) and RRP_{model} versus RRP_{EQ} (blue circles) for cells in different Ca_e (same as C, unity line shown as a dashed line). **F** Plot of versus p_{train} (red circles) and p_{EQ} (blue circles) for cells in different Ca_e. **G** Plot of the two linear extrapolation estimates of RRP size normalized to RRP_{model} versus p_{model} (RRP_{train}/RRP_{model}, red circles; RRP_{EQ}/RRP_{model}, blue circles). The line y=1 is shown as a dashed line. **H** Plot of the two linear extrapolation estimates of *p* normalized to p_{model} versus p_{model} (p_{train}/p_{model}, red circles; p_{EQ}/p_{model}, blue circles). The line y=1 is shown as a dashed line.

Figure 3.2 (Continued)

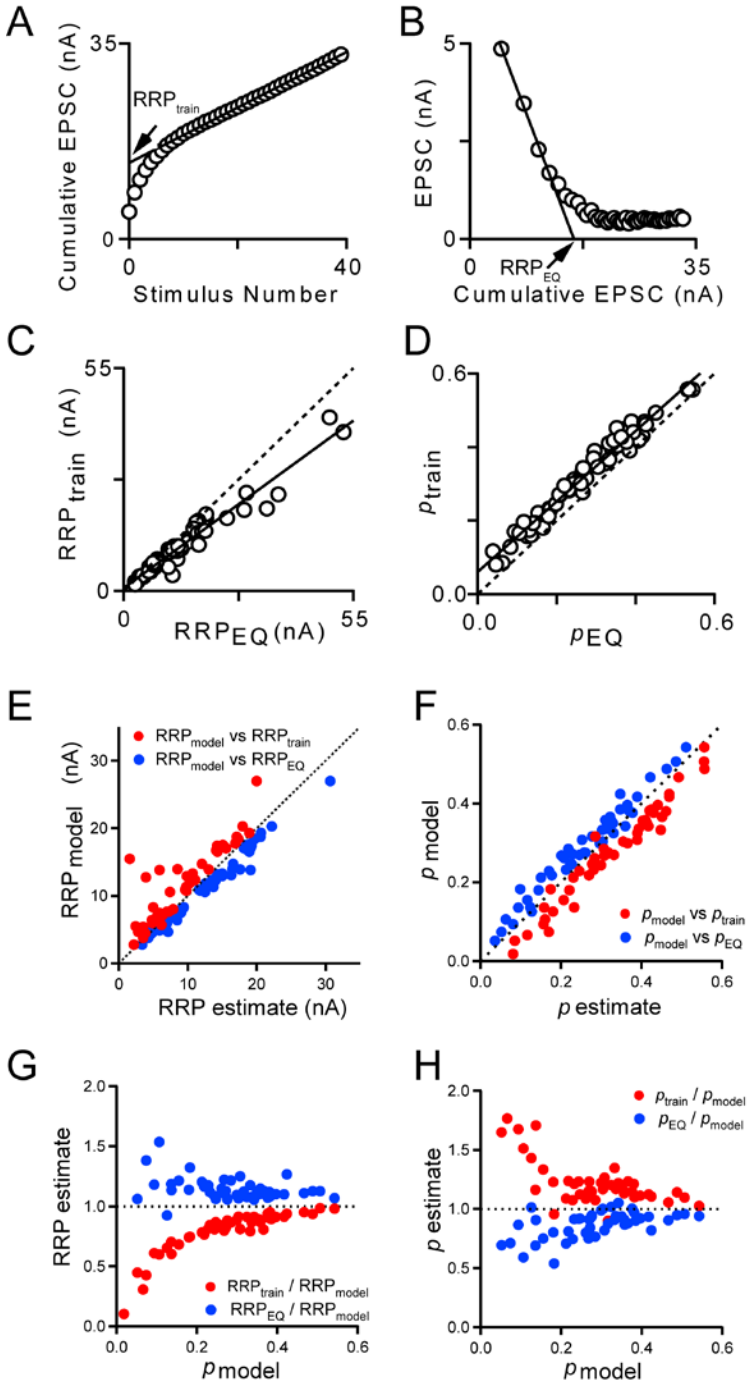

Table 3.1. **Key assumptions that characterize methods of estimating the size of the RRP and *p*.**

Assumptions	RRP_{train}	RRP_{EQ}	RRP_{model}
Single pool depletion	**Yes**	**Yes**	**Yes**
Constant *p*	**No**	**Yes**	**Yes**
Constant replenishment	**Yes; maximal**	**Yes; none**	**No; variable**
Direct estimate of *p*	**No**	**No**	**Yes**

estimates of RRP size by the RRP_{train} method are consistently smaller than RRP_{EQ} estimates of RRP size (**Figure 3.2 C**). Additionally, neither linear extrapolation technique provides a direct measure of *p*; rather, the amplitude of the first EPSC is divided by the estimated RRP size to give an estimate of *p*. $p_{train} = EPSC_0/RRP_{train}$, and $p_{EQ} = EPSC_0/RRP_{EQ}$. Since these indirect measures of *p* are inversely related to the estimate of RRP size, it makes sense that p_{train} is consistently larger than p_{EQ} (**Figure 3.2 D**). In contrast, our model uses an iterative curve-fitting function custom-written in IgorPro (see Methods) in which N, *p*, and R are optimized. The data is entered into the model as a single one-dimensional data array containing the amplitude of each EPSC in response to a stimulus train as a function of stimulus number. The curve-fitting function is given a set of starting values of N, *p*, and R, from which it can change each variable systematically to determine the optimal values of N, *p*, and R to fit the data given (see **Materials and Methods** for detailed description). We find a remarkable agreement between the new estimate of RRP size, which we will call RRP_{model}, and our existing back-extrapolation estimates of RRP size (**Figure 3.2 E**). Interestingly, RRP_{model} is typically larger than RRP_{train}, but smaller than RRP_{EQ} (**Figure 3.2 E**). This makes sense, due to the allowance for a varied rate of replenishment during the

stimulus train which eventually reaches the maximal rate assumed to be constant by the RRP_{train} technique. The model therefore attributes more of the cumulative release during a stimulus train to replenishment (thus excluding it from an RRP measurement) than RRP_{EQ}, but attributes more of the cumulative release during a stimulus train to replenishment than RRP_{train}. The estimated value of *p* by this model, or p_{model}, can also be compared to the values of *p* generated by the two linear extrapolation techniques. We find that p_{model} is well-correlated with our two other estimates of *p,* and that p_{model} is typically larger than p_{EQ} but smaller than p_{train} (**Figure 3.2 F**). Normalizing the linear extrapolation estimates of RRP and *p* to the estimates provided by the model leads to some interesting observations. Estimates of RRP size by the two linear extrapolation methods seem to be in better agreement for high *p* values, with significant deviations when p_{model} is low (**Figure 3.2 G**). It also seems very clear that the estimates of *p* obtained by the two linear extrapolation techniques are in close agreement when p_{model} is high, but that for low *p* cases (i.e., $p_{model}<0.2$), the differences between p_{train} and p_{EQ} become more substantial (**Figure 3.2 H**).

Having performed a basic characterization of our model, we then ran simulations in which we systematically varied one parameter while holding the other two constant to observe how synaptic responses might change and how existing estimates of RRP size perform. First, we varied *p* while holding N and R constant (N=1, R=0.01). We chose an RRP size equal to one for simplicity, since this value can correspond to a relative RRP size (not a specific number of vesicles). Significant deviation of estimated RRP size from a value of one indicates an inaccurate estimate of RRP size. We chose a replenishment rate, R, equal to 0.01, which is on the lower end of typical replenishment rates our model estimates for standard recording conditions (room temperature recordings with 100 Hz trains in 2 mM Ca_e). Interestingly, the ability of the RRP_{train}

technique to accurately estimate RRP size is very dependent on the value of *p*; for high *p*, the RRP_{train} technique performs very well, with estimates of RRP size close to one (**Figure 3.3 A**, *p*=0.4 and 0.2), while its ability to accurately estimate RRP size is compromised at lower *p* values (**Figure 3.3 A**, *p*=0.1 and 0.05). When *p*=0.01, RRP_{train}=0.748, and when *p*=0.05, RRP_{train}=0.427. These simulations can be summarized to show the relationship between RRP_{train} estimates of RRP size versus the actual RRP size as dictated by the simulation (**Figure 3.3 B**). These simulations suggest that the RRP_{train} technique can give excellent estimates of RRP size for synapses with high *p*. They also suggest that for low *p* synapses (i.e., for *p*<0.1), changes in *p* could manifest as changes in the value of RRP_{train}. This suggests that the RRP_{train} technique can falsely report changes in *p* as changes in RRP for experimental manipulations, and should only be used under relatively high *p* conditions.

The ability of our model to generate a direct estimate of *p* is likely due in large part to the time constant of decay that the exponential fit function in generates. Lower values of *p* would be expected to produce longer time constants, and higher values of *p* would produce shorter time constants. This is illustrated in **Figure 3.4 A**, depicting the postsynaptic responses in an MNTB cell in response to a 100 Hz train under low Ca_e and standard Ca_e conditions. Under low Ca_e conditions, where *p* is considerably reduced from its control value (see **Figure 2.3**), the time constant of decay of EPSC amplitudes is higher than the time constant seen under standard Ca_e conditions. We decided to determine whether the decay of EPSC amplitudes alone could be used to accurately estimate *p*. Using the equation $p=1-e^{-(1/\tau)}$, where τ equals the time constant of decay of EPSC amplitudes (expressed as the number of stimuli, not time), we generated an estimate of *p* that we will call p_τ. Plots of p_τ versus the two established linear extrapolation methods of estimating *p* show that there is very good agreement between p_τ and p_{train} (red circles, **Figure 3.4**

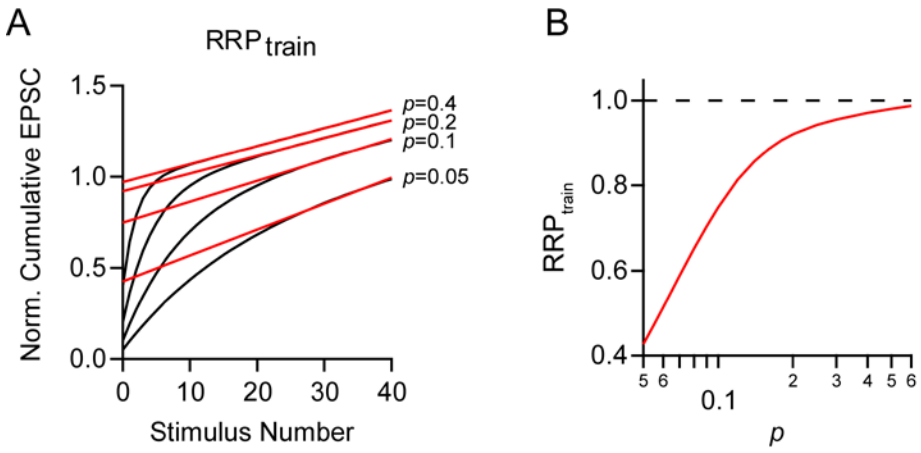

Figure 3.3. Effect of changing *p* on the estimated RRP size. A Simulations were performed using the variables N, *p*, and R values of {1, x, 0.01}. The values of *p* shown are (a) 0.4, (b) 0.2, (c) 0.1, and (d) 0.05. The last fifteen points of cumulative EPSCs were fit with a line and back-extrapolated to x=0 to measure RRP_{train}. The cumulative EPSCs resulting from the same simulated train frequencies are plotted with pool size measurements performed using the RRP_{train} technique. **B** The measured pool size as a function of frequency for RRP_{train} (red). The actual pool size is equal to one (dotted black line).

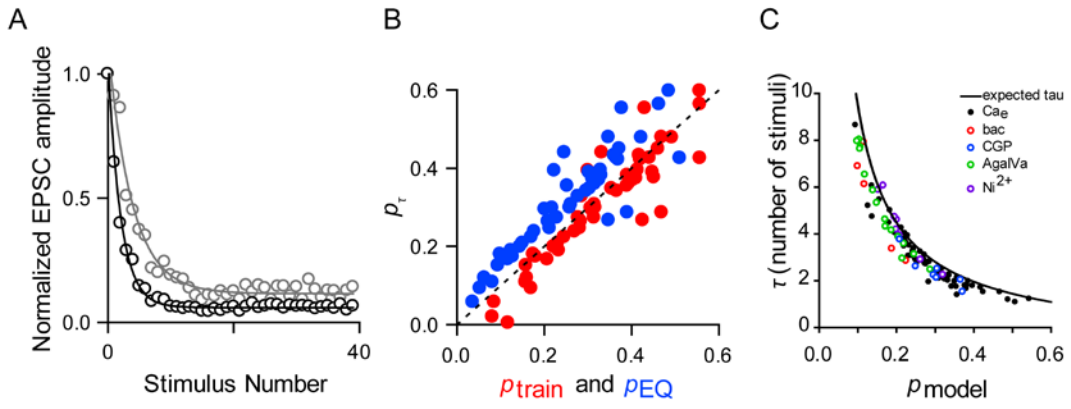

Figure 3.4. Direct estimation of *p* from decay time constant of EPSC amplitudes. A Plot of EPSC amplitudes versus stimulus number for 100 Hz stimulus trains in 1.5 mM external calcium (gray circles) and 2 mM external calcium (black circles) with single exponential curve fits. Lower external calcium, and consequently lower values of *p*, leads to slower depletion of the RRP. **B** Comparison of *p* estimates from the time constant of decay of EPSC amplitudes using the equation $p=1-e^{-(1/\tau)}$) versus indirect linear extrapolation methods of estimating *p*. p_τ versus p_{train} (red), p_τ versus p_{EQ} (blue), and the unity line (dashed black line). **C** Pharmacological manipulations of neurotransmitter release and their effects on EPSC decay time constant and p_{model}. The predicted τ for a given value of *p* is shown (solid black line) with data taken in various external calcium concentrations (black circles), the $GABA_B$ receptor agonist baclofen (100 µM, red open circles), the $GABA_B$ receptor antagonist CGP 55845 (20 µM, blue open circles), nickel (100 µM open purple circles), and ω-agatoxin IVA (50 nM, open green circles).

B) as well as between p_τ and p_{EQ} (blue circles), with slightly better agreement observed for p_{train}. This suggests that the time course of decay of EPSCs provides enough information to give a reasonable estimate of *p*. We also see excellent agreement between the expected time constant of EPSC amplitude decay (τ) for a given value of *p* (solid black line, **Figure 3.4 C**) with p_{model} calculated for a variety of pharmacological manipulations (much of room temperature data presented in **Chapter 2**; **Figure 3.4 C**). This suggests that for a wide variety of *p* values, p_{model} is probably mostly generated from the time course of decay of EPSC amplitudes.

We then decided to systematically vary the replenishment rate, R, to determine how relative changes in replenishment might affect estimates of RRP size. The size of the RRP (N) and the probability of release (*p*) were held constant (N=1, *p*=0.2). An RRP size of one was again chosen for simplicity, as in the previous figure. The probability of release, *p*, was set to 0.2, since this is a typical value for the calyx of Held under standard recording conditions and sufficiently high to provide reliable estimates of RRP size (**Figure 3.3** and **Figure 3.4**). For realistic replenishment rates at 100 Hz ($R \approx 0.02$-0.03), both the RRP_{train} technique and RRP_{EQ} technique provide good assessments of true RRP size (**Figure 3.5 A, B**). Significant increases in replenishment rate are not well-tolerated by the RRP_{train} technique; when R=0.1, RRP_{train}=0.530, although N=1 (**Figure 3.5 A**). In contrast, the RRP_{EQ} technique appears to tolerate high levels of replenishment relatively well, although RRP_{EQ} does overestimate the RRP size for high rates of replenishment (for R=0.1, RRP_{EQ}=1.231). These findings are summarized in **Figure 3.5 C**.

A determinant of synaptic responses to high-frequency activity that is not directly accounted for in the current version of this model is the frequency of the stimulus train. At the

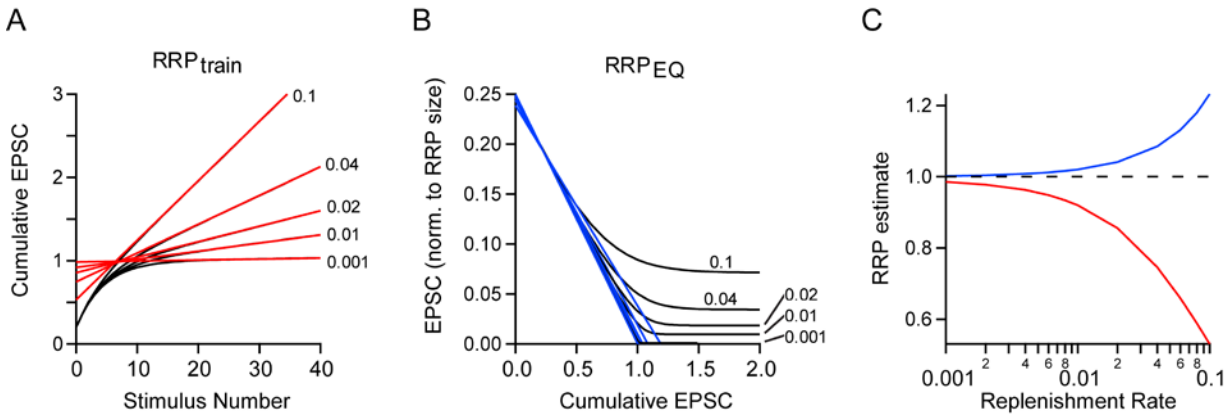

Figure 3.5. Effect of changing replenishment rate of the estimated RRP size. A Simulations were performed using the variables N, *p*, and R values of {1, 0.2, x}, where x varies from 0.001 to 0.1. The last fifteen points of cumulative EPSCs were fit with a line and backextrapolated to x=0 to measure RRP_{train}. **B** Plots of the simulated EPSC amplitude versus cumulative EPSC are shown. Linear fits to the first four points of each curve are extended to y=0, indicating the value of RRP_{EQ}. **C** The measured pool size as a function of replenishment rate for two methods of RRP estimation: RRP_{train} (red) and RRP_{EQ} (blue). The actual RRP size is equal to one (dotted black line).

calyx of Held, it is appreciated that trains of at least 100 Hz and perhaps up to 300 Hz are required to provide reliable estimates of RRP size, with observations of larger estimated RRP size by the RRP_{train} technique at higher frequencies (Taschenberger and von Gersdorff, 2000). At other synapses, lower frequencies are typically considered adequate to deplete and measure the RRP (Liu et al., 2014; Stevens and Wesseling, 1998; Wesseling and Lo, 2002). Here, we assess the frequency-dependence of RRP estimates. We performed postsynaptic voltage-clamp recordings from MNTB cells and stimulated the presynaptic axon with stimulus trains of 100 Hz and 200 Hz. The example cell shown in **Figure 3.6 A** shows that the initial EPSC is of similar amplitude but that the steady state EPSC amplitude late in the stimulus train is somewhat larger for slower trains. This is what would be expected, since the longer interstimulus interval for the slower 100 Hz train allows for more replenishment of the RRP, and thus a larger resulting EPSC upon stimulation. The cumulative EPSCs shown in **Figure 3.6 B** for the same cell reveal that the value of RRP_{train} is larger for the 200 Hz train (black) than for the 100 Hz train (gray). The summary data shown in **Figure 3.6 C** (n=4) shows that RRP_{train} is consistently higher for 200 Hz trains than for 100 Hz trains. Consequently, p_{train} is lower for 200 Hz trains than for 100 Hz trains, since $p_{train}=EPSC_0/ RRP_{train}$. This is an interesting observation—is the effective size of the RRP truly frequency-dependent? To explore this question, we studied the time course of recovery from depression at the calyx of Held synapse to inform simulations of synaptic transmission at different stimulus frequencies.

We ran our model on a large dataset (n=27) of postsynaptic recordings during stimulation at 100 Hz performed in standard Ca_e (2 mM) to determine the average replenishment rate under control conditions. The average replenishment rate was 0.0295 ± 0.0014 (mean $\pm$SEM; data not shown).

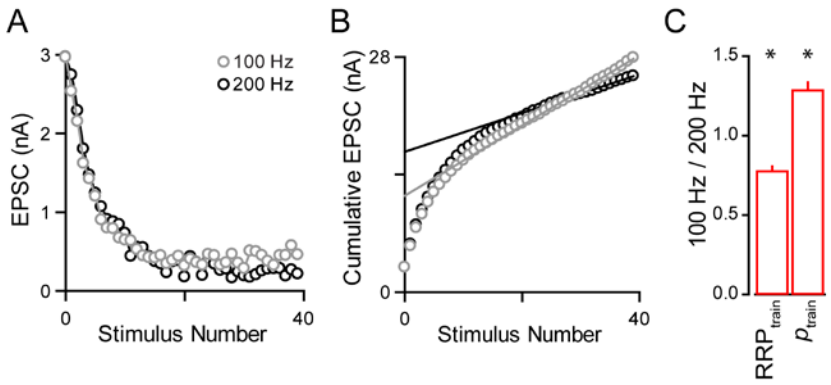

Figure 3.6. Apparent change in RRP_{train} with different stimulus frequencies. A Example of postsynaptic responses from an MNTB cell stimulated with a 100 Hz stimulus train (gray open circles) and a 200 Hz stimulus train (black open circles) plotted versus stimulus number. **B** Cumulative EPSCs plotted for the same example cell shown in A. RRP_{train} is larger for the 200 Hz train (black) than for the 100 Hz train (gray). **C** Summary data showing the average change in p_{train} and RRP_{train} in cells stimulated with a 100 Hz train as compared to a 200 Hz train. p_{train} is larger during a 100 Hz train than for a 200 Hz train, and RRP_{train} is smaller at 100 Hz than at 200 Hz.

We reasoned that this replenishment rate, plus information on the time course of recovery from depression, would allow us to estimate replenishment rates for frequencies higher and lower than 100 Hz. In a separate set of experiments, we used a depleting train of action potentials (at least 25 action potentials) to study recovery from depression. Similar data was shown in **Figure 2.2 E**, but here we include more data points for short Δt intervals. These data was collected by delivering a long train of stimuli at 100 Hz and, after 25 stimuli, altering the interstimulus interval for every tenth stimulus (**Figure 3.7 A**). This larger data set was well-fit by a double exponential function of the form $EPSC(\Delta t)=A-Be^{(-\Delta t/\tau 1)}-Ce^{(-\Delta t/\tau 2)}$, with $\{A, B, \tau_1, C, \tau_2\}$ equal to {1, 0.246, 185 ms, 0.697, 2900 ms}, which conforms to the data at short time intervals (**Figure 3.7 B**) and longer time intervals (**Figure 3.7 C**) quite well.

We simulated postsynaptic responses to stimulus trains of different frequencies by scaling the average replenishment rate at 100 Hz (R=0.0295) with the double-exponential fit shown in **Figure 3.7 C**. This assumes that recovery from depression at different frequencies has similar kinetics, which may not be the case, since the concentration and spatial extent of calcium that accumulates in the presynaptic terminal during activity may be frequency-dependent. Future experiments will be conducted to determine whether the time course of recovery from depression is frequency-dependent.Here, we make a preliminary attempt to determine whether the effective size of the RRP is frequency-dependent, or whether changing the frequency of stimulation might lead to inaccurate estimates of effective RRP size. We simulated responses to stimulus trains of varying frequencies. **Figure 3.8 A** shows simulated EPSC amplitudes plotted for N, *p*, and R of {1, 0.2, x} as a function of time. To mimic the effects of varying frequency in our simulations, we used the double-exponential fit from **Figure 3.7 B, C** to estimate the amount of replenishment that would occur at between stimuli at 20 Hz (interstimulus interval, or ISI=50

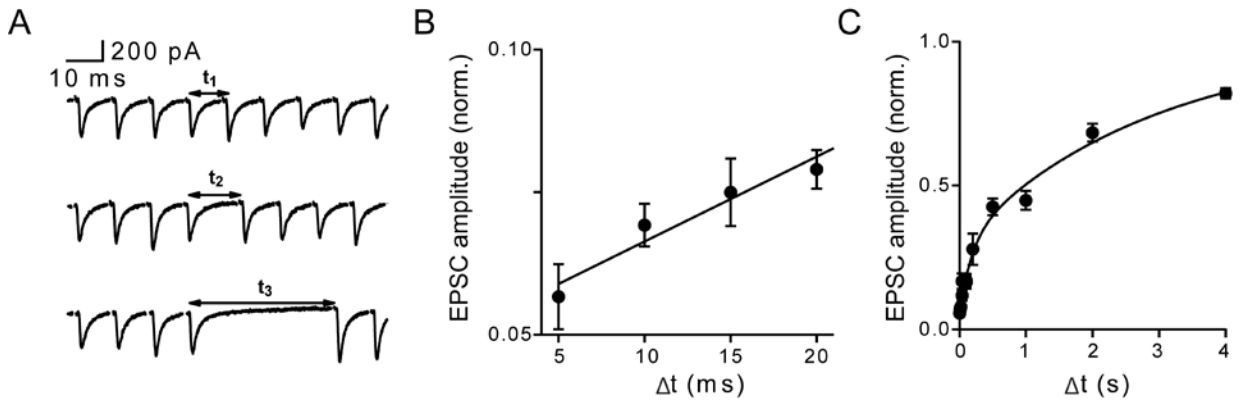

Figure 3.7. Time course of recovery from depression. A Three example traces showing the experimental paradigm used to determine the extent of calcium-dependent recovery from depression for short Δt values (≤40 ms), with t_1 = 10 ms, t_2 = 15 ms, and t_3 = 40 ms. 25 stimuli are delivered at 100 Hz to deplete the RRP, after which every tenth interstimulus interval is varied from 10 ms to assess the extent of recovery. The amplitude of the resulting EPSC reflects the extent of replenishment to the RRP, or recovery from depression, that occurs. **B** Recovery of EPSC amplitude during trains for short time intervals. EPSC amplitudes were normalized to the first EPSC in the stimulus train. Summarized data for experiments performed as described in A. A double exponential fit is shown (*black line*) $y=A + 0.246e^{(185\ ms)} + 0.697e^{(2900\ ms)}$. **C** Recovery of EPSC during trains for longer Δt values with the same double exponential fit. For Δt>40 ms, the RRP was depleted with a standard 100 Hz stimulus train for 40 pulses, after which a single stimulus was delivered to assess recovery from depression.

Figure 3.8. Effect of changing stimulus frequency on the estimated RRP size. Simulations were performed using the variables N, *p*, and R values of {1, 0.2, x }. x was scaled to simulate firing at different frequencies, and was determined from our characterization of recovery from depression (see text for details). The frequencies shown are 20 Hz, 40 Hz, 100 Hz, and 300 Hz. **A** EPSC amplitude (normalized to RRP size) versus time shown for simulations at different frequencies. **B** Plots of EPSC size (norm. to RRP size) versus stimulus number. **C** The last fifteen points of cumulative EPSCs were fit with a line and backextrapolated to x=0 to measure RRP_{train}. **D** Magnified view of the plot in C. **E** Plots of the simulated EPSC amplitude versus cumulative EPSC are shown. Linear fits to the first four points of each curve are extended to y=0, indicating the value of RRP_{EQ}. **F** The measured pool size as a function of frequency for two methods of RRP estimation: RRP_{train} (red) and RRP_{EQ} (blue). The actual RRP size is equal to one (dashed black line).

Figure 3.8 (Continued)

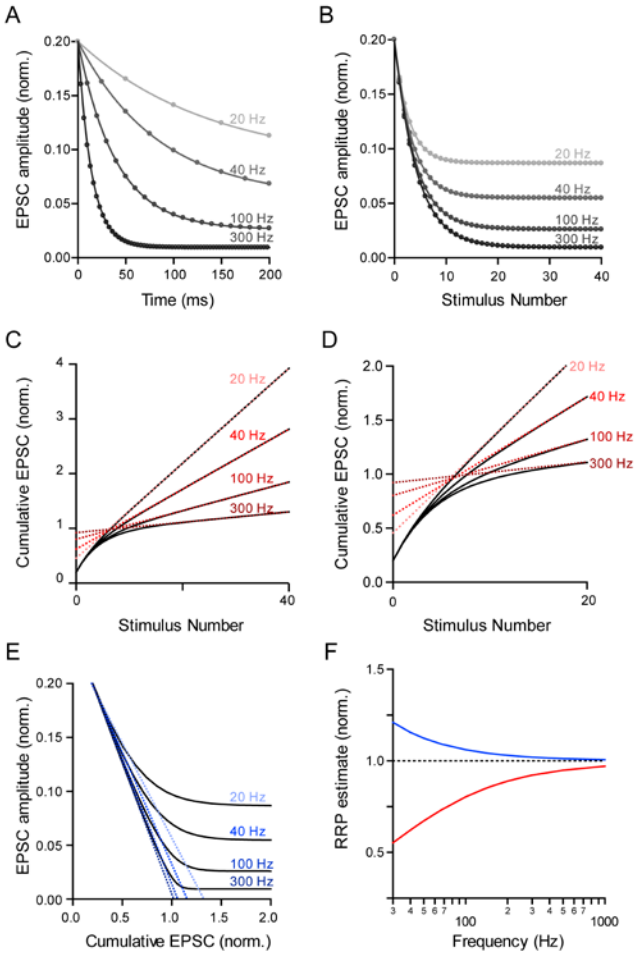

ms), 40 Hz (ISI=25 ms), 100 Hz (ISI=10 ms), and 300 Hz (ISI=3.3 ms) stimulation (for details, see **Materials and Methods**). Higher-frequency stimulus trains lead to rapid decay of EPSC amplitudes, while slower stimulus trains lead to more slowly-decaying EPSC amplitudes. Additionally, the steady-state EPSC amplitude is much larger for slower stimulus trains than for fast stimulus trains (**Figure 3.8 B**). Interestingly, for simulations in which only stimulus frequency is changed, and not the RRP size, *p*, or replenishment rate per unit of time, there are substantial differences in the value of RRP_{train}, with low-frequency trains leading to considerable underestimates of RRP size (**Figure 3.8 C, D**). Estimates of RRP size made with the RRP_{EQ} technique are also affected by stimulus frequency, with low-frequency trains leading to overestimates of RRP size (**Figure 3.8 E**). Summary plots of estimated RRP size versus stimulus frequency are shown in **Figure 3.8 F**. At 100 Hz, RRP_{train} underestimates the RRP size by approximately 20%, while RRP_{EQ} overestimates the RRP size by only about 6% (RRP_{train}=.803, RRP_{EQ}=1.061). This suggests that under our recording conditions, RRP_{EQ} may provide a much better estimate of RRP size than does RRP_{train}, and that apparent frequency-dependent changes in RRP_{train} may be due to estimation error rather than a true change in RRP size. Higher frequency trains provide more accurate estimates of RRP size (300 Hz: RRP_{train}=0.921, RRP_{EQ}=1.020). It is quite apparent that sufficiently high stimulus frequencies must be used to accurately assess the size of the RRP, and that the RRP_{EQ} technique is slightly more resistant to error than the RRP_{train} technique for frequencies typically used at the calyx of Held synapse (100-300 Hz).

The summary of simulations shown in **Figure 3.8 F** was performed with realistic values of *p* (*p*=0.2) and R (R=0.0295) for 100 Hz stimulus trains delivered at room temperature. First, we performed the same simulations except with both higher and lower values of *p* (**Figure 3.9**

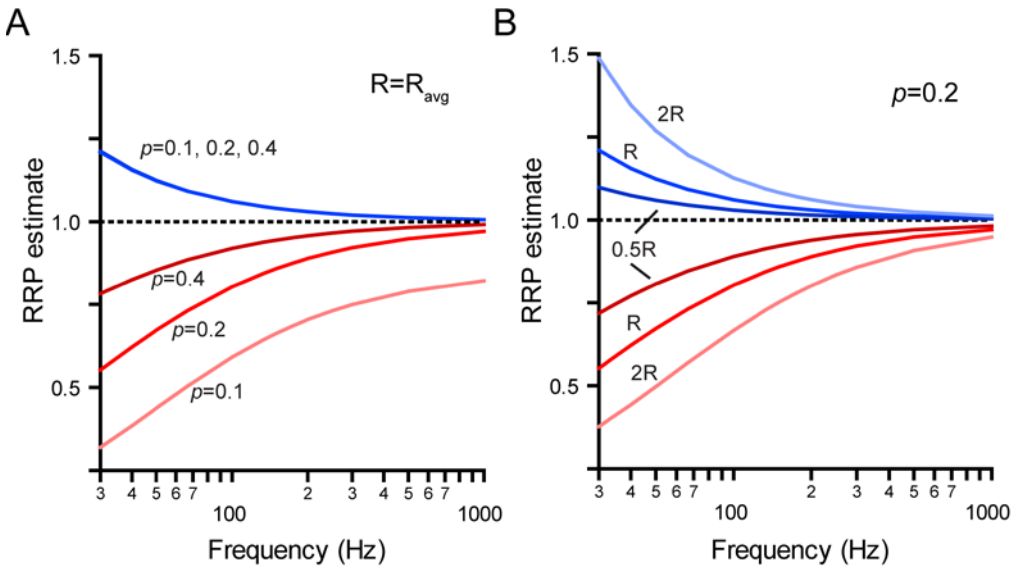

Figure 3.9. Effect of varying *p* and R on estimated RRP size. A Effect of changing *p* on linear extrapolation estimates of RRP size. Simulations were performed with {N, *p*, R}={1, x, 0.00295} with x=0.1, 0.2, and 0.4. Linear extrapolation techniques were then used to estimate the RRP size from the simulated data. RRP_{train} was very sensitive to changes in *p*, with RRP_{train} values becoming much lower than the actual RRP size (*p*=0.1, light red; *p*=0.2, red; and *p*=0.4, dark red). RRP_{EQ} for the same values of *p* were very similar and overlap on this graph (p_{EQ} for *p*=0.1, 0.2, and 0.4 shown in blue). **B** Effect of changing R on linear extrapolation measures of RRP size. Simulations were performed with {N, *p*, R}={1, 0.2, x} with x=0.0148, 0.0295, and 0.0590. Linear extrapolation techniques were then used to estimate the RRP size from the simulated data. RRP_{train} was very sensitive to changes in R, with RRP_{train} values becoming much lower than the actual RRP size for high replenishment rates. We halved (labeled 0.5 R) and doubled (labeled 2R) the average value of R for simulations (0.5R: R=0.0148, dark red; R: R=0.0295, red; and 2R: R=0.0590, light red). RRP_{EQ} for the same values of R were also very different, with high replenishment leading to overestimates of RRP size (0.5R: R=0.0148, dark blue; R: R=0.0295, blue; and 2R: R=0.0590, light blue).

A). Here, we chose p=0.1, 0.2, and 0.4. The size of the RRP and replenishment rate per unit time were kept constant (N=1, R=0.0295). Interestingly, the RRP_{EQ} technique is very resistant to changes in p in our simulated data. The values of RRP_{EQ} calculated for various p values are very similar (p=0.1, RRP_{EQ}=1.060; p=0.2, RRP_{EQ}=1.061; and p=0.4, RRP_{EQ}=1.061). In stark contrast, changing p has a considerable impact on RRP_{train} estimates of RRP size. For p=0.4, RRP_{train}=0.920, but for p=0.2, RRP_{train}=0.803 and for p=0.1, RRP_{train}=0.591. Our model does not account for facilitation, which is a relatively minor factor at the calyx of Held under normal conditions, but does begin to play a substantial role under low p conditions, such as in the presence of a VGCC antagonist or in reduced Ca_e. Facilitation is a complicating factor, especially for the RRP_{EQ} method. This is because the RRP_{EQ} method depends exclusively on the amplitudes of the first few EPSCs in response to a stimulus train, and these responses are the ones most affected by facilitation. As a result, RRP_{EQ} is likely to not provide as much of an advantage under low p conditions as **Figure 3.9 A** indicates. Future experiments will be conducted to determine the time course and extent of facilitation under control conditions and under conditions of low p (i.e., in low Ca_e) in an attempt to incorporate facilitation into a future version of this model.

We also wanted to assess the role of changing stimulus frequency under conditions of reduced or enhanced replenishment of the RRP. We halved and doubled the replenishment rate from our experimentally-obtained value (R=0.0295 ±0.0014) and performed simulations and estimations of RRP size with both linear extrapolation techniques (**Figure 3.9 B**). We find that both techniques are sensitive to changes in replenishment, as would be expected from the results shown in **Figure 3.5**. At 100 Hz, doubling the replenishment rate reduces RRP_{train} considerably (R=0.0295, RRP_{train}=0.803, red curve; R=0.0590, RRP_{train}=0.667, light red curve). Halving the

replenishment rate improves the ability of the RRP_{train} method to accurately assess RRP size (R=0.0148, RRP_{train}=0.890, dark red curve). Doubling the replenishment rate increases RRP_{EQ} (R=0.0295, RRP_{EQ}=1.061, blue curve; R=0.059, RRP_{EQ}=1.126, light blue curve), and halving it reduces RRP_{EQ} (R=0.0148, RRP_{train}=1.030, dark blue curve).

In light of these simulations, we analyzed experimental data collected at 100 Hz and 200 Hz with our three techniques. Here, we show the same example cell shown in **Figure 3.6 A, B** with the RRP_{train} technique applied and see a large difference between the RRP estimate at 100 Hz (light red arrow) and 200 Hz (red arrow). We also used the RRP_{EQ} method to estimate RRP size at 100 Hz (**Figure 3.10 B**, light blue arrow) and 200 Hz (**Figure 3.10 B**, blue arrow). We find very little difference in these estimates of RRP size. Finally, we used our model to determine optimal values of N, *p*, and R for the same cell at 100 Hz versus 200 Hz and found that the modeling function was able to fit the data very well (**Figure 3.10 C**), with little difference between RRP size estimates. Our summary data (**Figure 3.10 D**) show that RRP_{train} estimates are smaller at 100 Hz as compared to at 200 Hz (78.0 ± 3.0% of 200 Hz, p-value<0.05) and that p_{train} is consequently increased at 100 Hz as compared to 200 Hz (128.8 ± 5.1% of 200 Hz, p-value<0.05). In contrast, RRP_{EQ} estimates are larger at 100 Hz than at 200 Hz (107.2 ± 6.9% of 200 Hz, p-value>0.05) and p_{EQ} estimates are smaller at 100 Hz than at 200 Hz (0.84 ± 2.0% of 200 Hz, p-value>0.05), although these differences are not statistically significant. However, the modeling function suggests a third possibility—that in fact the size of the RRP is not significantly changed (96.9 ± 6.3% of 200 Hz), nor is *p* (104.4 ± 9.1% of 200 Hz), but rather that the replenishment rate R_{model} per interstimulus interval is just increased for slower frequencies (276.4 ± 13.5% of 200 Hz, p<0.05).

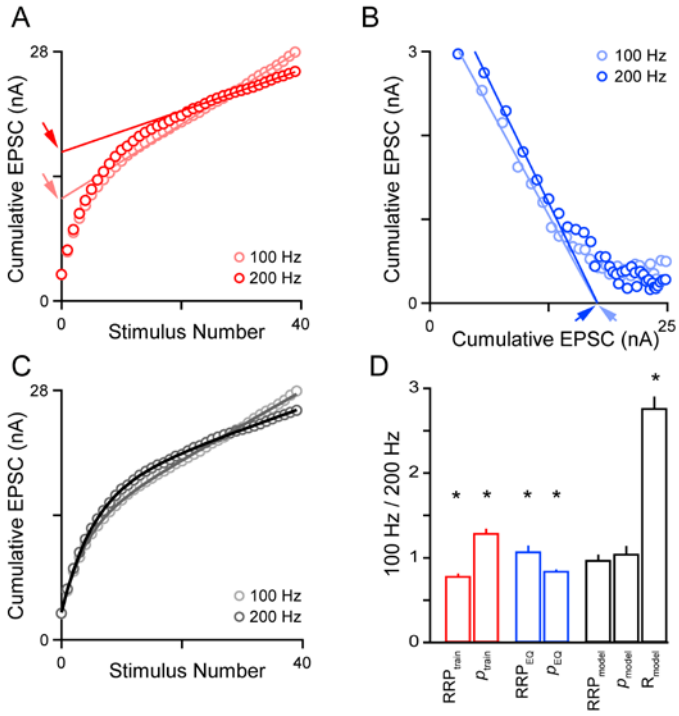

Figure 3.10. Apparent frequency dependence of RRP_{train} may be due to differences in replenishment per interstimulus interval. A Cumulative EPSC plotted for an example cell show that RRP_{train} is larger for the 200 Hz train (red arrow) than for the 100 Hz train (light red arrow). **B** EPSC amplitude versus cumulative EPSC shows that RRP_{EQ} is very similar for 100 Hz (light blue arrow) and 200 Hz (blue arrow) stimulus trains in an example cell. **C** Cumulative EPSCs with model fits plotted for 100 Hz (gray line) and 200 Hz (black line) can be used to estimate RRP size. **D** Summary data for all three techniques of measuring RRP size (n=4).

Discussion

In this chapter, we explore methods for estimating *p* and effective RRP size at the calyx of Held synapse, with the future goal of generalizing the lessons learned here to other synapses.

The original purpose of this model was for use as a reality check for the types of experiments performed in **Chapter 2**. Based on our experimental observations, we suspected that the RRP_{train} technique is inaccurate under certain conditions, such as low *p* or low stimulus frequency, but did not have a quantitative way to determine the conditions under which the technique would be accurate or inaccurate. To strengthen our confidence in our interpretation of the results, we applied the technique of Elmqvist and Quastel (Elmqvist and Quastel, 1965), which makes very different assumptions than the RRP_{train} technique, to our data, and came up with similar results. We then developed a third method of estimating RRP size and *p*, which we called the corrected RRP_{train} technique, which sought to correct for the availability of release sites in determining the rate of replenishment of the RRP. The agreement of all three methods convinced us that the calcium-dependence of RRP size that we observed was indeed real and not an artifact of our estimation techniques. Aware of the limitations of each technique (**Table 3.1**), we decided to develop and implement a simple model of postsynaptic responses to high-frequency synaptic transmission that could help characterize the strengths and weaknesses of each of the three extrapolation techniques, and perhaps also be used as an improved method of estimating *p* and RRP size.

We first compared the model (**Figure 3.1** and **Equations 3.2-3.10**) to the train and EQ techniques, and found that it shows excellent agreement with these two extrapolation-based measures under most conditions, with deviations apparent in low *p* conditions (**Figure 3.2**).

Interestingly, the fact that RRP_{model} tends to lie in between RRP_{train} and RRP_{EQ} may indicate that it is a fairly accurate estimate of RRP size. As previously discussed (**Discussion**, **Chapter 2**), the RRP_{train} method assumes a maximal replenishment rate throughout the stimulus train, which likely makes it an underestimate of true RRP size, while the RRP_{EQ} method assumes no replenishment, which likely makes it an overestimate.

We also found that the values of p_{model} obtained in varying Ca_e were typically in between p_{train} and p_{EQ}. This did not necessarily have to be the case, since the model provides a direct estimate of *p*, unlike both linear extrapolation techniques. Again, we previously suggested that p_{train} is likely an overestimate of *p* and that conversely p_{EQ} is likely an underestimate, which gives us renewed confidence in the accuracy of p_{model}. Based on the equations used to define our model, we expected that the decay of EPSC amplitudes during a stimulus train were primarily responsible for the model's estimation of *p*. We found that the decay time constant of EPSC amplitudes alone could provide a very good estimate of *p* that agrees very well with values generated by linear extrapolation techniques, and that p_τ and p_{model} were very similar (**Figure 3.4**). The ability of our model to provide a direct estimate of *p* is a particular strength of the model, since it indicates that accurate estimation of *p* is possible even if perfect depletion of the RRP cannot be achieved with AP stimuli.

Another particular strength of our model is its direct estimation of RRP replenishment. We drew inspiration from other approaches (Wesseling and Lo, 2002) at other synapses which found that the replenishment rate of the RRP could be determined using the relative difference between the amplitudes of the first EPSC in response to a stimulus train ($EPSC_0$) and the steady-state EPSC amplitude (EPSCss) after depletion of the RRP with high-frequency stimulation. Use

of our model to characterize neuromodulators or genetic manipulations that might affect the rate of RRP replenishment could uncover interesting mechanisms by which synaptic transmission is regulated. Examples of potential candidates to test our ability to detect altered replenishment could involve genetic manipulation of synaptotagmin 7 (Syt7), which has been suggested by others to affect replenishment of the RRP (Liu et al., 2014), or to use pharmacological inhibition of calmodulin (CaM), which has also been shown to be important for replenishment of the RRP (Sakaba and Neher, 2001a).

Simulations and their implications for linear extrapolation methods

We performed simulations according to our three-parameter model of release to validate and test the limits of the train and EQ methods. Strikingly, the train method is very sensitive to low p; according to our simulations, when $p<0.1$ the train technique can underestimate the size of the RRP by approximately 25% (**Figure 3.3**). This is the case even for a replenishment rate that is on the lower end of normal at the calyx of Held; when replenishment of the RRP is increased, RRP_{train} will underestimate the true RRP size even more significantly.

We also find that linear extrapolation techniques are sensitive to the rate of replenishment, and that high rates of replenishment can lead to inaccurate assessments of RRP size. Under our standard recording conditions, the replenishment rate is fairly low ($R=0.0295 \pm 0.0014$), which suggests that RRP_{EQ} is an accurate estimate of RRP size and that RRP_{train} is still a fairly accurate estimate of RRP size. However, recordings performed at near-physiological

temperature (data not shown) exhibit much higher rates of replenishment, suggesting that special care needs to be taken to accurately assess RRP size under these conditions.

An important caveat to interpreting the results of these simulations is that we have not included facilitation in our model of neurotransmitter release. Facilitation does occur at this synapse, and while it is not prominent under standard recording conditions, can affect EPSC amplitudes more substantially under low *p* conditions. Many other models of neurotransmitter release have incorporated a parameter to model facilitation (Varela et al., 1999), while other studies of strongly depressing synapses have chosen to omit facilitation because a simpler model is sufficient for their purposes (Abbott et al., 1997; Kusano and Landau, 1975; Varela et al., 1999). We feel that the current version of our model describes release at the calyx of Held quite well under standard recording conditions, but that in low *p* conditions (such as in the presence of a neuromodulator or low Ca_e) facilitation ought to be included in the model. Future experiments will be conducted in which postsynaptic responses to repeated stimulus trains in low Ca_e will be recorded and analyzed to determine the average time course and magnitude of facilitation at this synapse. We hope that by including facilitation in our model, it can be applied to other synapses with lower *p* and more substantial facilitation.

Chapter 4

Regulation of Initial Release Probability by Tonic Activation of Presynaptic G-protein Coupled Receptors

Abstract

A critical characteristic of a given synapse is its initial synaptic strength. The parallel fiber to Purkinje cell (PF-PC) synapse has a low *p*, with marked paired-pulse facilitation. This work shows that antagonizing several presynaptic G protein-coupled receptors (GPCRs) significantly increases the efficacy of the PF-PC synapse. This suggests that basal GPCR signaling is important for setting its low initial synaptic strength. In this chapter, we determine which GPCRs set initial synaptic strength under basal conditions at this synapse. We find that inhibition of adenosine A1 receptors, endocannabinoid type 1 (CB1) receptors, and metabotropic GABA ($GABA_B$) receptors individually play a small role in regulating basal synaptic release properties. However, all three together play a significant role in limiting neurotransmitter release, as revealed by simultaneous pharmacological blockade of A1Rs, CB1Rs, and $GABA_B$Rs. These GPCRs also mediate basal release properties at near-physiological temperature. When A1Rs, CB1Rs, and $GABA_B$Rs are inhibited, EPSC amplitudes increase by more than two-fold, with minimal effects on the paired-pulse ratio. We hypothesize that these GPCRs may modulate synaptic transmission by controlling presynaptic influx. In bulk calcium imaging experiments, we find that simultaneous pharmacological blockade of A1Rs, CB1Rs, and $GABA_B$Rs significantly increases presynaptic influx at room temperature and elevated temperature. Inhibition of individual GPCRs (A1Rs, CB1Rs, or $GABA_B$Rs) leads to smaller effects on calcium influx. We conclude that multiple GPCRs are important for regulating basal neurotransmitter release properties at the PF-PC synapse, which may have physiological relevance for information flow through the cerebellar cortex.

Introduction

Crucial to our understanding of synaptic function is the basal synaptic strength, which corresponds to the number and size of presynaptic connections onto a postsynaptic target neuron. Much is known about the mechanisms that change synaptic strength, but much less is known about the mechanisms that set and maintain the initial strength of a synapse. Initial synaptic strength is fundamental to low-frequency synaptic transmission. Factors such as the density and distribution of presynaptic calcium channels, calcium sensitivity of the release machinery, and various presynaptic signaling cascades are all presynaptic characteristics of synapses thought to influence initial synaptic strength. However, it is not understood which of these factors are most important at specific synapses and how these factors may interact to set synaptic strength. In this proposal, I will address one question regarding the regulation of synaptic strength: is tonic presynaptic inhibition important for setting basal release properties?

Here, I study the regulation of basal neurotransmitter release at the cerebellar parallel fiber to Purkinje cell (PF-PC) synapse. This synapse offers important advantages, including its well-characterized anatomy and electrophysiology. Additionally, presynaptic inhibition is known to occur through four $G_{i/o}$–coupled receptors at the PF-PC synapse: adenosine A1 receptors, cannabinoid type 1 (CB1) receptors, γ-aminobutryic acid class B ($GABA_B$) receptors, and type 4 metabotropic glutamate (mGlu4) receptors. Applying an agonist that activates these receptor types reduces synaptic strength. This can occur by various presynaptic mechanisms.

A1 receptors. A1Rs are present in PF boutons, where they are known to mediate presynaptic inhibition (Dittman and Regehr, 1996). They are activated by adenosine, which may accumulate in the synaptic cleft by degradation of adenosine triphosphate (ATP) or by active

release of adenosine. A1 receptor agonists inhibit presynaptic calcium influx, likely through direct modulation of presynaptic calcium channels, at synapses including the PF-PC synapse (Dittman and Regehr, 1996; Dolphin et al., 1986). Additionally, modulation of presynaptic potassium channels and the adenylyl cyclase (AC)/protein kinase A (PKA) pathway have been implicated in A1R signaling (van Calker et al., 1979; Jeon et al., 2003; Londos et al., 1980; Yum et al., 2008)**,** as has activation of p38 mitogen-activated protein kinase (MAPK) (Brust et al., 2006).

CB1 receptors. CB1 receptors are activated by endocannabinoids, which usually function as retrograde messengers. It has been proposed that the CB1R inhibits release by direct modulation of calcium channels or by modulation of presynaptic potassium currents. At the PF-PC synapse, a CB1 agonist causes a decrease in presynaptic calcium influx that can fully explain the observed depression of postsynaptic currents. An indirect effect of the potassium current on modulating calcium influx at the PF-PC synapse has been proposed (Daniel and Crepel, 2001; Daniel et al., 2004). However, this seems unlikely because application of a CB1 agonist (1) does not affect fiber volley waveform or velocity (Brown, Safo, and Regehr 2004; Lévénés et al. 1998; Takahashi and Linden 2000) (2) does not change the timecourse of presynaptic calcium influx (Brown et al., 2004), and (3) differentially affects calcium influx through different calcium channel types (Brown et al., 2004).

$GABA_B$ receptors. $GABA_B$ receptors also modulate presynaptic calcium influx to inhibit release at many synapses, including the PF-PC synapse (Takahashi, Kajikawa, and Tsujimoto 1998; Dittman and Regehr 1996). While GABA release does not occur at the PF-PC synapse, GABA released by interneurons during elevated activity can spill over to affect neighboring

excitatory synapses (Dittman and Regehr, 1997; Isaacson, 1998). $GABA_B$ receptors are negatively coupled to adenylyl cyclase (AC) at many central synapses (Kamatchi and Ticku, 1990; Knight and Bowery, 1996) reduce synaptic strength by downregulating production of cyclic AMP (cAMP) by AC. $GABA_B$Rs also can modulate presynaptic calcium channels to reduce calcium influx (Dittman and Regehr, 1996). Inhibition by $GABA_B$ receptors has been suggested to be modulated by protein kinase C because activation of PKC suppresses agonist-induced presynaptic inhibition (Dutar and Nicoll, 1988; Kubota et al., 2003; Taniyama et al., 1992). A clear mechanism for modulation of signaling through PKC has not yet been elucidated.

mGlu4 receptors. Metabotropic glutamate receptors are found at many presynaptic terminals (Anwyl, 1999), and have been shown to depress vesicular release by activating presynaptic potassium channels and to facilitate release by increasing action potential-evoked release of intracellular calcium from stores (Cochilla and Alford, 1998). Specifically, mGlu4 receptors are present at PF boutons (Kinoshita et al., 1996; Mateos et al., 1998), and activation of these receptors has been shown to decrease synaptic strength (Pekhletski et al., 1996). mGlu4 receotirsactivation reduces action potential-induced presynaptic calcium influx at PF presynaptic terminals (Daniel and Crepel, 2001), and it has been suggested that mGlu4 receptors may indirectly inhibit voltage-gated calcium channels by activating 4AP-sensitive presynaptic K^+ channels in PF boutons (Daniel and Crepel, 2001). mGlu4 receptor activation also inhibits AC (Knöpfel and Grandes, 2002).

Ligand-dependent vs. ligand-independent GPCR activation

In most cases, presynaptic inhibition by adenosine, endocannabinoids, GABA, and glutamate have been studied by application of agonists to increase signaling of presynaptic receptors. A less-explored phenomenon is tonic presynaptic inhibition by GPCRs under basal conditions. There are two mechanisms by which persistent GPCR signaling might occur, one ligand-dependent and the other ligand-independent. Ligand-dependent signaling occurs by persistent transmitter release and/or slow clearance of transmitter from the synaptic cleft. Tonic activation of A1Rs has not been reported at the PF-PC synapse, but it has been reported in the hippocampus at the CA3-CA1 synapse (Wu and Saggau, 1994). Tonic inhibition of granule cells by GABA release has been studied by several groups (Brickley et al., 1996; Rossi et al., 2003), although these studies only report tonic inhibition through ionotropic $GABA_A$ receptors. Persistent presynaptic inhibition via $GABA_B$ receptors has been demonstrated at synapses between granule cells and inhibitory interneurons (Mapelli et al., 2009), but not at PF-PC synapses. Finally, tonic activation of CB1Rs by persistent endocannabinoid release has been demonstrated at inhibitory synapses in various brain regions (Hentges et al., 2005; Neu et al., 2007; Zhu and Lovinger, 2005).

In contrast, ligand-independent GPCR activity occurs by constitutive GPCR activation. In the classical two-state model, inactive receptors spontaneously undergo a conformational change to transition from the inactive state (R) to the active state (R*). The active state can also be achieved by binding of a partial or full agonist. In either case, the conformational change promotes the dissociation of bound GDP from G-proteins, which increases GPCR signaling (Gilman, 1987; Iiri et al., 1998). Evidence suggests that the two-state model may be too simple

and that there may in fact be differences in the signaling capacities of constitutively-active and agonist-activated GPCRs (Seifert and Wenzel-Seifert, 2002). However, easy ways to distinguish between different active states in living tissue have not been developed. The most common way to distinguish between ligand-dependent and ligand-independent GPCR activation is by comparing the effects of neutral antagonists and inverse agonists. A neutral antagonist, which prevents binding of agonist or inverse agonist to the receptor, causes no change in the conformational state of the receptor. In contrast, inverse agonists can reduce GPCR signaling by two mechanisms: prevention of agonist binding and stabilization of the inactive R state of the GPCR. Together, inverse agonists and neutral antagonists can be used to distinguish between agonist-induced and constitutive signaling in basal GPCR activity. If tonic release of ligand is responsible for GPCR activation, then both a neutral antagonist and inverse agonist will prevent signaling. This would manifest at the PF-PC synapse as an increase in neurotransmitter release with either type of pharmacological agent. However, a neutral antagonist can only block tonic release, since true neutral antagonists do not affect the conformational state of the receptor to which they bind. Because inverse agonists block agonist binding, many inverse agonists have been treated as neutral antagonists (Seifert and Wenzel-Seifert, 2002). Ideally, studies of tonic GPCR signaling should differentiate between constitutive and agonist-induced activity by using properly classified pharmacological tools.

Mechanisms by which presynaptic inhibition regulates neurotransmitter release

Once activated, GPCRs can modulate the presynaptic cell in several ways to reduce neurotransmitter release. At many synapses, G-protein βγ subunits inhibit vesicle release. This

can occur by two main mechanisms, one calcium-dependent and the other calcium-independent. The calcium-dependent mechanism is well-characterized and can be mediated by many types of neuromodulator-activated GPCRs. Interestingly, channel modulation occurs through a direct action of free Gβγ dimers on voltage-gated calcium channels, with the identity of the βγ subunits being important for modulation selectivity of specific channel types (García et al., 1998; Herlitze et al., 1996; Ikeda, 1996; Ruiz-Velasco and Ikeda, 2000; Zhou et al., 2000)**.** Modulation of presynaptic calcium currents by GPCRs has been demonstrated at the PF-PC synapse, where activation of $G_{i/o}$-coupled GPCRs modulates Ca_v2 calcium channels in presynaptic boutons to reduce calcium influx (Brown et al., 2004; Dittman and Regehr, 1996; Kreitzer and Regehr, 2001). The precise site of modulation is unknown, although the N terminus of the $Ca_v\alpha1$ subunit and possibly the I-II loop are important for GPCR-mediated inhibition (Agler et al., 2005; Page et al., 1997, 1998). Because of the exponential calcium dependence of vesicular release, subtle changes in presynaptic calcium influx can have large effects on synaptic transmission.

A second role for Gβγ in presynaptic inhibition lies downstream of calcium influx; upon GPCR activation, liberated βγ dimers inhibit release by interfering with the binding of synaptotagmin to the soluble *N*-ethylmalemide-sensitive factor attachment protein receptor (SNARE) complex (Blackmer et al., 2001; Gerachshenko et al., 2005; Wells et al., 2012; Yoon et al., 2007). This mechanism has been primarily studied at giant synapses in the lamprey spinal cord due to the accessibility of their large presynaptic terminals. It is unknown whether similar calcium-independent effects might exist at synapses such as the PF-PC synapse. Studies of the

mechanism of GPCR-mediated presynaptic inhibition at the PF-PC synapse should consider both calcium-dependent and calcium-independent mechanisms of reducing neurotransmitter release.

Possible interactions between tonic presynaptic GPCR signaling pathways

With multiple inhibitory GPCRs at the presynaptic terminal, the potential for interactions between signaling systems arises. These interactions may be complicated, and it is not clear whether they would lead to super-additive or sub-additive effects on the extent of tonic presynaptic inhibition. Both types of interactions have been described for GPCR signaling in other systems, and can even coexist in the same system. For example, interactions between adenosine, somatostatin, and serotonin GPCRs can have either a sub-additive or super-additive effect on a GIRK channel-mediated potassium current in hippocampal CA3 neurons. Sub-additive effects are achieved at saturating agonist concentrations, while lower, more physiologically-relevant agonist concentrations lead to super-additivitity (Sodickson and Bean, 1998).

Evidence for crosstalk between GPCRs involved in presynaptic inhibition has been demonstrated at the axon terminals of Schaffer collaterals in hippocampal slices. In these terminals, tonic activation of A1Rs by endogenous adenosine blocks presynaptic inhibition by CB1Rs (Hoffman et al., 2010). The authors suggest that this interaction is most likely due to overlap in the sets of Gα subunits that can couple to A1Rs and CB1Rs. Tonic A1R signaling may also inhibit CB1R signaling by inhibiting a significant fraction of voltage-gated calcium channels such that the effect of CB1 signaling is occluded. Because at least three of the four GPCRs

present at PF boutons (A1Rs, CB1Rs, and $GABA_BRs$) can couple to overlapping sets of α subunits (Straiker et al., 2002) and also may inhibit overlapping classes of voltage-gated calcium channels (Brown et al., 2004), similar interactions may occur at the PF-PC synapse.

The interactions that may arise between different presynaptic GPCR-mediated signaling pathways are likely to be complex and multi-faceted, which makes it very difficult to predict how these interactions might affect the extent of presynaptic inhibition. Experimental approaches are important to determine whether interactions multiple types of presynaptic GPCRs may affect the extent tonic presynaptic inhibition and whether these interactions increase or decrease tonic inhibition.

Materials and Methods

Slice preparation

Sprague Dawley rats (P17-P18) are deeply anesthetized with isofluorane and decapitated. Brains are removed and placed into an ice-cold sucrose cutting solution containing (in mM): 82.7 NaCl, 65 sucrose, 23.8 $NaHCO_3$, 23.7 glucose, 6.8 $MgCl_2$, 2.4 KCl, 1.4 NaH_2PO_4, and 0.5 $CaCl_2$. Transverse or parasagittal slices (250-300 μm thick) are made from the vermis of the cerebellum in the cutting solution. Slices are incubated at 32˚C for 30 minutes in ACSF solution containing (in mM): 125 NaCl, 26 $NaHCO_3$, 25 glucose, 2.5 KCl, 1.5 $CaCl_2$, 1.25 NaH_2PO_4, and 1 $MgCl_2$, adjusted to 315 ± 2 mOsm. Slices are then incubated for 30 minutes at room temperature in ACSF. All solutions in contact with the whole brain or slices are bubbled with 95% O_2/5% CO_2.

Electrophysiology

Whole-cell voltage-clamp recordings of PCs are made with 1.0-1.7 MΩ borosilicate glass electrodes containing (in mM): 110 Cs_2SO_4, 5.5 $MgSO_4$, 15 HEPES, 10 EGTA, 1.5 $MgCl_2$, 4 $CaCl_2$, 2 Na_2-ATP, 0.1 D600, adjusted to 310-315 mOsm and pH 7.3. Recordings are obtained at 25 ± 1 ˚C (room temperature) or at 34 ± 1 ˚C (near-physiological temperature) as noted. Access resistance and leak current were monitored and experiments were rejected if either parameter changed significantly. During bulk calcium imaging experiments, presynaptic fiber volleys were recorded with an extracellular electrode filled with ACSF placed in the molecular layer close to the imaging site.

Pharmacology

To record EPSCs in the absence of fast inhibitory currents, 20 μM picrotoxin was used to block $GABA_A$ receptors. Various pharmacological agents were used either alone or in combination to inhibit GPCR activity: AM251 (CB1Rs, 2 μM), CGP 55845 (GABABRs, 2 μM), and DPCPX (A1Rs, 5 μM), and were all purchased from Tocris Bioscience/R&D Systems, (Minneapolis, MN). All antagonists/inverse agonists were dissolved in dimethylsulfoxide (DMSO). For each dataset, ACSF used in baselines, in controls, and in applications of single drugs were supplemented with extra DMSO to keep the DMSO concentration constant in all experiments.

Presynaptic calcium imaging

Presynaptic calcium signals in PFs were measured as described previously (Regehr and Tank, 1991; Mintz et al., 1995; Regehr and Atluri, 1995). Briefly, PFs were labeled by local application of a solution containing the membrane-permeant calcium indicator Magnesium Green AM (Life Technologies). Positive pressure was applied to a delivery pipette of 8-15 µm diameter in order to apply a stream of dye onto a spot in the molecular layer, and a large-diameter suction pipette to remove excess dye. Slices were incubated for at least one hour to allow for dye equilibration in PFs. PFs were stimulated with an single borosilicate glass electrode in the molecular layer. Fluorescence changes were measured at a 50 µm diameter spot that was more than 200 µm away from the loading site. An Olympus BX50WI microscope with a 60x 0.9 NA water immersion objective (Olympus) was used to visualize the slice. Magnesium Green AM was excited using a 470-nm LED (Thorlabs). Collected light was focused onto a custom-built photodiode, converted to a voltage signal, and digitally recorded. Background fluorescence was subtracted before determining $\Delta F/F$ values. All experiments were performed in standard ACSF at 32 ± 1 °C.

Data acquisition and analysis

Data were acquired using an ITC-18 interface (Instrutech) at 10 and 1 kHz for electrophysiology and fluorescence data, respectively, and a Multiclamp 700A (Axon Instruments/Molecular Devices, Union City, CA) amplifier. Data were digitally filtered using an

eight-pole Bessel filter at 5 kHz for electrophysiology data and 500 Hz for fluorescence data. All data were analyzed using Igor Pro (Wavemetrics, Lake Oswego). Averages are presented as mean ± SEM. Wilcoxon signed-rank tests or paired Student's t test was performed to determine statistical significance ($p < 0.05$) where indicated.

Results

Identification of individual presynaptic GPCRs that regulate synaptic transmission.

At the PF-PC synapse, we examined basal activity of A1Rs, CB1Rs, and $GABA_BRs$. These experiments were performed by recording from PCs (cerebellar schematic, **Figure 4.1 A**) in whole-cell mode with the cell voltage-clamped to -70 mV (**Figure 4.1 B**). To simulate physiological conditions, all recordings are performed at 34±1˚C and in artificial cerebrospinal fluid (ACSF) containing 1.5mM $CaCl_2$. Extracellular glass electrodes were used to activate either one or two regions in the molecular layer near the PC dendrites. The positions of the electrodes and stimulus intensities were adjusted to obtain reliable EPSCs of 200-350 pA. After establishing a baseline response, one of three pharmacological agents was added to the superfused ACSF: 2 µM AM251, 2 µM CGP 54626, or 5 µM DPCPX. These drugs are used to inhibit CB1Rs, $GABA_BRs$, or A1Rs, respectively. These drugs will be referred to as “antagonists/inverse agonists” since it is not clear whether they exhibit inverse agonist or neutral antagonist properties

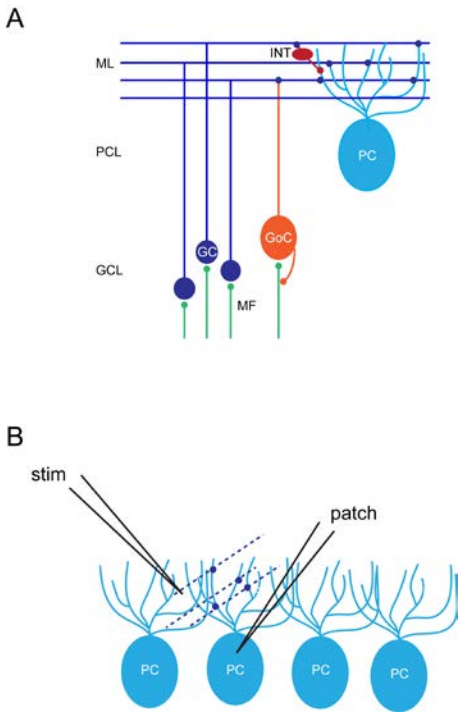

Figure 4.1. Schematic of cerebellar circuitry and recording configuration. A The cerebellar cortex is divided into three distinct layers: the granule cell layer (GCL), the Purkinje cell layer (PCL), and the molecular layer (ML). Excitatory input to the cerebellar cortex is carried by mossy fibers (MFs, green) that form synapses onto granule cells (GCs, dark blue) and Golgi cells (GoCs, orange). GoCs in turn inhibit MFs. Granule cells send an axon up into the molecular layer (ML) that bifurcates. These axons are called parallel fibers (PFs) and form excitatory synapses onto the dendrites of Purkinje cells (PCs, light blue), GABAergic interneurons in the ML (INTs, red), and GoCs. INTs form inhibitory synapses onto PCs. **B** Recording configuration for whole-cell voltage clamp experiments. In sagittal slices, PCs (light blue) are oriented with their dendrites in the plane of the slice and PFs are oriented perpendicularly to the surface of the slice (dark blue dashed lines). A patch electrode is used to record postsynaptic currents from a PC while an extracellular stimulating electrode is used to activate PFs.

under these conditions. My data indicate that application of all three inverse agonists/antagonists together greatly enhanced EPSC amplitudes (**Figure 4.2 A**). However, application of AM251 or CGP 55845 alone each caused a very small or negligible increase in EPSC amplitude, and DPCPX caused a moderate increase in EPSC amplitude (**Figure 4.2 B, C, Table 4.1**). Simultaneous application of all three inverse agonists/antagonists led to the largest effect on EPSC amplitude, with an approximate doubling of EPSC size which was statistically significant (normalized EPSC increase; 235 ± 23%, Wilcoxon signed-rank test with complete statistics in **Table 4.1**). These results suggest that at room temperature, there is significant basal activation of GPCRs that maintains the extent of neurotransmitter release, and that inhibiting GPCR activation can uncover the true capacity for neurotransmitter release at this synapse.

Because the release, diffusion, and clearance of neurotransmitters can be temperature-dependent (Asztely et al., 1997; Diamond and Jahr, 2000; Rusakov et al., 2011), we replicated these experiments at near-physiological temperature (34 ± 1°C). Simultaneous application of AM 251, CGP 55845, and DPCPX again resulted in an approximate doubling of EPSC amplitude (**Figure 4.3 A, C, E**), which was not quite statistically significant (p=0.0625; see **Table 4.2**). The effects of inhibiting A1Rs, CB1Rs, and $GABA_BRs$ in isolation was also examined by application of individual GPCR inverse agonists/antagonists. We observed very small, statistically insignificant changes in EPSC amplitudes with AM 251, CGP 55845, and DPCPX (**Figure 4.3 C, E, Table 4.2**). It is difficult to directly measure *p* using an extracellular stimulating electrode, since this procedure activates many PF-PC synapses. Quantifying the changes in paired-pulse ratio (PPR) is often used as an indirect way to detect changes in *p*. We used a paired-pulse protocol with an interstimulus interval of 30 ms to measure changes in PPR elicited by drug application (**Figure 4.3 C, D**). Surprisingly, inhibitors of A1Rs, CB1Rs, and $GABA_BRs$ did not

Figure 4.2. Inhibition of $G_{i/o}$ coupled GPCRs increases synaptic strength. A An example EPSC recorded in voltage clamp configuration under baseline conditions (gray) and after application of AM 251 (2 µM), CGP 55845 (2 µM), and DPCPX (5 µM). The amplitude of the EPSC increases substantially with no discernible effects on its kinetics. **B** Summary of average enhancement of EPSC amplitudes (normalized to baseline amplitude) after pharmacological inhibition of GPCRs with AM 251 (2 µM), CGP 55845 (2 µM), DPCPX (5 µM), simultaneous application of all three inhibitors at the same concentrations or control. The increases in EPSC amplitude caused by DPCPX and by simultaneous application of AM251, CGP 55845, and DPCPX are statistically significant (asterisks; see Table 4.1). **C** Time course of normalized EPSC amplitudes during application of GPCR inhibitors: AM251 (blue), CGP 55845 (green) DPCPX (red), simultaneous application of all three inhibitors (black) or control (purple). Drug application begins at time=0.

Figure 4.2 (Continued)

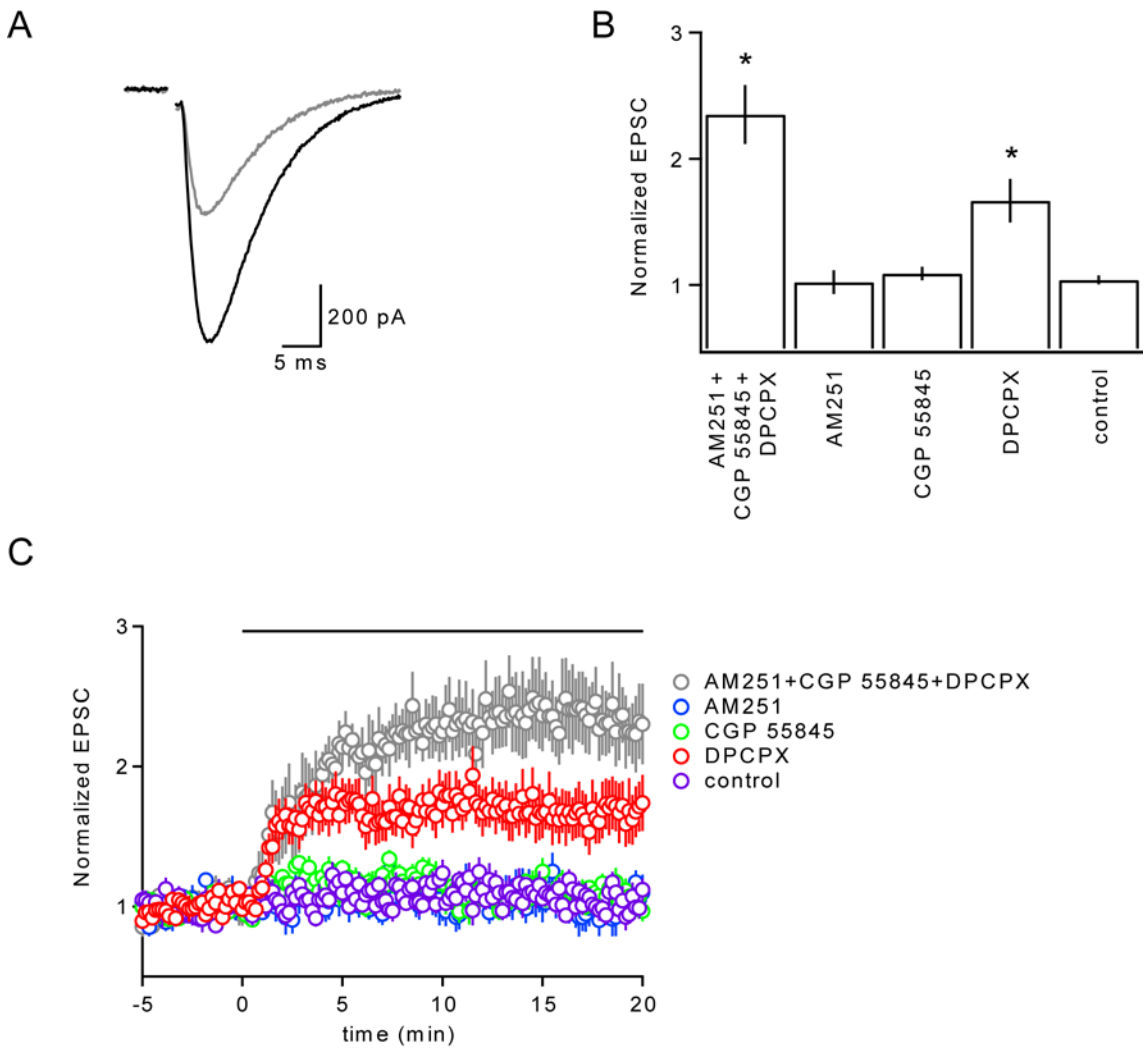

Table 4.1. Statistics summary for GPCR-mediated tonic effects on EPSC amplitude at room temperature.

Wilcoxon Two-tailed Signed Rank Test	AM251 + CGP 55845 + DPCPX	AM251	CGP 55845	DPCPX	Control
Number of Cells	7	7	10	13	7
Mean	2.351	1.023	1.092	1.667	1.04
Std. Error	0.2322	0.0946	0.0539	0.1707	0.0353
Theoretical median	1	1	1	1	1
Actual median	2.064	1.041	1.091	1.423	1.03
p-value (two-tailed)	0.0156	0.9375	0.1055	0.0002	0.2969
Significance (alpha=0.05)	Yes	No	No	Yes	No

Figure 4.3. Inhibition of $G_{i/o}$ coupled GPCRs increases synaptic strength at near-physiological temperature. A *Left* Example EPSCs recorded in voltage clamp configuration under baseline conditions (gray) and after application of AM 251 (2 µM), CGP 55845 (2 µM), and DPCPX (5 µM) (black). The amplitude of the EPSC increases substantially with no discernible effects on its kinetics. *Right* The same example synaptic responses shown in A, now normalized to the amplitude of the first response. No change in the paired-pulse ratio (PPR) is apparent. **B** Summary of average enhancement of EPSC amplitudes (normalized to baseline amplitude) after pharmacological inhibition of GPCRs with AM 251 (2 µM), CGP 55845 (2 µM), DPCPX (5 µM), or simultaneous application of all three inhibitors at the same concentrations noted. **C** Summary of average change in PPR (normalized to baseline PPR) after pharmacological inhibition of GPCRs with AM 251 (2 µM), CGP 55845 (2 µM), DPCPX (5 µM), or simultaneous application of all three inhibitors at the same concentrations noted. **D** Time course of normalized EPSC amplitudes during application of GPCR inhibitors: AM251 (blue), CGP 55845 (green) DPCPX (red), or simultaneous application of all three inhibitors (black). Drug application begins at time=0.

Figure 4.3 (Continued)

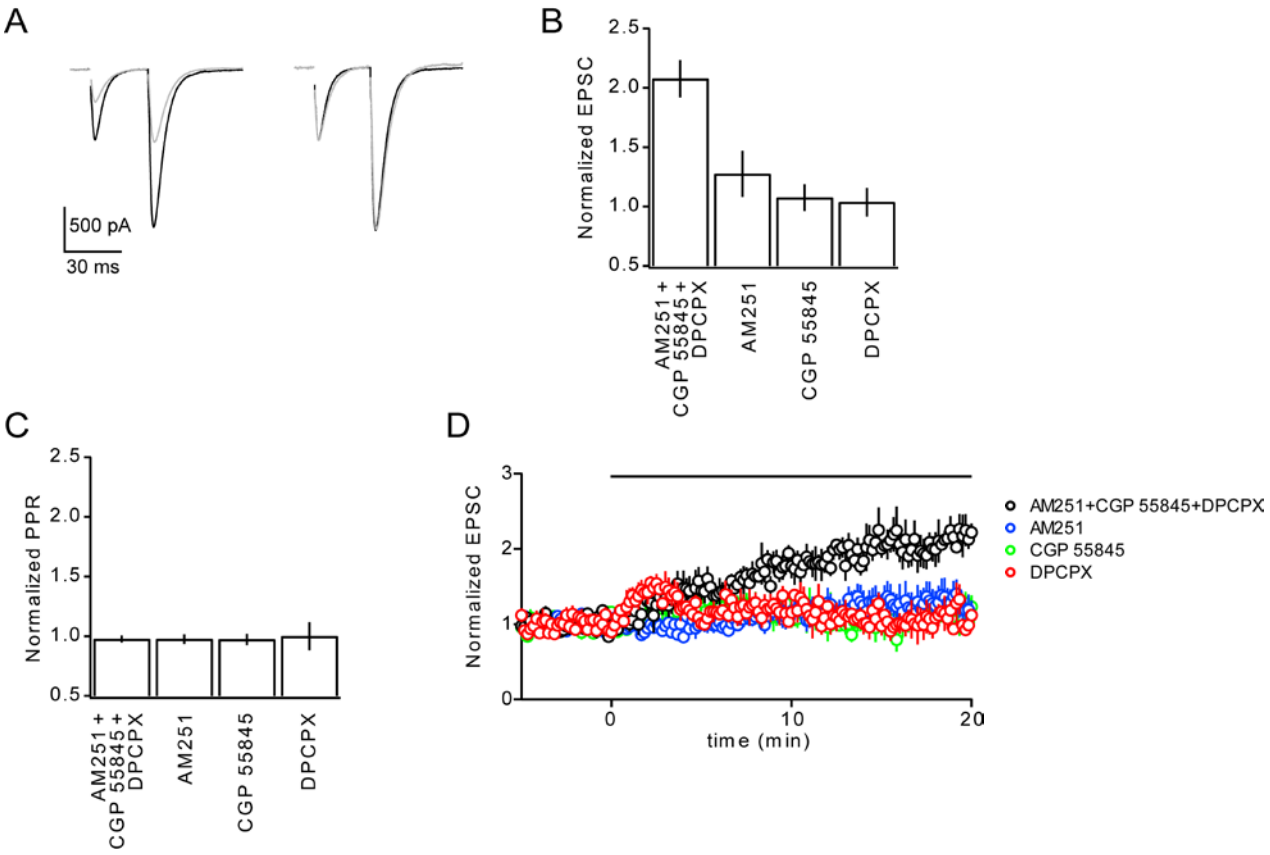

Table 4.2. Statistics summary for GPCR-mediated tonic effects on EPSC amplitude and PPR at near-physiological temperature.

	AM251 + CGP 55845 + DPCPX	AM251	CGP 55845	DPCPX
Number of Cells	5	7	6	3
Wilcoxon two-tailed signed rank test (EPSC)				
Mean EPSC	2.077	1.274	1.075	1.036
Std. Error of EPSC	0.1578	0.1941	0.1132	0.1203
Theoretical median of EPSC	1	1	1	1
Actual median of EPSC	1.903	1.056	1.05	0.9693
p-value (two-tailed) for EPSC	0.0625	0.4688	1	1
Significance (alpha=0.05) for EPSC	No	No	No	No
Wilcoxon two-tailed signed rank test (PPR)				
Mean PPR	0.9755	0.9754	0.9731	1
Std. Error of PPR	0.0298	0.0414	0.0459	0.1172
Theoretical median of PPR	1	1	1	1
Actual median PPR	0.943	0.944	0.952	0.8969
p-value (two-tailed) for PPR	0.625	0.5781	0.5625	1
Significance (alpha=0.05) for PPR	No	No	No	No

affect the PPR. However, unavoidable series resistance errors might cause incomplete voltage-clamp for large synaptic currents, leading to inaccurate measurements of the second EPSC in a pair.

Quantification of the collective effects of presynaptic GPCR on synaptic transmission.

It is well known that activation of presynaptic GPCRs coupled to $G_{i/o}$ can reduce presynaptic calcium influx by modulating presynaptic calcium channels. Previous work has

shown that small changes in calcium influx have dramatic effects on the amplitude of evoked PC EPSCs (Dittman and Regehr, 1996; Mintz et al., 1995; Sabatini and Regehr, 1997) This can be summarized by the power law EPSC= $k(Ca^{2+}\ influx)^n$ with n=2-3 at the PF-PC synapse (Mintz et al., 1995). Therefore, even small reductions in presynaptic calcium influx, each caused by a different class of $G_{i/o}$-coupled GPCR, will have considerable inhibitory effects on synaptic transmission. It follows that inhibiting multiple GPCRs that mediate presynaptic inhibition should cause an increase in synaptic transmission that exceeds the sum of the effects caused by inhibition of each individual GPCR. My experiments suggest that the collective effect of inhibiting A1, CB1, and $GABA_B$ receptors is considerably larger than the sum of their individual effects (**Figure 4.2 A, B**). The mean enhancement of EPSC size is approximately two-fold (2.14 ± 0.16 –fold enhancement) for the three antagonists/inverse agonists combined.

Determination of the effects of GPCR-mediated inhibition of presynaptic calcium influx.

Previous experiments at the PF-PC synapse have indicated that activation of presynaptic A1, CB1, and $GABA_B$ receptors leads to a reduction in presynaptic calcium influx upon action potential invasion of the parallel fibers (Brown et al., 2004; Dittman and Regehr, 1996). Here, we test whether tonic activation of presynaptic GPCRs inhibits calcium influx through the VGCCs coupled to vesicle release. It is known that agonist-induced presynaptic inhibition at PF boutons occurs through three types of calcium channels, N-type, P/Q-type, and R-type channels ($Ca_v2.1$-2.3). Changes in influx through these types of channels can be visualized by loading calcium indicators into presynaptic terminals.

These experiments use bulk loading of a membrane-permeant calcium indicator to load a band of parallel fibers running through the molecular layer (**Figure 4.4 A**), taking advantage of the fact that most of the lipid membranes in this region belong to granule cell axons (Atluri and Regehr, 1995; Sabatini and Regehr, 1995). Although this method includes non-boutons in the determination of ΔF/F, an estimated 75% of the volume of the PFs consists of presynaptic boutons, and PFs are by far the largest volume contributor to the molecular layer (Palay and Chan-Palay, 1974). Additionally, the concentration of voltage-gated calcium channels is much lower in granule cell axons as compared to presynaptic boutons (Cohen et al., 1991; Robitaille and Charlton, 1992; Stephen et al., 1993), indicating that the changes in fluorescence observed in a labeled volume of the molecular layer is likely to reflect changes in calcium levels in the presynaptic boutons of granule cells.

Using the low-affinity calcium indicator magnesium green AM (K_d=7μM; Zhou and Neher, 1993) loaded into parallel fibers in the slice and measurements of presynaptic calcium influx, calcium transients were recorded while stimulating a beam of parallel fibers with an extracellular electrode (**Figure 4.4 A, B**). After establishing a baseline ΔF/F associated with the stimulus, either one antagonist/inverse agonist against A1Rs, CB1Rs, $GABA_BRs$, or mGluR4s alone, or all four antagonists together, was applied. The peak ΔF/F change was measured (**Figure 4.4 C**), which can be can be used as a linear measure of presynaptic calcium influx for the low-affinity indicator used (Regehr and Atluri, 1995). One limitation of using an AM dye is that it is extruded from the membrane more rapidly at physiological temperatures, which limits the duration of each experiment to 20-60 minutes (Beierlein et al., 2004). This time frame was sufficient to complete single wash-in experiments. We find that the mean peak ΔF/F value is significantly higher after simultaneous application of all three inverse agonists/antagonists

Figure 4.4. Inhibition of $G_{i/o}$ coupled GPCRs increases presynaptic calcium influx. A Schematic depicting bulk calcium indicator loading technique. A delivery pipette filled with magnesium green AM ejects a pressurized stream of dye (shown in green) onto the parallel fibers in a transverse cerebellar slice. A suction pipette removes excess dye. After dye equilibration in parallel fibers, a stimulating electrode is placed in the labeled beam of fibers near the loading site and labeled fibers are imaged from a site several hundred microns away from the loading site. The orientation of PCs in the slice is shown by the example PC (blue). **B** An example average calcium transient recorded during baseline conditions (gray) and after simultaneous application of AM 251 (2 µM), CGP 55845 (2 µM), and DPCPX (5 µM) (black). **C** Time course of normalized EPSC amplitudes during application of GPCR inhibitors at the concentrations noted in B: AM251 (blue), CGP 55845 (green) DPCPX (red), or simultaneous application of all three inhibitors (32°C, black; 25°C, gray). Drug application begins at t=0. **D** Summary of average enhancement of ΔF/F (normalized to baseline amplitude) after pharmacological inhibition of GPCRs with AM 251, CGP 55845, DPCPX, or simultaneous application of all three inhibitors at the concentrations noted in C at 25°C and 32°C. **E** Summary of average change in fiber volley amplitude (normalized to baseline amplitude) after pharmacological inhibition of GPCRs with AM 251, CGP 55845, DPCPX, or simultaneous application of all three inhibitors at the concentrations noted in C at 25°C and 32°C. **F** Summary of average change in average calcium transient decay time constant (normalized to baseline decay time constant) after pharmacological inhibition of GPCRs with AM 251, CGP 55845, DPCPX, or simultaneous application of all three inhibitors at the concentrations noted in C at 25°C and 32°C.

Figure 4.4 (Continued)

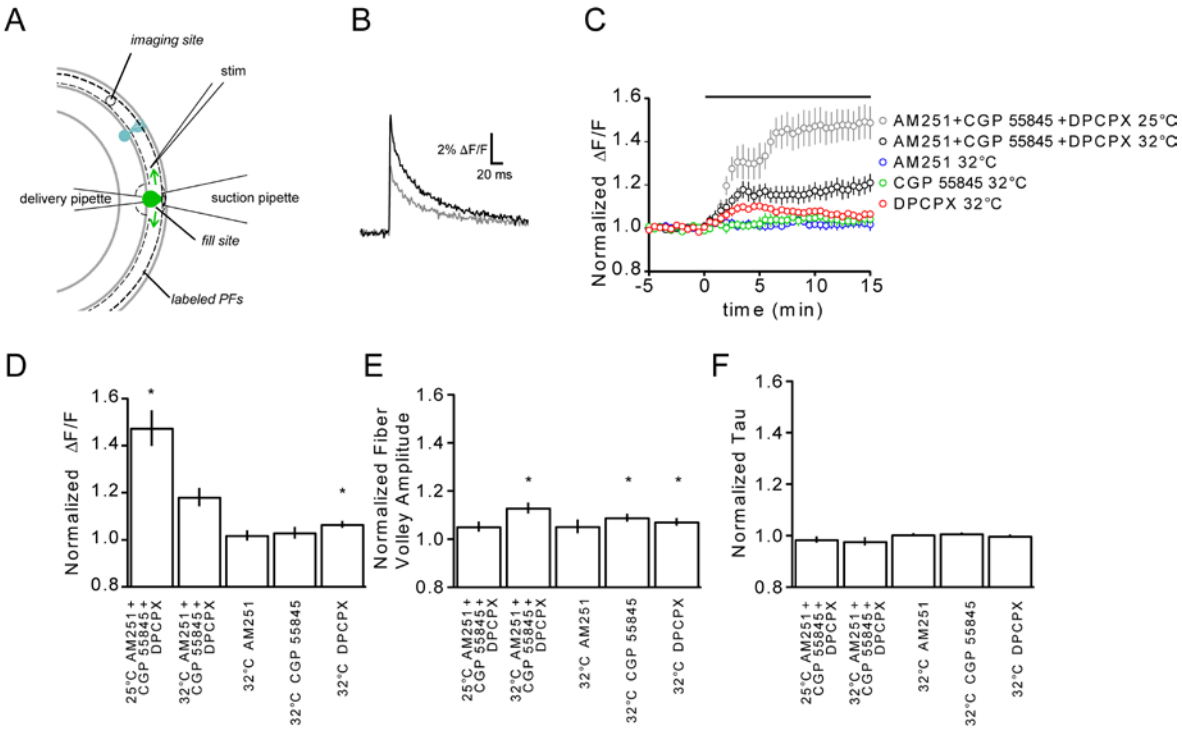

Table 4.3 Statistics summary for GPCR-mediated tonic effects on ΔF/F, presynaptic fiber volley, and calcium decay time constant at elevated temperature (32°C).

Treatment	AM251 + CGP 55845 + DPCPX	AM251 + CGP 55845 + DPCPX	AM251	CGP 55845	DPCPX
Temperature	25°C	32°C	32°C	32°C	32°C
Number of Slices	6	8	7	7	8
Wilcoxon two-tailed signed rank test (ΔF/F)					
Mean ΔF/F, normalized to baseline	1.556	1.177	1.01	1.033	1.059
Standard error (SEM) of ΔF/F, normalized	0.1036	0.03752	0.02623	0.02488	0.01694
Theoretical median	1	1	1	1	1
Median ΔF/F, normalized to baseline	1.555	1.136	1.014	1.028	1.072
p-value (two-tailed)	0.0313	0.0078	0.6875	0.2969	0.0234
Significance (alpha=0.05)	Yes	No	No	No	Yes
Wilcoxon two-tailed signed rank test (fiber volley)					
Mean fiber volley amplitude, normalized to baseline	1.052	1.13	1.053	1.089	1.072
Standard error (SEM) of fiber volley amplitude, normalized	0.02134	0.02278	0.02821	0.01684	0.01565
Theoretical median	1	1	1	1	1
Median fiber volley amplitude, normalized to baseline	1.071	1.134	1.052	1.102	1.061
p-value (two-tailed)	0.1563	0.0078	0.2188	0.0156	0.0078
Significance (alpha=0.05)	No	Yes	No	Yes	Yes
Wilcoxon two-tailed signed rank test (decay time constant)					
Mean decay time constant, normalized to baseline	0.9848	0.9777	1.004	1.008	0.9984
Standard error (SEM) of decay time constant, normalized	0.01212	0.0159	0.006285	0.004513	0.006824
Theoretical median	1	1	1	1	1
Median decay time constant, normalized to baseline	0.988	0.9683	1.01	1.007	1.001
p-value (two-tailed)	0.3125	0.25	0.8125	0.2188	0.9453
Significance (alpha=0.05)	No	No	No	No	No

against A1Rs, CB1Rs, and $GABA_BRs$ than before application at both 25°C and 34°C (25°C, 55.6 ± 10.3% increase; 32°C, 17.7 ± 3.8% increase; **Figure 4.4 C, D, Table 4.3** for detailed statistics), strongly suggesting that the increases in synaptic strength resulting from GPCR inhibition are at least partially due to the effect of increased calcium influx on vesicular release. This result also suggests that a presynaptic mechanism is likely to account for the effects of GPCR inhibitors on EPSC size. Inhibition of individual GPCRs led to considerably smaller effects on presynaptic calcium influx, or ΔF/F (AM251, 1.0 ± 2.6% increase; CGP 55845, 3.3 ± 2.5% increase; DPCPX, 5.9 ± 1.7% increase; **Figure 4.4 C, D**). Of the three inverse agonists/antagonists applied in isolation, only the increased ΔF/F observed in DPCPX was significant, while the contributions of AM 251 and CGP 55845 were insignificant (detailed statistics in **Table 4.3**).

To test whether the observed increases in ΔF/F could be attributed to changes in PF excitability, an extracellular recording electrode was placed in the molecular layer close to the imaging site. Small increases in excitability were observed for all treatments (**Figure 4.4 E**), as measured by the amplitude of the fiber volley peak to the fiber volley trough. Application of all three GPCR antagonists simultaneously at 25°C led to a small but insignificant increase in the amplitude of the fiber volley (5.2 ± 2.1% increase), which became significant at elevated temperature (13 ± 2.3% increase). Increases in the fiber volley amplitude were observed during application in individual GPCR antagonists, as well (AM251, 5.3 ± 2.8% increase; CGP 55845, 8.9 ± 1.7% increase; DPCPX, 7.2 ± 1.6% increase). The changes in fiber volley amplitude during application of DPCPX or CGP 55845 were small but statistically significant (statistics in **Table 4.3**).

Finally, to test whether changes in calcium buffering in cells were occurring during experiments, we measured the decay time constant of calcium transients by fitting a single exponential function to the falling phase of the calcium signal. In all cases, the change in the decay time constant was very small and statistically insignificant (**Figure 4.4 F,** statistics in **Table 4.3**).

Discussion

My results reveal that a large enhancement in EPSC size occurs when A1Rs, CB1Rs, and $GABA_BRs$ are inhibited (**Figures 4.2 and 4.3**). Small to moderate effects are observed when inhibiting only one receptor type in isolation, with A1Rs having the largest apparent impact on synaptic transmission, particularly at room temperature (**Figure 4.2**). These results have two important immediate implications. First, these results indicate that slice electrophysiology experiments may be typically conducted under considerable modulation, even in the absence of external stimulation. Tonic inhibition of neurotransmitter release likely affects estimates of release probability and RRP size, and will decrease the apparent extent of neurotransmitter release. Secondly, the relatively minor effects of inhibiting individual GPCR types, particularly at near-physiological temperature (**Figure 4.3**), suggest that the collective effect of simultaneously inhibiting all three types of GPCRs may exceed the sum of the individual effects. This would suggest that there may be interactions between presynaptic A1R, CB1R, and/or $GABA_BR$ signaling pathways. Signaling by each of these three receptors proceeds via the $G_{i/o}$ pathway and likely depends upon the availability of free Gβγ dimers, as described previously. Preventing activation of each type of GPCR might lead to a decrease in free Gβγ, since the dimer

is only liberated from the heterotrimeric Gαβγ complex upon receptor activation. Under basal conditions, ongoing activity of multiple signaling pathways might prove mutually beneficial to the other pathways in ensuring that enough free Gβγ exists to support basal activity levels. In this way, superadditive effects might be achieved by blocking multiple $G_{i/o}$ pathways.

Presynaptic calcium seems to be at least partially responsible for the increase in synaptic strength caused by blocking presynaptic GPCRs (**Figure 4.4**). Using the power law described previously, with $2<n<3$ (Mintz et al., 1995), we would predict that the 55.6% increase in calcium influx observed during application of all three GPCR inhibitors at room temperature can explain an increase in synaptic strength of 242-377% . In our room temperature experiments, we observe a 235 ± 23% increase in synaptic strength, which agrees with the power law prediction. Thus, the effects on EPSC size observed during the application of GPCR antagonists are likely to be mostly explained by changes in presynaptic calcium influx. Certainly, other calcium-independent mechanisms could contribute to the enhancement in EPSC size observed. These mechanisms could include an upregulation of cAMP/PKA signaling, a downregulation of PKC activity, changes to other presynaptic conductances, and/or direct effects on the exocytosis machinery. It has recently been shown at hippocampal synapses that different $G_{i/o}$ coupled receptor types present at the same synapse can have differential effects on presynaptic calcium influx, while both still inhibiting neurotransmitter release (Hamid et al., 2014). Therefore, the relative individual contributions of A1Rs, CB1Rs, and $GABA_BRs$ to regulating calcium influx need not correlate with their relative effects on EPSC amplitude. The data presented here are insufficient for evaluating these possibilities, but if calcium-independent mechanisms do play a role, it is likely to be less prominent than the effect of tonic GPCR-mediated inhibition of presynaptic calcium channels.

Discrepancies between room temperature and elevated temperature data sets

One issue that is difficult to resolve here are the discrepancies between the effects of individual GPCRs on synaptic transmission at room temperature versus near-physiological temperature. At room temperature, A1 receptors seem to play a moderate, statistically-significant role in regulating basal release properties (167 ± 17% of initial EPSC amplitude, **Figure 4.2 C**), which decreases at near-physiological temperature (104 ± 12% of initial EPSC amplitude, **Figure 4.3 C, E**). It is possible that adenosine clearance is accelerated at elevated temperatures, such that the effect of A1 receptor signaling at elevated temperature does not decrease synaptic strength as significantly *in vivo*. However, at 32°C, there is a statistically-significant, small effect of DPCPX on presynaptic calcium influx (**Figure 4.4 C, D**). Ideally, it would be possible to perform presynaptic calcium imaging experiments at 34°C so that it could be directly compared with the electrophysiology data presented in **Figure 4.2**. However, obtaining high-quality bulk presynaptic calcium data becomes very difficult at near-physiological temperatures due to increased calcium indicator extrusion.

Additionally, the effects of simultaneously inhibiting A1Rs, CB1Rs, and $GABA_BRs$ on presynaptic influx seems to be very temperature-dependent. At room temperature, we observed a 55.6 ± 10.4% increase in ΔF/F, while we observed only a 17.7 ± 3.8% increase in ΔF/F at 32°C. This difference may be caused by a true difference in the extent of GPCR-mediated inhibition of presynaptic calcium influx at different recording temperatures. This difference could also reflect a difference of the sensitivity of magnesium green AM at different temperatures. With the bulk loading technique we used here, it is difficult to convert ΔF/F values to estimated calcium

concentrations. Instead, a ratiometric indicator or calcium indicator paired with a calcium-insensitive dye would have to be used. Potential heterogeneity of dye concentration in neighboring PFs would still be a complicating factor in determining the change in calcium concentrations in cells.

The electrophysiology experiments presented in **Figures 4.2** and **4.3** depend upon the activation of many PF-PC synapses; each PC is estimated to receive about 175,000 synaptic inputs from granule cells (Napper and Harvey, 1988), and I am likely to activate many hundreds to thousands of inputs with an extracellular electrode. Therefore, we used bulk imaging techniques to image a band of fibers, judging that these bulk changes would be a more appropriate way to evaluate the changes in the population of PF boutons that synapse onto a PC. Other studies use finer-resolution imaging of calcium dyes in individual presynaptic boutons, which allows for quantification of calcium concentrations (Brenowitz and Regehr, 2007; Zhang and Linden, 2009), which could be attempted in future experiments. However, calcium influx and dynamics at individual presynaptic boutons is highly variable (Brenowitz and Regehr, 2007; Zhang and Linden, 2009), increasing the number of experiments necessary to obtain accurate estimates of the effect of each GPCR inhibitor on average presynaptic influx at PF boutons.

Importance of basal release properties at the PF-PC synapse

Additionally, a tonic reduction of basal release by GPCR-mediated presynaptic inhibition is likely to have important implications for short-term plasticity at the PF-PC synapse. The characteristic low initial *p* of this synapse is considered a result of prominent residual calcium

buildup in the presynaptic terminal paired with fairly low levels of synaptic vesicle depletion. This low initial *p* is crucial for the facilitation observed during stimulus trains and results in large PC EPSC amplitudes at high frequencies of PF firing (Dittman et al., 2000). In the absence of tonic presynaptic inhibition, the effects of synaptic vesicle depletion are likely more prominent, which would decrease the extent of facilitation observed during high-frequency stimulus trains. Additionally, the largest PC EPSC amplitudes might be produced by lower-frequency stimulus trains (Abbott and Regehr, 2004). If GPCR-mediated tonic inhibition acts by reducing initial *p*, it is likely to play an important role in regulating transmission at the PF-PC synapse and information flow through the cerebellar cortex.

The observation that relieving presynaptic inhibition by GPCRs does not change the PPR (**Figure 4.3 C, D**) indicates that changes in initial *p* may not be responsible for increased synaptic strength in the absence of GPCR activation. Instead, changes to the effective RRP size, which we have shown to be calcium-dependent (**Chapter 2**), may produce the observed increase in synaptic strength without significant changes in short-term plasticity. Directly probing the effective RRP size at the PF-PC synapse is very difficult, due to its low initial *p* and prominent synaptic facilitation. Furthermore, it is difficult to ensure that the same subset of PF boutons is activated with each electrical stimulus, which complicates studies of the properties of neurotransmitter release.

Modulation of the basal release properties at the PF-PC synapse, whether by regulating initial *p* or RRP size, may have significant effects on information transfer to the DCN. Experimental studies have shown that the firing rate of a PC is linearly dependent on the synaptic charge received from its PF inputs (Walter and Khodakhah, 2006). In the study, the authors used

increases in the number of activated presynaptic fibers instead of increases in neurotransmitter released per bouton to increase the number of synaptic inputs, but the two manipulations should affect synaptic currents in the same manner. Tonic presynaptic inhibition may then increase the number of PF inputs required to produce a certain increase in PC firing rate.

Chapter 5

Conclusion

Calcium dependence of effective RRP size

In this thesis, we present three distinct chapters studying two very different excitatory synapses. We begin by focusing on the calyx of Held synapse and show that changes to calcium influx into the presynaptic terminal affects neurotransmitter release by two processes: first, by altering *p*, which has already been well established, and second, by altering effective RRP size, which is much more controversial. Other groups have made observations similar to ours (Schneggenburger et al., 1999) in that changing the external calcium concentration had a large effect on RRP_{train}. However, the interpretation of these data was that the stimulus train delivered in standard external calcium (2 mM calcium) was insufficient to deplete the RRP, and that the larger value measured in 4 mM calcium corresponded to the true, constant effective RRP size. We wished to test this claim, and did so by altering calcium influx by 1) changing the external calcium concentration, 2) reducing calcium influx by antagonizing R-type VGCCs, which are in the minority at this synapse, 3) reducing calcium influx by partially antagonizing P/Q-type VGCCs, which are primarily responsible for release at this synapse (**Figure 2.5** and **Figure 2.7**) (Wu et al., 1999), and finally 4) by applying the $GABA_B$ receptor agonist baclofen (**Figure 2.6** and **Figure 2.7**). Three different extrapolation techniques all conclude that changes to both *p* and the number of vesicles released over time occur under these experimental conditions.

Towards a model of neurotransmitter release at the calyx of Held synapse

We pursued the topic of changes in neurotransmitter release properties with a modeling approach in **Chapter 3**. We developed and implemented a basic depletion model that accounts for replenishment of the RRP (**Figure 3.1**) in order to analyze postsynaptic responses to high-frequency stimulus trains and observed an excellent agreement between RRP_{model} and p_{model} across a variety of initial *p* values (**Figure 3.2**). The model also qualitatively agrees with the conclusions of linear extrapolation methods on the effects of pharmacological manipulation of VGCCs (**Figure 3.4**). With confidence in the ability of our model to simulate realistic neurotransmitter release in response to train stimuli, we used our model to simulate postsynaptic responses over ranges of *p*, R, and stimulus frequency. As these properties of neurotransmitter release are very difficult to experimentally manipulate in isolation, we feel that this model has the potential to provide insights into experimental data that cannot be gained from experiments alone. We find that the model supports ideas that we intuitively thought might be true—we find that low *p*, high R, and low stimulus frequency can jeopardize accurate assessments of effective RRP size and *p* (**Figures 3.3-3.10**). Future studies at other synapses may benefit for performing similar analyses to verify whether the RRP estimation method applied will be accurate, and perhaps even to see whether this model can provide new insight into the particular characteristics of a specific synapse.

Functional significance of regulating RRP size versus release probability

An important question that emerges from **Chapters 2** and **3** pertains to the benefit of regulating RRP size versus *p*. For the first response to a stimulus train, there need be no difference between the two scenarios (**Figure 2.8**), but there is a difference in the shape of

responses to prolonged stimulus trains. It is well established that changes in *p* are important for the time course of synaptic depression and therefore important in defining a neural code (Tsodyks and Markram, 1997), but what can be added by the ability to regulate RRP? Changing the effective RRP size is a fairly straightforward way to dynamically alter the number of spikes that effectively cause a postsynaptic spike, and will produce a different effect than regulation of *p*. The size of an EPSC is proportional to the amount of depolarizing current that flows in, and this determines whether a spike will be generated in the postsynaptic cell. If a neuromodulator were to regulate a synapse only by increasing *p*, for example, the efficacy of early stimuli in eliciting postsynaptic responses would be enhanced, but the postsynaptic current amplitudes will decay more quickly, possibly leading to fewer spikes in the postsynaptic cell due to a stimulus train. In contrast, increasing the size of the RRP by the same percentage would improve the efficacy of all stimuli in generating postsynaptic spikes, since an increase in RRP size simply scales up the amplitude of postsynaptic responses to a train.

A remaining question is whether regulation of calcium influx by different means can have different fractional effects on RRP and *p*. The data presented here cannot provide a clear answer, but future experiments performed in the presence and absence of various neuromodulators could reveal differential regulation of RRP size and *p*. For now, we observe simultaneous regulation of both properties of neurotransmitter release.

Finally, our understanding of replenishment at the juvenile calyx of Held suggests a parallel between observations at depressing cortical pyramidal cell synapses (Abbott et al., 1997), that the total charge transfer when changing frequency may be unchanged. However, in the tens of milliseconds after a frequency change, there will be differential charge transfer. This

suggests that the calyx of Held may use this ability to detect changes in activity and selectively enhance that information flowing to higher order auditory regions.

Regulation of basal neurotransmitter release at the PF-PC synapse

Chapter 4 describes tonic regulation of neurotransmitter release in an *in vitro* slice preparation from rodent cerebellum. We found that simultaneous inhibition of A1 receptors, CB1 reeptors, and $GABA_B$ receptors with inverse agonists/neutral antagonists leads to a large potentiation of synaptic strength at the PF-PC synapse (**Figures 4.2** and **4.3**), likely due to increased calcium influx when basal activation of GPCRs is disrupted (**Figure 4.4**). To us, this was a very surprising finding, and one that we believe is not currently appreciated in the field. Something that would be fascinating to explore in the future is whether basal levels of adenosine, GABA, and endocannabinoids can collaboratively regulate neurotransmitter release *in vivo*. Although *in vivo* pharmacology experiments are often difficult, it is possible to apply these inhibitors of GPCRs to the cerebellum *in vivo* and record calcium transients in parallel fibers to look for regulation of calcium influx. A preliminary *in vivo* experiment performed in our lab (data not shown) suggested that tonic regulation of calcium influx may occur.

Similarities and differences between observations at the calyx of Held and PF-PC synapses

The calyx of Held synapse and PF-PC synapse are both glutamatergic synapses that have been well-studied for decades, but in most other ways are vastly different. The two synapses display very different convergences: more than one hundred thousand PF synapses are estimated to contact a PC (Napper and Harvey, 1988), but post-hearing principal neurons of the MNTB

typically have only one presynaptic terminal that contacts it (Borst and Soria van Hoeve, 2012). This difference is indicative of very different roles of these synapses in neuronal computations.

The calyx of Held synapse, with its large RRP, axosomatic architecture, and monosynaptic contact is optimally poised to act as a powerful, high-fidelity relay synapse on the way to higher level auditory brain regions (Borst and Soria van Hoeve, 2012). Despite the size and strength of this synapse, modulation of presynaptic calcium influx by a $GABA_B$ receptor agonist (**Figure 2.6**) (Takahashi et al., 1998) can powerfully limit synaptic strength. The presence of inhibitory interneurons in the MNTB suggests that $GABA_B$ receptors may play an important role during periods of high, sustained firing.

In contrast, the PF-PC synapse has a very low *p* under control conditions and is likely to serve as an integrator of neuronal activity for a large population of granule cells. Only if a large fraction of granule cells fire can the AP threshold of a PC be met, leading to inhibition of the PC's targets. Despite these differences, it is evident that the PF-PC synapse contains multiple targets of GPCRs, leading to a rich ability of neuromodulators to regulation the basal release of neurotransmitter (**Figures 4.2-4.4**).

Our studies at the calyx of Held prompt the question, might neuromodulators at a variety of synapses regulate neurotransmitter release by controlling *p* and RRP size? This question is extremely difficult to address at the PF-PC synapse, due to its very low *p* and the relative difficultly of stimulating the same set of presynaptic axons and to deplete the RRP, even with very high frequency stimuli. Experiments that use minimal fiber stimulation or optical activation of a subset of PFs may allow for further analysis of this question, although the ability to deplete the RRP will not be improved by these techniques. We hope to study synapses such as the climbing fiber-PC synapse, the endbulb of Held synapse, where *p* is likely high enough to allow

for depletion of the RRP with high frequency stimulation, in order to determine whether our results at the calyx of Held might be generalizable.

An interesting potential similarity between PF-PC and calyx of Held synapses lies in their presynaptic calcium domains. The immature calyx of Held synapse, which has been studied by many, has been shown to exhibit loose, microdomain coupling (Meinrenken et al., 2002), and coupling at the PF-PC synapse may be similar, although coupling at this synapse is less well understood (Augustine et al., 2003). This suggests that that the effect of GPCR agonists like baclofen at the calyx may regulate the effective size of the RRP by exclusion of primed vesicles from the effective RRP under basal conditions, and that a similar effect could occur in the cerebellum. More rigorous experiments, again using minimal fiber stimulation of optical activation of presynaptic axons, might provide a readout of *p* and RRP size that could be compared under control conditions and in the presence of a neuromodulator. The conjecture here certainly indicates that greater understanding of local calcium and the molecules effecting release will be important to further dissect mechanisms of neurotransmitter release.

The final data chapter of this thesis (**Chapter 4**) has a common theme with the experiments and modeling at the calyx of Held in that it indicates the need for more rigorous dissection of regulating neurotransmitter release. Unlike the calyx of Held, the lack of synaptic depression at the PF-PC synapse suggests that changes in PF firing rate could have a significant effect on charge transfer per unit time at this synapses, providing an important way to modulate information flow through the cerebellar cortex. Our observations are particularly interesting if they persist *in vivo*, which we were unable to test here. It is possible that superadditive effects of different neuromodulators on calcium influx can only be seen in slices, where there can be artificial accumulation of neurotransmitters, and where the temperature is lower, which can slow

clearance by transporter proteins. Even if the observed tonic inhibition of neurotransmitter release is exclusively an *in vitro* phenomenon, it is an important one to consider when analyzing previous work. Typically, inhibitors of all possible GPCRs are not necessarily included in the recording solution in slice experiments, suggesting that many studies may not have studied the true basal state of the PF-PC synapse, but instead a modulated state that may be very different *in vivo*.

Chapter 6

Appendix A

Hyperpolarization Induces a Long-Term Increase in the Spontaneous Firing Rate of Cerebellar Golgi Cells

Court Hull, YunXiang Chu*, Monica Thanawala*, Wade G. Regehr

*these authors made equal contributions

Journal of Neuroscience 2013 Apr; 33(14): 5895-902.

Author contributions:

C.A.H. and W.G.R. designed research; C.A.H., Y.C., and M.T. performed research; C.A.H. and W.G.R. analyzed data; C.A.H. and W.G.R. wrote the paper

Abstract

Golgi cells (GoCs) are inhibitory interneurons that influence the cerebellar cortical response to sensory input by regulating the excitability of the granule cell layer. While GoC inhibition is essential for normal motor coordination, little is known about the circuit dynamics that govern the activity of these cells. In particular, while GoC spontaneous spiking influences the extent of inhibition and gain throughout the granule cell layer, it is not known whether this spontaneous activity can be modulated in a long-term manner. Here we describe a form of long-term plasticity that regulates the spontaneous firing rate of GoCs in the rat cerebellar cortex. We find that membrane hyperpolarization, either by mGluR2 activation of potassium channels, or by somatic current injection, induces a long-lasting increase in GoC spontaneous firing. This spike rate plasticity appears to result from a strong reduction in the spike afterhyperpolarization (AHP). Pharmacological manipulations suggest the involvement of calcium-calmodulin dependent kinase II (CaMKII) and calcium-activated potassium channels in mediating these firing rate increases. As a consequence of this plasticity, GoC spontaneous spiking is selectively enhanced, but the gain of evoked spiking is unaffected. Hence this plasticity is well-suited for selectively regulating the tonic output of GoCs rather than their sensory-evoked responses.

Introduction

Mossy fibers provide the main source of sensory input to the cerebellar cortex by exciting granule cells, Golgi cells, and other interneurons in the granule cell layer (Eccles et al., 1967; Ito, 2006). In turn, Golgi cells (GoCs) provide the sole source of inhibition onto granule cells, and can hence regulate activation of both the granule cell layer and ultimately the entire cerebellar cortical circuitry (Eccles et al., 1964).

Cerebellar GoCs characteristically fire spontaneous action potentials (APs) at frequencies between 1 and 20 Hz (Forti et al., 2006; Ruigrok et al., 2011). This produces a continuous barrage of fast inhibitory currents onto both granule cells and other GoCs. The GABA released by GoCs also activates extrasynaptic high-affinity α6 $GABA_A$ receptors on granule cells to produce a tonic inhibitory current (Brickley et al., 1996; Hamann et al., 2002). Recent evidence suggests that this tonic current accounts for the majority of granule cell inhibitory charge *in vivo*, and plays a crucial role in regulating sensory evoked responses (Duguid et al., 2012). In addition to tonically inhibiting granule cells, GoC spiking can inhibit release from mossy fibers by activating presynaptic $GABA_B$ receptors (Mitchell and Silver, 2000). In these ways, the firing rate of GoCs critically determines the ongoing excitability of the granule cell layer.

The rate of GoC firing is also likely important at the behavioral level, as manipulations that alter GoC firing can lead to ataxia in rodents (Cheron et al., 2009; Watanabe and Nakanishi, 2003). Such severe behavioral consequences could arise from an overall change in the level of GoC inhibition provided to the granule cell layer. It is also possible that the tendency of GoCs to fire synchronously as a population depends on the frequency of GoC spontaneous firing (Dugué et al., 2009; Gibson et al., 2005; Vervaeke et al., 2010). Thus, modulating the tonic rate of GoC

firing could provide an important mechanism for regulating activity throughout the granule cell layer.

In this study, we demonstrate that brief hyperpolarization produces a robust long-term increase in the spontaneous firing rate of cerebellar GoCs. This modulation likely involves CaMKII as well as BK-type calcium-activated potassium channels, and is similar to a form of spike rate plasticity termed firing rate potentiation (FRP) that has been described in the vestibular nucleus (Nelson et al., 2003, 2005). Hence, these results suggest that modulation of calcium-activated potassium channels by CaMKII could represent a more widespread mechanism for spontaneously active cells to adjust their activity. However, we find that BK-type channel modulation cannot explain all of the observed plasticity in GoCs. Moreover, we find a strong frequency dependence of the plasticity, with lower initial spike rates allowing larger changes in spiking. Finally, in contrast with cells in the vestibular nucleus, GoC FRP selectively regulates spontaneous spiking without altering the gain of evoked spiking. These data hence suggest that FRP in GoCs is specifically tailored to modulate their tonic inhibitory output rather than their evoked activity.

Materials and Methods

Slices and Recordings

Acute sagittal slices (250 µm thick) were prepared from the cerebellar vermis of postnatal day 17 (P17) - P23 Sprague-Dawley rats of either sex. Slices were cut and stored as described previously (Hull and Regehr, 2012). Visually guided whole-cell recordings were obtained with patch pipettes (3-6 MΩ) pulled from borosilicate capillary glass (World Precision Instruments). Electrophysiological recordings were performed at 31-33º C.

Spontaneous IPSCs (sIPSCs) were recorded at 0 mV using an internal pipette solution containing (in mM): 140 Cs-gluconate, 15 HEPES, 0.5 EGTA, 2 TEA-Cl, 2 MgATP, 0.3 NaGTP, 10 phosphocreatine-$tris_2$, 2 QX 314-Cl, pH = 7.2. Current clamp recordings were performed with an internal solution containing (in mM): 150 K-gluconate, 3 KCl, 10 HEPES, 0.5 EGTA, 3 MgATP, 0.5 GTP, 5 phosphocreatine-$tris_2$, and 5 phosphocreatine-Na_2, pH = 7.2.

For FRP experiments, it was critical to avoid exposing cells to internal solution prior to patching, because this produced a prolonged depolarization block of spiking and greatly reduced the amount of subsequent FRP (likely by pre-inducing plasticity when spiking was blocked). Hence, pipettes were not positioned near the cell prior to patching, and positive pressure was not applied until immediately before approaching to form a seal. To check that cells were not in depolarization block, we recorded in cell-attached mode prior to break-in, and then confirmed after break-in that the spike rate was within 1 Hz of the cell-attached spike rate.

No current was injected to regulate GoC spiking before or after induction of FRP. Current clamp experiments were performed in synaptic blockers of AMPA receptors (NBQX, 5 µM), NMDA receptors (R-CPP, 2.5 µM), $GABA_A$ receptors (picrotoxin, 20 µM), and $GABA_B$ receptors (CGP55845, 1 µM). Voltage clamp experiments used the same drugs, except without picrotoxin. For incubation experiments, slices were placed in the recording chamber and

perfused with the appropriate drug for approximately 30 minutes prior to patching. Drugs were purchased from Sigma-Aldrich, Tocris or Abcam.

Electrophysiolgical data were acquired using a Multiclamp 700B amplifier (Axon Instruments), digitized at 20 kHz with either a National Instruments USB-6229 or ITC-18 board, and filtered at 2 kHz. Acquisition was controlled with custom software written in IgorPro (Matthew Xu-Friedman, SUNY Buffalo).

Analysis

Linear fits were used to describe input/output relationships. Mean AP waveforms were generated by averaging 5 seconds of spikes per condition in each experiment, and then by averaging these mean waveforms across experiments. Changes in the AP waveforms were determined by subtraction of the average waveforms for each individual cell per condition, and then by averaging these subtracted waveforms across cells. These difference waveforms were quantified 2ms after the peak of the AP (ΔVm_{2ms}) to provide a sensitive measure of spike broadening. Changes in the spike after-hyperpolarization (AHP) were quantified at ΔVm_{20ms}, a time where the AHP is near maximal. Data are reported as mean ± SEM, and statistical analysis was carried out using a two-tailed Student's t-test.

Results

Our recent study of the inhibitory connection between GoCs provided a clue that GoC spontaneous activity can be modulated (Hull and Regehr, 2012). We took advantage of the fact that GoCs are the only inhibitory cerebellar interneuron that expresses mGluR2 (Ohishi et al., 1994). Consistent with the known role of mGluR2 in opening potassium channels (Watanabe and Nakanishi, 2003), we found that activating these receptors with APDC reduced evoked inhibition onto other GoCs. Here we find that APDC (2 μM) also reduces the frequency of sIPSCs onto other GoCs (**Figure 6.1A**, 65 ± 8% reduction, n=6). Surprisingly, however, when APDC was washed out of the slice, there was an immediate increase in the rate of sIPSCs onto GoCs (**Figure 6.1A**, 46 ± 27% mean increase). Based on our previous finding that GoCs provide the majority of GABAergic inhibition onto other GoCs, this observation led us to hypothesize that transient APDC application could increase the rate of spontaneous GoC firing.

To test this hypothesis, we recorded GoC spontaneous spiking before, during and after APDC application (2 μ□M for ~ 3 minutes,**Figure 6.1 B**). In these experiments, APDC hyperpolarized GoCs to an average membrane potential of -61 ± 2 mV (n=8). Upon washout of APDC, there was an immediate increase in the rate of GoC spiking. GoCs spike rates then continued to increase for approximately 10 minutes before stabilizing at a rate that was more than 2-fold faster than it had been prior to APDC (148.7 ± 37% increase, 5.2 ± 1.2 to 11.6 ± 1.4 Hz, n=8). This firing rate potentiation (FRP) lasted for the duration of our recordings.

To investigate possible cellular mechanisms underlying this plasticity, we compared the action potential (AP) waveforms in control conditions to those at least 15 minutes after APDC application (**Figure 6.1 C**). By averaging mean AP waveforms across all experiments in control and post-APDC conditions, we observed a consistent decrease in the magnitude of the GoC

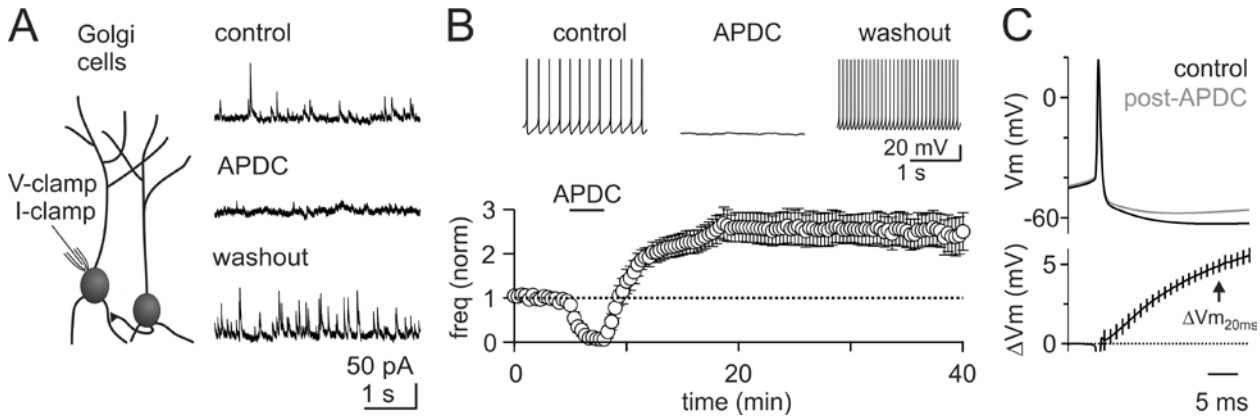

Figure 6.1. Transient activation of GoC mGluR2 receptors increases spontaneous inhibition by producing a long-term increase in tonic spiking. **A** *left*, recording configuration for all experiments. *right*, Voltage-clamp recording of sIPSCs at 0 mV (top). Example recording shows that the mGluR2 agonist APDC reduces the sIPSC rate (middle), and upon washout the sIPSC rate is elevated (bottom). **B** *top***,** current-clamp recording reveals that APDC eliminates GoC spontaneous spiking, and spike rate is elevated upon washout. *Bottom*, Summary timecourse showing the effect of transient mGluR2 activation on the GoC spike rate (n=8). **C** Average AP waveform in control (top, *black*) and 15 minutes post-APDC (top, *blue*) reveals a reduction in the AHP (n=8). *Bottom*. Subtracted AP waveforms illustrating the mean difference (±SEM) quantified 20ms after the AP peak (ΔVm_{20ms}).

after-hyperpolarization (AHP) without any change in the spike width. Subtraction of the mean waveforms (ΔVm) revealed a decrease in the AHP following washout of APDC, as measured 20 ms after the AP peak (ΔVm_{20ms} = 4.9 ± 0.4 mV).

To determine whether mGluR2 activation produced FRP simply by hyperpolarizing GoCs and transiently suppressing their spontaneous firing, or whether a downstream cascade initiated by mGluR2 activation was required, we performed additional current-clamp experiments. Negative current injections for 3 minutes were used to suppress spontaneous firing by hyperpolarizing GoCs to approximately -65 mV (-64 ± 1 mV, n = 20, **Figure 6.2 A**). Following hyperpolarization, there was an immediate increase in GoC spike rates. The spike rates then continued to increase for 10-15 minutes before stabilizing at nearly double the initial control rate (84 ± 14% increase, 4.3 ± 0.5 to 7.9 ± 0.8 Hz, n=20). At the same time, we observed a consistent decrease in the magnitude of the GoC AHP that closely mirrored the timecourse of spike rate increases. There was a consistent decrease in the AHP 15 minutes after hyperpolarization (**Figure 6.2 B**, ΔVm_{20ms} = 2.9 ± 0.3 mV). These experiments indicate that a brief suppression of GoC firing is sufficient to induce FRP, and mGluR2 activation is not required.

The reduction in spike AHP following FRP induction could reflect modulation of an ion channel, or it could simply be a consequence of increased GoC spike rates. To discriminate between these possibilities, we modulated GoC spike rates with positive current injections under control conditions and measured the resulting AP waveform changes (**Figure 6.2 C**). In these experiments, we matched the absolute spike rates to the averages obtained in FRP experiments (4.4 ± 0.1 Hz and 7.7 ± 0.1 Hz, n=11). The waveform changes associated with differences in

Figure 6.2. Transient hyperpolarization induces a long-term increase in GoC spiking and a corresponding decrease in spike AHPs. A *top,* Example experiment showing that a 3 minute negative current injection of -50 pA hyperpolarizes the GoC membrane to approximately -65 mV, and suppresses spiking. An increase in GoC spiking occurred following hyperpolarization. *Bottom,* Summary of all experiments (n=20) where GoCs were hyperpolarized with current injection shows a long-term increase in spontaneous spiking, and a decrease in AHP amplitudes. **B** Mean AP waveform before (*top, black*) and after (*top, blue*) hyperpolarization, and difference waveforms (*bottom*) reveal a reduction in AHPs (n=20). Inset shows 1 second of spiking from an example cell before and after induction of FRP with a 3 min. current injection of -75 pA. **C** Current injection was used to adjust GoC spike to the average mean rates observed before and after hyperpolarization in A. Averaged APs at low frequency (4.4 ± 0.1 Hz, *top black*), high frequency (7.7 ± 0.1 Hz, top red), and the mean difference trace (*bottom, black*) reveals little change in the waveforms at low and high frequency. Inset shows 1 second of spiking from an example cell before and after a 7 pA current injection.

Figure 6.2 (Continued)

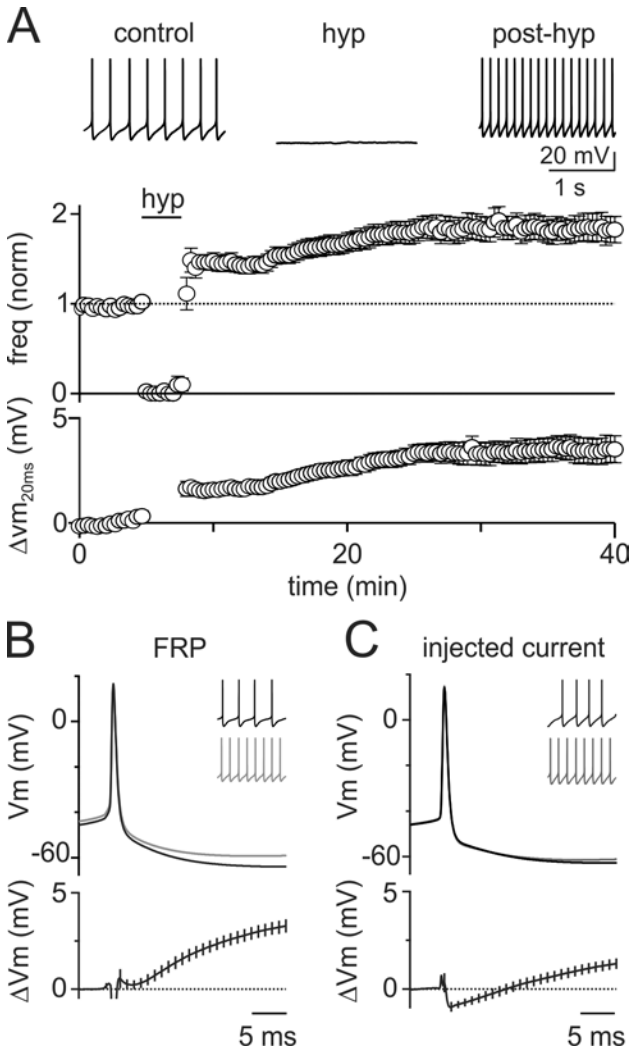

firing frequency were significantly smaller than those associated with FRP (ΔVm_{20ms} = 1.0 ± 0.3 mV, p=0.0003). These data suggest that FRP may involve modulation of the currents underlying the spike AHP.

To investigate the cellular mechanism underlying this AHP change, we began by testing the involvement of CaMKII, which has been implicated in a similar form of spike rate plasticity in the vestibular nucleus (Nelson et al., 2005). In the vestibular nucleus, membrane hyperpolarization reduces CaMKII activity by lowering AP-evoked calcium influx, which in turn leads to a long-term reduction in the overall BK channel conductance by reducing the open probability of individual channels (van Welie and du Lac, 2011). This mechanism decreases the AHP of vestibular nucleus cells, and produces a long-term increase in their spontaneous firing rate (Nelson et al., 2003). If this mechanism also controls GoC FRP, then inhibiting CaMKII should mimic FRP by increasing spontaneous firing rates, and should also occlude subsequent induction of FRP by hyperpolarization.

In GoCs, we found that the CaMKII inhibitor KN-62 (10 μM) increased spike rates to a similar degree as the induction of FRP with hyperpolarization (**Figure 6.3 A**, 65 ± 19 % increase, n=7). This increase in spike rate was also associated with a decrease in the GoC AHP, similar to what was observed during FRP (ΔVm_{20ms} = 3.1 ± 0.5 mV, p=0.736). Moreover, incubation of slices in KN-62 largely occluded hyperpolarization-evoked FRP (**Fi ure 6.3 B**, freq. = 19 ± 8 % of control, n=6), and produced a much smaller change in the AHP following hyperpolarization as compared to controls (ΔVm_{20ms} = 1.3 ± 0.5 mV, p=0.012). These data suggest that GoC FRP involves a CaMKII-dependent long term modification of an ion channel involved in the GoC AHP.

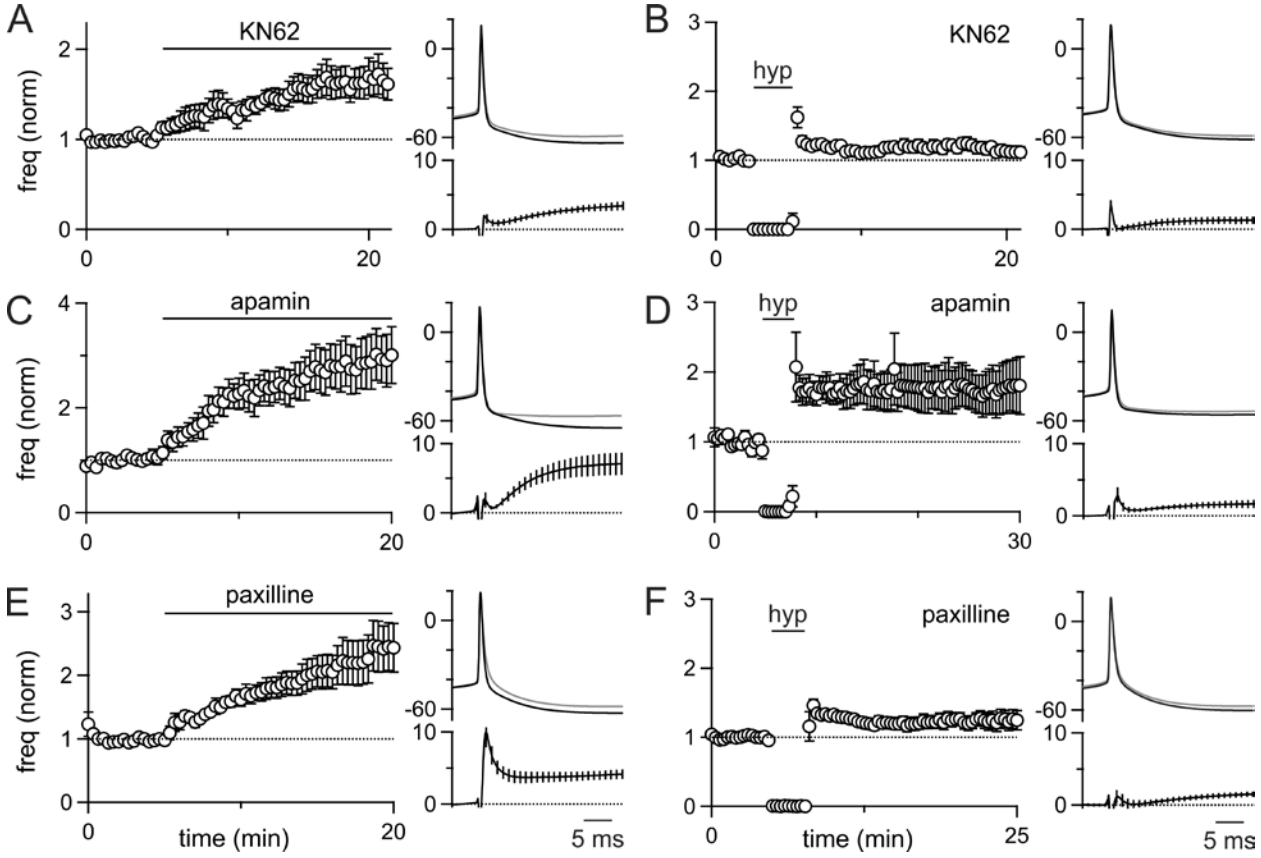

Figure 6.3. Firing rate potentiation involves CaMKII and BK-type potassium channels. Current-clamp experiments were performed in which the spontaneous firing of GoCs and the GoC spike waveform was monitored. The wash-in effect of the CaMKII inhibitor KN-62 (**A**, n=7), the SK-type potassium channel antagonist apamin (**C**, n=7) and the BK-type potassium channel inhibitor paxilline (**E**, n=10) were assessed. The effect of a 3 minute somatic hyperpolarization was also assessed in slices incubated in the presence of KN-62 (**B**, n=6), apamin (**D**, n=10) and paxilline (**F**, n=17).

To identify the target of CaMKII modulation, we focused on GoC conductances known to regulate spontaneous firing and contribute to their AHP. We therefore tested the role of small and large conductance calcium-activated potassium channels (SK and BK channels, respectively), both of which are present in GoCs (Forti et al., 2006). Application of the selective SK channel antagonist apamin (150 nM) significantly increased spontaneous GoC firing (192 ± 50% increase, n=7), and greatly reduced the GoC AHP (ΔVm_{20ms} = 6.9 ± 1.5 mV) (**Figure 6.3 C**). Many GoCs that were incubated in apamin entered a sustained depolarized state and were unable to fire normal rhythmic action potentials (6/16). In GoCs that fired spontaneously in the presence of apamin, hyperpolarization was still able to evoke FRP (**Fig. 3D**, 76 ± 36% increase, n=10), suggesting that the bulk of FRP is not a consequence of SK channel modulation. Changes in the AHP following hyperpolarization, however, were smaller than in controls (ΔVm_{20ms} = 1.6 ± 0.5 mV, p=0.036) (**Figure 6.3 D**). These data suggest that following the dramatic decrease in the GoC AHP when SK channels are blocked, additional small changes in the AHP can significantly change the overall spike rate.

We also examined the involvement of BK channels in FRP. The selective BK-channel antagonist paxilline (10 µM) increased GoC spike rates more than 2-fold (**Figure 6.3 E**, 145 ± 38% increase, n=10), and greatly reduced the GoC AHP (ΔVm_{20ms} = 4.0 ± 0.6 mV). In addition, paxilline also broadened the APs (control ΔVm_{2ms} = 0.3 ± 0.2 mV, paxilline ΔVm_{2ms} = 6.8 ± 1.3 mV, p=0.0001). Paxilline incubation, however, largely occluded FRP (**Figure 6.3 F**, 24 ± 13% increase, n=17), and there was very little change in the GoC AHP following hyperpolarization compared with controls (ΔVm_{20ms} = 1.3 ± 0.4 mV, p=0.0025).

It was not always possible to test the contribution of different channel types to FRP using pharmacology. For example, the role of I_h in FRP could not be assessed because the selective I_h blocker ZD7288 disrupted firing and led to unstable, depolarized membrane potentials along with prolonged membrane oscillations following FRP induction. We also tried to determine whether simultaneous blockade of SK and BK channels led to a more complete suppression of FRP. However, co-application of paxilline and apamin had such a profound effect on membrane repolarization that most GoCs went into a depolarized state and could not fire action potentials. These findings indicate that stable spontaneous activity in GoCs involves multiple channels, and removing more than one channel type critically destabilizes their pacemaking ability. Moreover, these findings place practical limitations on the use of pharmacological approaches to study the role of ion channels in FRP.

Our findings suggest that the mechanism of FRP in GoCs has many similarities to the FRP previously described in vestibular nucleus neurons. These similarities include a comparable decrease in the AHP, insensitivity to SK channel blockade, and occlusion of FRP by BK channel blockade. However, in GoCs we find that paxilline both reduces the spike AHP and broadens the spikes. These data suggest that BK channels with both fast and slow kinetics are present in GoCs, and that the contributions of BK channels to GoC firing might be complex.

To clarify the role of BK channels in GoC FRP, we performed additional experiments. First, we sought to resolve the differential effect of paxilline and FRP on the GoC action potential by applying paxilline after FRP induction. In contrast with experiments where paxilline was applied without inducing FRP, we found that paxilline had a very small effect on the AHP following FRP induction (ΔVm_{20ms} = 1.8 ± 0.4 mV, p=0.0061). Furthermore, paxilline did not

further increase GoC firing rates above FRP levels (**Figure 6.4 A**, FRP =170 ± 42% of control, paxilline = 167 ± 41% of control, n=7). However, paxilline still had a large effect on the width of APs (ΔVm_{2ms} = 5.0 ± 1.2 mV). This selective effect on AP width was quite different from the effect of paxilline application before inducing FRP, which both broadened APs and reduced the spike AHP (**Figure 6.4 B**). These experiments reveal that the slow component of the AHP modulated by FRP is much smaller than the total paxilline-sensitive component of the AHP (**Figure 6.4 B,** arrow). In addition, they suggest that paxilline blocks BK channel subtypes with both fast and slow kinetics (Brenner et al., 2005), while FRP involves a selective modulation of a subset of slow BK channels active during the AHP.

The finding that BK channels can contribute both rapidly to the width of APs and more slowly to spike AHPs is consistent with the behavior of these channels in other cell types. Previous studies have established that the presence or absence of the β4 subunit can influence the kinetics of BK channels (Brenner et al., 2005). The peptide inhibitor iberiotoxin is thought to target a subset of BK channels lacking the β4 subunit (Meera et al., 1997), and is thus a promising tool for identifying the subpopulation of BK channels that specifically contribute to FRP. In the vestibular nucleus, iberiotoxin selectively affects the slow AHP and completely occludes FRP (Nelson et al., 2003).

To segregate the contribution of distinct subtypes of BK channels to GoC FRP, we tested the effects of iberiotoxin on GoC spiking and plasticity. Iberiotoxin (150 nM) increased the spike rate of GoCs (**Figure 6.4 C**, 124 ± 36% increase, n=7), and reduced the GoC spike AHP (ΔVm_{20ms} = 2.5 ± 0.3 mV) without broadening the AP waveform (ΔVm_{2ms} = 0.3 ± 0.2 mV). However, when slices were incubated in iberiotoxin, membrane hyperpolarization still produced

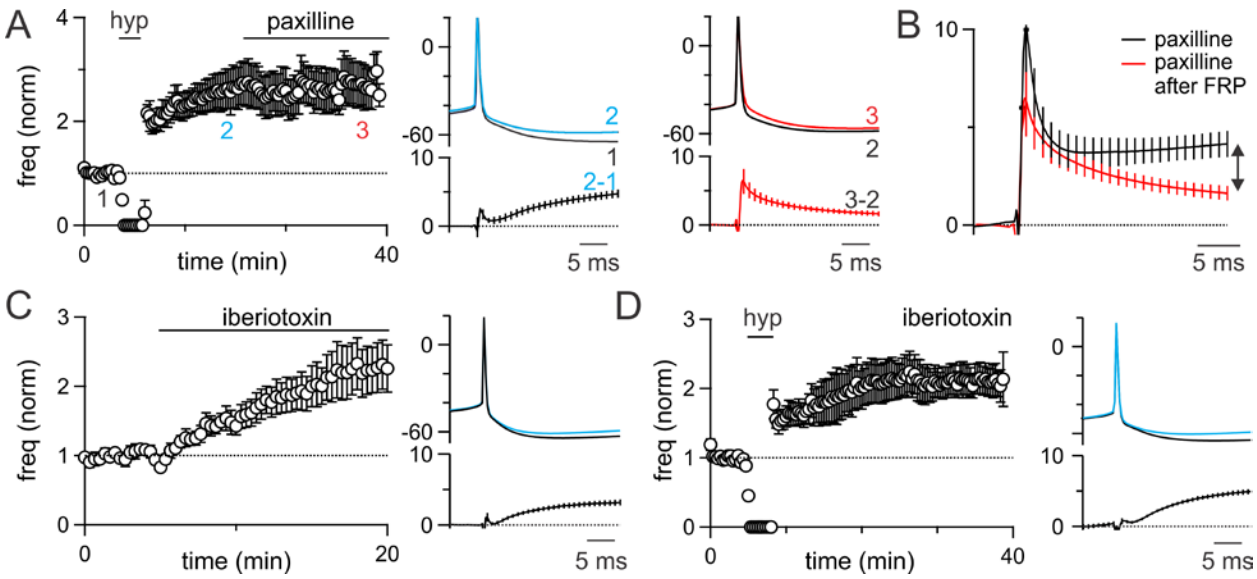

Figure 6.4 GoC FRP involves a sub-set of BK-type potassium channels A *left,* Paxilline was applied following the induction of FRP (n=7). *Right,* FRP reduced the spike AHP (blue), while paxilline selectively broadened the AP (red). **B** Comparison of the difference waveforms for paxilline applied without FRP induction (*black, from Fig. 3*) and following FRP induction (*red*) reveals that paxilline has a much larger effect on the AHP (later time points) when applied without inducing FRP. The paxilline sensitive component of FRP is small and late in the AHP (double arrow). **C** Iberiotoxin wash-in elevates the spike rate of GoCs, and selectively decreases the spike AHP. **D** Iberiotoxin incubation does not occlude FRP, and the spike AHP is still significantly reduced following induction of plasticity.

robust FRP (**Figure 6.4 D**, FRP = 111 ± 22% of control, n=8) and a decrease in the spike AHP (ΔVm_{20ms} = 3.2 ± 0.4 mV). It is surprising that FRP remained intact in the presence of iberiotoxin given that 1) paxilline blocked FRP, 2) iberiotoxin selectively decreased the AHP without affecting the spike width, and 3) iberiotoxin completely occludes FRP in the vestibular nucleus (Nelson et al., 2003).

These surprising differences between BK channel antagonists led us to re-examine our FRP experiments and test whether any other recording parameter might provide further insight to our pharmacological manipulations. Hence, we tested the role of initial spike rate in all our experiments on an individual cell basis (**Figure 6.5**). We first examined the firing rate of GoCs following each pharmacological drug wash-in as a function of initial spike rate (**Figure 6.5 A**). For wash-ins of each drug, this analysis revealed a strong correlation, with lower initial spike rates favoring larger rate enhancements. At initial spike rates greater than 5 Hz, there was little or no increase in spiking in for drug wash-ins.

These data led us to question whether FRP might have a similar frequency dependence. For FRP induced with both hyperpolarization and APDC, also found that lower initial spike rates led to larger FRP (**Figure 6.5 B**). In these experiments, however, even spike rates above 5 Hz consistently lead to an approximately 50% enhancement of spiking (FRP, >5 Hz initial spike rate: 52 ± 8% of control, n=9). These data suggest that some of the differences we observed between pharmacological conditions may involve variability in the initial spike rates. Therefore, we next examined the magnitude of FRP in different drug conditions as a function of initial spike rates (**Figure 6.5 C**).

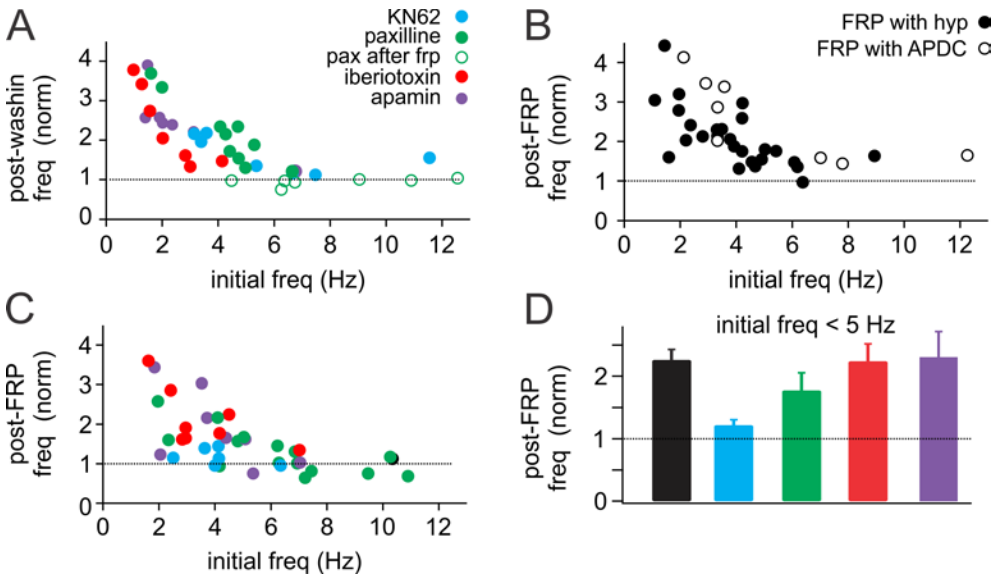

Figure 6.5. The magnitude of GoC FRP depends on initial firing rate. A In all drug wash-ins, the increase in firing rate was greatest for cells with low initial firing rates. Little or no increase in firing rate was observed for initial firing rates above 5 Hz. **B** The magnitude of FRP was also dependent on initial firing rates, with lower firing rates producing the largest FRP. However, FRP was present at initial rates above 5 Hz. **C** For most drug conditions, FRP was also dependent on initial firing rate, and little or no FRP was evident for initial firing rates greater than 5 Hz. **D** Summary of FRP magnitude for cells with initial firing rates below 5 Hz. While FRP was still occluded by KN62, the effect of paxilline was reduced in cells with lower initial firing rates.

For most drug conditions, we observed larger FRP following lower initial spike rates (**Figure 6.5 C**). In addition, we observed little or no enhancement of spiking in any drug condition where initial spike rates were above 5 Hz. Interestingly, while apamin and iberiotoxin increased spike rates to a similar extent as paxilline in our wash-in experiments (**Figures 6.3, 6.4**), we found very few cells with spike rates above 5 Hz in apamin or iberiotoxin after incubation of slices in these drugs. These data may suggest some type of compensation that allows spike rates to return to near control levels after extended periods of SK or β4-lacking BK channel blockade. To determine whether variability in the initial spike rates could affect our interpretation of FRP experiments in various drug conditions, we re-analyzed our FRP data for all cells with initial spike rates lower than 5 Hz (**Figure 6.5 D**).

FRP induced by hyperpolarization (control) was increased in cells with initial spike rates below 5 Hz (control FRP = 127 ± 17%, n=20). However, KN62 still largely occluded FRP in this restricted population (FRP = 21 ± 9% of control, n=5). In contrast, paxilline had less impact on FRP for cells with low initial firing rates (FRP = 77 ± 28% of control, n=5). As in the total population, apamin and iberiotoxin had no significant effect on FRP (apamin FRP = 130 ± 41% of control, n=5, p=0.925, iberiotoxin FRP = 123 ± 28% of control, n=7, p=0.930). While FRP in paxilline was still somewhat reduced relative to control cells that had initial spike rates below 5 Hz, these data suggest that BK channel modulation cannot account for the all of the FRP in GoCs.

To further explore the conditions required for inducing FRP in GoCs, we tested the duration of hyperpolarization necessary for plasticity (**Figure 6.6**). Spike rates were stable in the absence of hyperpolarization (1 ± 20% of control, n=8, **Figure 6.6 A**), or following 5 s of

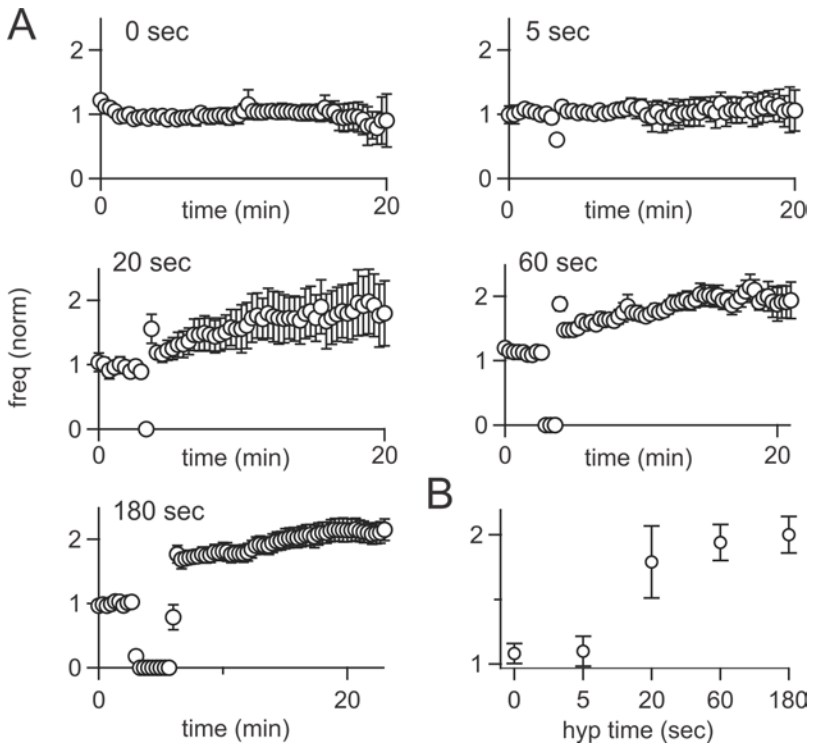

Figure 6.6. Time dependence of FRP induction. A GoC spike rates were recorded following hyperpolarizations of 0 (n=8), 5 (n=6), 20 (n=10), 60 (n=15) and 180 (n=22) seconds. While 5 second hyperpolarizations did not increase spike rates, longer durations each produced a nearly 2-fold increase in spiking. Note that data points represent 20 second intervals, resulting a non-zero spiking value for 5 seconds of hyperpolarization **B** Summary of GoC spike rates as a function of hyperpolarization time.

hyperpolarization (8 ± 23% of control, n=6). In contrast, hyperpolarizing for 20 s induced robust FRP (84 ± 45% increase, n=10). This plasticity was slightly less, but not significantly different from FRP induced by 1 minute (97 ± 19 % increase, n = 15, p=0.766) or 3 minutes of hyperpolarization (112 ± 17% increase, n=22, p=0.472 **Figure 6.6 B**). Hence, a hyperpolarization of just 20 s is sufficient to induce large increases in GoC spiking.

To explore the consequences of FRP on GoC function, we tested their responses to injected current (F/I curves) before and after induction of FRP (**Figure 6.7**). In the vestibular nucleus, FRP prominently increases the slope of F/I curves (Nelson et al., 2003), which is thought to be important for setting the gain of the vestibulo-ocular reflex (VOR) at the behavioral level. In GoCs, however, we find that FRP produces only an offset change in the F/I relationship (control intercept = 1.67 ± 1.10 Hz, FRP intercept = 5.03 ± 1.43 Hz, n=10), without altering the slopes of the F/I curves (control slope = 0.078 ± 0.006 Hz/pA, FRP slope = 0.077 ± 0.007 Hz/pA, p=0.91). Hence, FRP produces the largest differences in firing rate in response to the smallest current injections, and there is essentially no change in the firing evoked by large current injections. These data suggest that FRP will play a primary role in regulating the tonic output of GoCs, but will have little influence on their sensory-evoked output.

Discussion

Here we have shown that a brief hyperpolarization leads to a robust long-term increase in the spontaneous firing rate of cerebellar GoCs. Previously, FRP had only been observed in the vestibular nucleus (Nelson et al., 2003, 2005). Our findings therefore suggest that this form of

Figure 6.7. FRP alters the offset but not the gain of GoC input/output transformations. A Example experiment showing the responses to injected current for a GoC before (*black*) and 15 minutes after (*blue*) inducing FRP with a 3 min. hyperpolarization. While FRP doubles the spontaneous spike rate, it has little influence on responses to injected current. **B** *top*, Summary of input/output relationships for injected current before and after inducing FRP with hyperpolarization. Lines represent linear fits to the averaged data (n=10). The mean slope prior to hyperpolarization was 0.078 ± 0.006 Hz/pA, and 15 minutes after hyperpolarization was 0.077 ± 0.007 Hz/pA, indicating that FRP does not change the gain of transmission. *Bottom*, Ratio of the firing rate evoked by a current injection (after inducing FRP)/ (before inducing FRP) reveals that the largest increase in spiking after induction of FRP occurs with no injected current, and this difference falls off rapidly with increasing current steps.

Figure 6.7 (Continued)

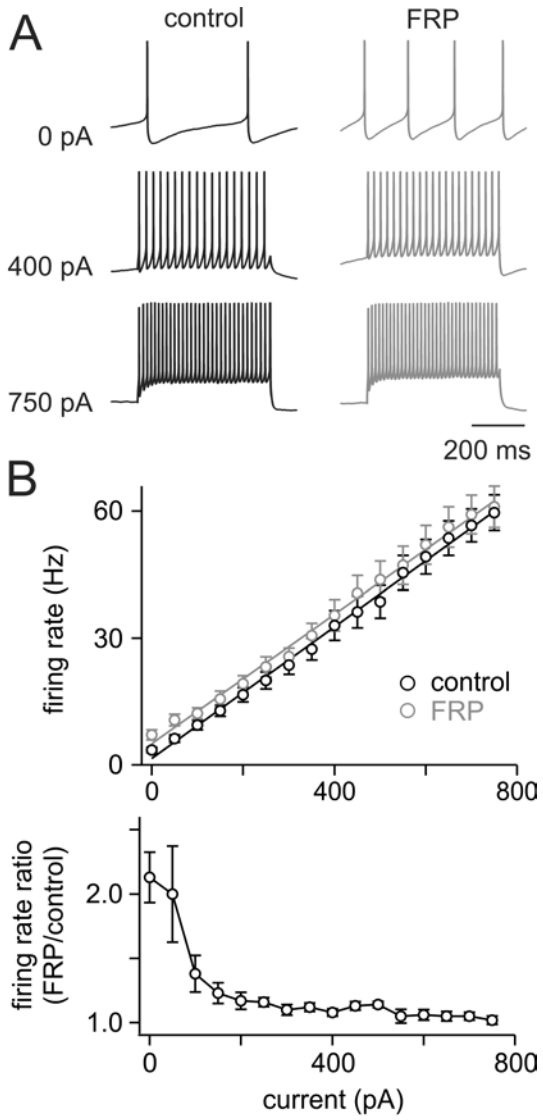

plasticity may be a more widespread means of regulating spontaneously active neurons. Despite sharing many similarities, however, the underlying mechanism of FRP and its influence on input/output transformations is markedly different in cerebellar GoCs. Here, we find that iberiotoxin-sensitive BK-type channels do not underlie plasticity as they do in the vestibular nucleus. Furthermore, GoC FRP selectively increases spontaneous firing rates without altering the gain of evoked transmission. Thus, FRP in GoCs is specialized to preferentially enhance tonic spiking while minimally altering evoked spiking.

Mechanism of FRP

The basic mechanism of FRP in GoCs shares some similarities to what has been described in neurons of the vestibular nucleus (Nelson et al., 2003, 2005). In both instances, FRP decreases the amplitude of spike AHPs, and these changes are largely occluded by inhibiting CaMKII. It therefore seems likely that FRP in GoCs also results from a decrease in CAMKII activation during hyperpolarization when AP-evoked calcium levels are reduced. However, in contrast with the vestibular nucleus, iberiotoxin-sensitive BK-type channels do not appear to contribute to FRP in GoCs, and blocking paxilline-sensitive BK channels can only partially occlude plasticity. Hence, our data suggest that in GoCs not all FRP is accounted for by a long-term reduction in BK channel activation, and that plasticity in these cells may be more complicated. It seems likely that GoC FRP results from the CaMKII-dependent regulation of multiple channel types, which could include a subset of BK channels involved in the spike AHP, or possibly the specific calcium channels that regulate their opening.

We find that FRP can be induced by hyperpolarizations as short as 20 seconds. This induction timecourse is consistent with the observation that CaMKII is only active for tens of seconds following depolarization-induced calcium influx (Lee et al., 2009). Furthermore, this short period of hyperpolarization may allow multiple types of GoC inputs to produce firing rate enhancement, depending on how this plasticity operates *in vivo*.

One possibility is that this plasticity acts as a homeostatic mechanism to keep GoC firing within an optimal range by elevating activity in response to a tonic inhibitory input, or by compensating for variability in potassium channel expression. This possibility seems to agree with our finding that GoC FRP is highly frequency dependent, and can increase lower spike rates to a much greater extent than rates above 5 Hz.

Another possibility, which is not mutually exclusive, is that GoC FRP is preferentially engaged by an acute inhibitory input and serves to dynamically regulate spiking. This could include a GABAergic or glycinergic synaptic input, mGluR2 activation, or possibly a neuromodulatory input. While GoCs do not receive the same type of powerful synaptic inhibition that vestibular nucleus cells receive from Purkinje cell synapses, they do receive inhibition from multiple other GoCs. This inhibition may be sufficient to suppress spiking *in vivo* on a timescale of 20 seconds. In fact, previous *in vivo* work has shown that the predominant response of GoCs to brief, single tactile stimuli is a depression of firing which lasts a few hundred milliseconds (Holtzman et al., 2006; Xu and Edgley, 2010). While the mechanism of this inhibition is not known, it seems reasonable that repetitive stimuli could lead to a depression of firing that lasts for 10s of seconds and would be appropriate for activating GoC FRP. Future

studies will be required to clarify the physiological conditions necessary for inducing FRP in GoCs.

Functional Consequences of FRP

It is remarkable that the effect on input/output transformations is so different in GoCs as compared to neurons in the vestibular nucleus despite sharing a similar mechanism. While both cell types exhibit a prominent increase in spontaneous activity, only the vestibular neurons have an increase in the gain of transmission (Nelson et al., 2003). This gain change is well suited to their physiological role in regulating the gain of the vestibulo-ocular reflex (VOR) (Bagnall et al., 2008). GoCs, however, do not appear to be involved in such a computation, and FRP accordingly produces no change in their gain of transmission. The differences between these two cell types illustrate the importance of the entire complement of ion channels in a neuron for determining the outcome of modulating a particular channel.

The observation that FRP preferentially affects spontaneous firing in GoCs suggests that this plasticity is tailored for modulating the level of tonic GABA release without dramatically changing the levels of fast, sensory-evoked inhibition they produce. Previous studies suggest that such an increase in tonic GoC spiking will significantly decrease the response of granule cells to mossy fiber inputs by activating α6-containing GABA receptors on granule cells (Chadderton et al., 2004; Crowley et al., 2009; Hamann et al., 2002; Mitchell and Silver, 2003), and possibly by increasing presynaptic inhibition of mossy fibers boutons (Mitchell and Silver, 2000). Recent *in vivo* work suggests that modulating tonic granule cell inhibition could play an important role in

regulating the signal-to-noise ratio of sensory-evoked transmission from mossy fibers (Duguid et al., 2012). GoC FRP may thus provide a mechanism to achieve this type of modulation, and hence regulate sensory processing in the cerebellar cortex.

References

Abbott, L.F., and Regehr, W.G. (2004). Synaptic computation. Nature *431*, 796–803.

Abbott, A.L.F., Varela, J.A., Sen, K., and Nelson, S.B. (1997). Synaptic Depression and Cortical Gain Control. Science *275*, 220–224.

Agler, H.L., Evans, J., Tay, L.H., Anderson, M.J., Colecraft, H.M., and Yue, D.T. (2005). G protein-gated inhibitory module of N-type (Ca(v)2.2) Ca2+ channels. Neuron *46*, 891–904.

Anwyl, R. (1999). Metabotropic glutamate receptors: electrophysiological properties and role in plasticity. Brain Res. Brain Res. Rev. *29*, 83–120.

Ariel, P., and Ryan, T. a (2010). Optical mapping of release properties in synapses. Front. Neural Circuits *4*, 1–10.

Asztely, F., Erdemli, G., and Kullmann, D.M. (1997). Extrasynaptic Glutamate Spillover in the Hippocampus: Dependence on Temperature and the Role of Active Glutamate Uptake. Neuron *18*, 281–293.

Augustine, G.J. (2001). How does calcium trigger neurotransmitter release? Curr. Opin. Neurobiol. *11*, 320–326.

Augustine, G.J., Santamaria, F., Tanaka, K., and Carolina, N. (2003). Local Calcium Signaling in Neurons Review. *40*, 331–346.

Bacaj, T., Wu, D., Yang, X., Morishita, W., Zhou, P., Xu, W., Malenka, R.C., and Südhof, T.C. (2013). Synaptotagmin-1 and synaptotagmin-7 trigger synchronous and asynchronous phases of neurotransmitter release. Neuron *80*, 947–959.

Bagnall, M.W., McElvain, L.E., Faulstich, M., and du Lac, S. (2008). Frequency-independent synaptic transmission supports a linear vestibular behavior. Neuron *60*, 343–352.

Beaumont, V., Llobet, A., and Lagnado, L. (2005). Expansion of calcium microdomains regulates fast exocytosis at a ribbon synapse. Proc. Natl. Acad. Sci. U. S. A. *102*, 10700–10705.

Berridge, M.J., Bootman, M.D., and Roderick, H.L. (2003). Calcium signalling: dynamics, homeostasis and remodelling. Nat. Rev. Mol. Cell Biol. *4*, 517–529.

Blackmer, T., Larsen, E.C., Takahashi, M., Martin, T.F., Alford, S., and Hamm, H.E. (2001). G protein betagamma subunit-mediated presynaptic inhibition: regulation of exocytotic fusion downstream of Ca2+ entry. Science *292*, 293–297.

Borst, J.G., and Sakmann, B. (1999). Effect of changes in action potential shape on calcium currents and transmitter release in a calyx-type synapse of the rat auditory brainstem. Philos. Trans. R. Soc. Lond. B. Biol. Sci. *354*, 347–355.

Borst, J.G.G., and Sakmann, B. (1996). Calcium influx and transmitter release in a fast CNS synapse. Nature *383*, 431–434.

Borst, J.G.G., and Soria van Hoeve, J. (2012). The calyx of held synapse: from model synapse to auditory relay. Annu. Rev. Physiol. *74*, 199–224.

Brenner, R., Chen, Q.H., Vilaythong, A., Toney, G.M., Noebels, J.L., and Aldrich, R.W. (2005). BK channel beta4 subunit reduces dentate gyrus excitability and protects against temporal lobe seizures. Nat. Neurosci. *8*, 1752–1759.

Brenowitz, S.D., and Regehr, W.G. (2007). Reliability and heterogeneity of calcium signaling at single presynaptic boutons of cerebellar granule cells. J. Neurosci. *27*, 7888–7898.

Brickley, S.G., Cull-Candy, S.G., and Farrant, M. (1996). Development of a tonic form of synaptic inhibition in rat cerebellar granule cells resulting from persistent activation of GABAA receptors. J. Physiol. *497 (Pt 3*, 753–759.

Brose, N., Petrenko, A.G., Südhof, T.C., and Jahn, R. (1992). Synaptotagmin: a calcium sensor on the synaptic vesicle surface. Science *256*, 1021–1025.

Brown, S.P., Safo, P.K., and Regehr, W.G. (2004). Endocannabinoids inhibit transmission at granule cell to Purkinje cell synapses by modulating three types of presynaptic calcium channels. J. Neurosci. *24*, 5623–5631.

Brust, T.B., Cayabyab, F.S., Zhou, N., and MacVicar, B.A. (2006). p38 mitogen-activated protein kinase contributes to adenosine A1 receptor-mediated synaptic depression in area CA1 of the rat hippocampus. J. Neurosci. *26*, 12427–12438.

Burgalossi, A., Jung, S., Meyer, G., Jockusch, W.J., Jahn, O., Taschenberger, H., O'Connor, V.M., Nishiki, T., Takahashi, M., Brose, N., et al. (2010). SNARE protein recycling by αSNAP and βSNAP supports synaptic vesicle priming. Neuron *68*, 473–487.

Caillard, O., Moreno, H., Schwaller, B., Llano, I., Celio, M.R., and Marty, a (2000). Role of the calcium-binding protein parvalbumin in short-term synaptic plasticity. Proc. Natl. Acad. Sci. U. S. A. *97*, 13372–13377.

Van Calker, D., Muller, M., and Hamprecht, B. (1979). Adenosine regulates via two different types of receptors, the accumulation of cyclic AMP in cultured brain cells. J. Neurochem. *33*, 999–1005.

Catterall, W.A., Leal, K., and Nanou, E. (2013). Calcium channels and short-term synaptic plasticity. J. Biol. Chem. *288*, 10742–10749.

Chadderton, P., Margrie, T.W., and Häusser, M. (2004). Integration of quanta in cerebellar granule cells during sensory processing. Nature *428*, 856–860.

Chard, P.S., Jordán, J., Marcuccilli, C.J., Miller, R.J., Leiden, J.M., Roos, R.P., and Ghadge, G.D. (1995). Regulation of excitatory transmission at hippocampal synapses by calbindin D28k. Proc. Natl. Acad. Sci. U. S. A. *92*, 5144–5148.

Cheron, G., Sausbier, M., Sausbier, U., Neuhuber, W., Ruth, P., Dan, B., and Servais, L. (2009). BK channels control cerebellar Purkinje and Golgi cell rhythmicity in vivo. PLoS One *4*, e7991.

Cochilla, a J., and Alford, S. (1998). Metabotropic glutamate receptor-mediated control of neurotransmitter release. Neuron *20*, 1007–1016.

Cohen, M.W., Jones, O.T., and Angelides, K.J. (1991). Distribution of Ca2+ channels on frog motor nerve terminals revealed by fluorescent omega-conotoxin. J. Neurosci. *11*, 1032–1039.

Cole, J.C., Villa, B.R.S., and Wilkinson, R.S. (2014). Rapid Report Disruption of actin impedes transmitter release in snake motor terminals. 579–586.

Cooper, R.L., Winslow, J.L., Govind, C.K., and Atwood, H.L. (1996). Synaptic structural complexity as a factor enhancing probability of calcium-mediated transmitter release. J. Neurophysiol. *75*, 2451–2466.

Crowley, J.J., Fioravante, D., and Regehr, W.G. (2009). Dynamics of fast and slow inhibition from cerebellar golgi cells allow flexible control of synaptic integration. Neuron *63*, 843–853.

Cuttle, M.F., Tsujimoto, T., Forsythe, I.D., and Takahashi, T. (1998). Facilitation of the presynaptic calcium current at an auditory synapse in rat brainstem. J. Physiol. *512 (3)*, 723–729.

Daniel, H., and Crepel, F. (2001). Control of Ca(2+) influx by cannabinoid and metabotropic glutamate receptors in rat cerebellar cortex requires K(+) channels. J. Physiol. *537*, 793–800.

Daniel, H., Rancillac, a, and Crepel, F. (2004). Mechanisms underlying cannabinoid inhibition of presynaptic Ca2+ influx at parallel fibre synapses of the rat cerebellum. J. Physiol. *557*, 159–174.

Denker, A., Bethani, I., Kröhnert, K., Körber, C., Horstmann, H., Wilhelm, B.G., Barysch, S. V, Kuner, T., Neher, E., and Rizzoli, S.O. (2011a). A small pool of vesicles maintains synaptic activity in vivo. Proc. Natl. Acad. Sci. U. S. A. *108*, 17177–17182.

Denker, A., Kröhnert, K., Bückers, J., Neher, E., and Rizzoli, S.O. (2011b). The reserve pool of synaptic vesicles acts as a buffer for proteins involved in synaptic vesicle recycling. Proc. Natl. Acad. Sci. U. S. A. *108*, 17183–17188.

Diamond, J.S., and Jahr, C.E. (2000). Synaptically Released Glutamate Does Not Overwhelm Transporters on Hippocampal Astrocytes During High-Frequency Stimulation. J Neurophysiol *83*, 2835–2843.

Dittman, J.S., and Regehr, W.G. (1996). Contributions of calcium-dependent and calcium-independent mechanisms to presynaptic inhibition at a cerebellar synapse. J. Neurosci. *16*, 1623–1633.

Dittman, J.S., and Regehr, W.G. (1997). Mechanism and kinetics of heterosynaptic depression at a cerebellar synapse. J. Neurosci. *17*, 9048–9059.

Dittman, J.S., and Regehr, W.G. (1998). Calcium dependence and recovery kinetics of presynaptic depression at the climbing fiber to Purkinje cell synapse. J. Neurosci. *18*, 6147–6162.

Dittman, J.S., Kreitzer, a C., and Regehr, W.G. (2000). Interplay between facilitation, depression, and residual calcium at three presynaptic terminals. J. Neurosci. *20*, 1374–1385.

Dobrunz, L.E., and Stevens, C.F. (1997). Heterogeneity of release probability, facilitation, and depletion at central synapses. Neuron *18*, 995–1008.

Dodge, F.A.J., and Rahamimoff, R. (1967). Co-operative action of calcium ions in transmitter release at the neuromuscular junction. J. Physiol. *193*, 419–432.

Dolphin, A.C., Forda, S.R., and Scott, R.H. (1986). Calcium-dependent currents in cultured rat dorsal root ganglion neurones are inhibited by an adenosine analogue. J. Physiol. *373*, 47–61.

Dugué, G.P., Brunel, N., Hakim, V., Schwartz, E., Chat, M., Lévesque, M., Courtemanche, R., Léna, C., and Dieudonné, S. (2009). Electrical coupling mediates tunable low-frequency oscillations and resonance in the cerebellar Golgi cell network. Neuron *61*, 126–139.

Duguid, I., Branco, T., London, M., Chadderton, P., and Häusser, M. (2012). Tonic inhibition enhances fidelity of sensory information transmission in the cerebellar cortex. J. Neurosci. *32*, 11132–11143.

Dutar, P., and Nicoll, R. a (1988). Pre- and postsynaptic GABAB receptors in the hippocampus have different pharmacological properties. Neuron *1*, 585–591.

Eggermann, E., Bucurenciu, I., Goswami, S.P., and Jonas, P. (2012). Nanodomain coupling between Ca^{2+} channels and sensors of exocytosis at fast mammalian synapses. Nat. Rev. Neurosci. *13*, 7–21.

Elmqvist, B.Y.D., and Quastel, D.M.J. (1965). A quantitave study of end-plate potentials in isolated human muscle. J. Physiol. *178*, 505–529.

Fedchyshyn, M.J., and Wang, L.-Y. (2005). Developmental transformation of the release modality at the calyx of Held synapse. J. Neurosci. *25*, 4131–4140.

Fernández-Chacón, R., Königstorfer, a, Gerber, S.H., García, J., Matos, M.F., Stevens, C.F., Brose, N., Rizo, J., Rosenmund, C., and Südhof, T.C. (2001). Synaptotagmin I functions as a calcium regulator of release probability. Nature *410*, 41–49.

Fogelson, A.L., and Zucker, R.S. (1985). Presynaptic calcium diffusion from various arrays of single channels. Implications for transmitter release and synaptic facilitation. Biophys. J. *48*, 1003–1017.

Forsythe, I.D., Tsujimoto, T., Barnes-Davies, M., Cuttle, M.F., and Takahashi, T. (1998). Inactivation of presynaptic calcium current contributes to synaptic depression at a fast central synapse. Neuron *20*, 797–807.

Forti, L., Cesana, E., Mapelli, J., and D'Angelo, E. (2006). Ionic mechanisms of autorhythmic firing in rat cerebellar Golgi cells. J. Physiol. *574*, 711–729.

García, D.E., Li, B., García-Ferreiro, R.E., Hernández-Ochoa, E.O., Yan, K., Gautam, N., Catterall, W. a, Mackie, K., and Hille, B. (1998). G-protein beta-subunit specificity in the fast membrane-delimited inhibition of Ca2+ channels. J. Neurosci. *18*, 9163–9170.

Geppert, M., Goda, Y., Hammer, R.E., Li, C., Rosahl, T.W., Stevens, C.F., and Südhof, T.C. (1994). Synaptotagmin I: A major Ca2+ sensor for transmitter release at a central synapse. Cell *79*, 717–727.

Gerachshenko, T., Blackmer, T., Yoon, E.-J., Bartleson, C., Hamm, H.E., and Alford, S. (2005). Gbetagamma acts at the C terminus of SNAP-25 to mediate presynaptic inhibition. Nat. Neurosci. *8*, 597–605.

Gibson, J.R., Beierlein, M., and Connors, B.W. (2005). Functional properties of electrical synapses between inhibitory interneurons of neocortical layer 4. J. Neurophysiol. *93*, 467–480.

Gilman, A.G. (1987). G proteins: transducers of receptor-generated signals. Annu. Rev. Biochem. *56*, 615–649.

Hamann, M., Rossi, D.J., and Attwell, D. (2002). Tonic and spillover inhibition of granule cells control information flow through cerebellar cortex. Neuron *33*, 625–633.

Hamid, E., Church, E., Wells, C.A., Zurawski, Z., Hamm, H.E., and Alford, S. (2014). Modulation of neurotransmission by GPCRs is dependent upon the microarchitecture of the primed vesicle complex. J. Neurosci. *34*, 260–274.

Helmchen, F., Borst, J.G., and Sakmann, B. (1997). Calcium dynamics associated with a single action potential in a CNS presynaptic terminal. Biophys. J. *72*, 1458–1471.

Hentges, S.T., Low, M.J., and Williams, J.T. (2005). Differential regulation of synaptic inputs by constitutively released endocannabinoids and exogenous cannabinoids. J. Neurosci. *25*, 9746–9751.

Herlitze, S., Garcia, D.E., Mackie, K., Hille, B., Scheuer, T., and Catterall, W.A. (1996). Modulation of Ca2+ channels by G-protein betagamma subunits. Nature *380*, 258–262.

Hoffman, A.F., Laaris, N., Kawamura, M., Masino, S. a, and Lupica, C.R. (2010). Control of cannabinoid CB1 receptor function on glutamate axon terminals by endogenous adenosine acting at A1 receptors. J. Neurosci. *30*, 545–555.

Holt, M., Cooke, A., Wu, M.M., and Lagnado, L. (2003). Bulk Membrane Retrieval in the Synaptic Terminal of Retinal Bipolar Cells. J. Neurosci. *23*, 1329–1339.

Holtzman, T., Rajapaksa, T., Mostofi, A., and Edgley, S.A. (2006). Different responses of rat cerebellar Purkinje cells and Golgi cells evoked by widespread convergent sensory inputs. J. Physiol. *574*, 491–507.

Hosoi, N., Sakaba, T., and Neher, E. (2007). Quantitative analysis of calcium-dependent vesicle recruitment and its functional role at the calyx of Held synapse. J. Neurosci. *27*, 14286–14298.

Hull, C., and Regehr, W.G. (2012). Identification of an inhibitory circuit that regulates cerebellar Golgi cell activity. Neuron *73*, 149–158.

Iiri, T., Farfel, Z., and Bourne, H.R. (1998). G-protein diseases furnish a model for the turn-on switch. Nature *394*, 35–38.

Ikeda, S.R. (1996). Voltage-dependent modulation of N-type calcium channels by G-protein betagamma subunits. Nature *380*, 255–258.

Isaacson, J.S. (1998). GABA B Receptor-Mediated Modulation of Presynaptic Currents and Excitatory Transmission at a Fast Central Synapse. 1571–1576.

Iwasaki, S., and Takahashi, T. (1998). Rapid Report Developmental changes in calcium channel types mediating synaptic transmission in rat auditory brainstem. J. Physiol. *509*, 419–423.

Jenkinson, D.H. (1957). The nature of the antagonism between calcium and magnesium ions at the neuromuscular junction. J. Phy *138*, 434–444.

Jeon, D., Yang, Y.-M., Jeong, M.-J., Philipson, K.D., Rhim, H., and Shin, H.-S. (2003). Enhanced learning and memory in mice lacking Na+/Ca2+ exchanger 2. Neuron *38*, 965–976.

Job, C. (1998). Calcium and Protein Kinase C Regulate the Actin Cytoskeleton in the Synaptic Terminal of Retinal Bipolar Cells. J. Cell Biol. *143*, 1661–1672.

Kamatchi, G.L., and Ticku, M.K. (1990). Functional coupling of presynaptic GABAB receptors with voltage-gated Ca2+ channel: regulation by protein kinases A and C in cultured spinal cord neurons. Mol. Pharmacol. *38*, 342–347.

Kinoshita, a, Ohishi, H., Nomura, S., Shigemoto, R., Nakanishi, S., and Mizuno, N. (1996). Presynaptic localization of a metabotropic glutamate receptor, mGluR4a, in the cerebellar cortex: a light and electron microscope study in the rat. Neurosci. Lett. *207*, 199–202.

Knight, a R., and Bowery, N.G. (1996). The pharmacology of adenylyl cyclase modulation by GABAB receptors in rat brain slices. Neuropharmacology *35*, 703–712.

Knöpfel, T., and Grandes, P. (2002). Metabotropic glutamate receptors in the cerebellum with a focus on their function in Purkinje cells. Cerebellum *1*, 19–26.

Kreitzer, a C., and Regehr, W.G. (2001). Retrograde inhibition of presynaptic calcium influx by endogenous cannabinoids at excitatory synapses onto Purkinje cells. Neuron *29*, 717–727.

Kubota, H., Katsurabayashi, S., Moorhouse, A.J., Murakami, N., Koga, H., and Akaike, N. (2003). GABAB receptor transduction mechanisms, and cross-talk between protein kinases A and C, in GABAergic terminals synapsing onto neurons of the rat nucleus basalis of Meynert. J. Physiol. *551*, 263–276.

Kuromi, H., and Kidokoro, Y. (1998). Two Distinct Pools of Synaptic Vesicles in Single Presynaptic Boutons in a Temperature-Sensitive Drosophila Mutant, shibire. Neuron *20*, 917–925.

Kusano, K., and Landau, E.M. (1975). Depression and recovery of transmission at the squid giant synapse. J. Physiol. *245*, 13–32.

Kushmerick, C., Renden, R., and von Gersdorff, H. (2006). Physiological temperatures reduce the rate of vesicle pool depletion and short-term depression via an acceleration of vesicle recruitment. J. Neurosci. *26*, 1366–1377.

Lee, S.-J.R., Escobedo-Lozoya, Y., Szatmari, E.M., and Yasuda, R. (2009). Activation of CaMKII in single dendritic spines during long-term potentiation. Nature *458*, 299–304.

Lévénés, C., Daniel, H., Soubrié, P., and Crépel, F. (1998). Cannabinoids decrease excitatory synaptic transmission and impair long-term depression in rat cerebellar Purkinje cells. J. Physiol. *510 (Pt 3*, 867–879.

Liley, A.W., and North, K.A.K. (1953). An electrical investigation of effects of repetitive stimulation on mammalian neuromuscular junction. J Neurophysiol *16*, 509–527.

Liu, H., Bai, H., Hui, E., Yang, L., Evans, C.S., Wang, Z., Kwon, S.E., and Chapman, E.R. (2014). Synaptotagmin 7 functions as a Ca2+-sensor for synaptic vesicle replenishment. Elife *3*, e01524.

Londos, C., Cooper, D.M., and Wolff, J. (1980). Subclasses of external adenosine receptors. Proc. Natl. Acad. Sci. U. S. A. *77*, 2551–2554.

Lou, X., Korogod, N., Brose, N., and Schneggenburger, R. (2008). Phorbol esters modulate spontaneous and Ca2+-evoked transmitter release via acting on both Munc13 and protein kinase C. J. Neurosci. *28*, 8257–8267.

Mann-Metzer, P., and Yarom, Y. (2002). Pre- and postsynaptic inhibition mediated by GABA(B) receptors in cerebellar inhibitory interneurons. J. Neurophysiol. *87*, 183–190.

Mapelli, L., Rossi, P., Nieus, T., and Angelo, E.D. (2009). Tonic Activation of GABA B Receptors Reduces Release Probability at Inhibitory Connections in the Cerebellar Glomerulus. 3089–3099.

Mateos, J.M., Azkue, J., Sarría, R., Kuhn, R., Grandes, P., and Knöpfel, T. (1998). Localization of the mGlu4a metabotropic glutamate receptor in rat cerebellar cortex. Histochem. Cell Biol. *109*, 135–139.

Matthews, E.A., Schoch, S., and Dietrich, D. (2013). Tuning local calcium availability: cell-type-specific immobile calcium buffer capacity in hippocampal neurons. J. Neurosci. *33*, 14431–14445.

Meera, P., Wallner, M., Song, M., and Toro, L. (1997). Large conductance voltage- and calcium-dependent K+ channel, a distinct member of voltage-dependent ion channels with seven N-terminal transmembrane segments (S0-S6), an extracellular N terminus, and an intracellular (S9-S10) C terminus. Proc. Natl. Acad. Sci. U. S. A. *94*, 14066–14071.

Meinrenken, C.J., Borst, J.G.G., and Sakmann, B. (2002). Calcium secretion coupling at calyx of held governed by nonuniform channel-vesicle topography. J. Neurosci. *22*, 1648–1667.

Mintz, I.M., Sabatini, B.L., and Regehr, W.G. (1995). Calcium control of transmitter release at a cerebellar synapse. Neuron *15*, 675–688.

Mitchell, S.J., and Silver, R.A. (2000). GABA spillover from single inhibitory axons suppresses low-frequency excitatory transmission at the cerebellar glomerulus. J. Neurosci. *20*, 8651–8658.

Mitchell, S.J., and Silver, R.A. (2003). Shunting inhibition modulates neuronal gain during synaptic excitation. Neuron *38*, 433–445.

Moulder, K.L., and Mennerick, S. (2005). Reluctant vesicles contribute to the total readily releasable pool in glutamatergic hippocampal neurons. J. Neurosci. *25*, 3842–3850.

Müller, M., Felmy, F., Schwaller, B., and Schneggenburger, R. (2007). Parvalbumin is a mobile presynaptic Ca2+ buffer in the calyx of held that accelerates the decay of Ca2+ and short-term facilitation. J. Neurosci. *27*, 2261–2271.

Napper, R., and Harvey, R. (1988). Number of parallel fiber synapses on an individual Purkinje cell in the cerebellum of the rat. J. Comp. Neurol. *274*, 168–177.

Nelson, A.B., Krispel, C.M., Sekirnjak, C., and du Lac, S. (2003). Long-lasting increases in intrinsic excitability triggered by inhibition. Neuron *40*, 609–620.

Nelson, A.B., Gittis, A.H., and du Lac, S. (2005). Decreases in CaMKII activity trigger persistent potentiation of intrinsic excitability in spontaneously firing vestibular nucleus neurons. Neuron *46*, 623–631.

Neu, A., Földy, C., and Soltesz, I. (2007). Postsynaptic origin of CB1-dependent tonic inhibition of GABA release at cholecystokinin-positive basket cell to pyramidal cell synapses in the CA1 region of the rat hippocampus. J. Physiol. *578*, 233–247.

Offermanns, S. (2003). G-proteins as transducers in transmembrane signalling. Prog. Biophys. Mol. Biol. *83*, 101–130.

Ohishi, H., Ogawa-Meguro, R., Shigemoto, R., Kaneko, T., Nakanishi, S., and Mizuno, N. (1994). Immunohistochemical localization of metabotropic glutamate receptors, mGluR2 and mGluR3, in rat cerebellar cortex. Neuron *13*, 55–66.

Oliet, S.H.R., Baimoukhametova, D. V, Piet, R., and Bains, J.S. (2007). Retrograde regulation of GABA transmission by the tonic release of oxytocin and endocannabinoids governs postsynaptic firing. J. Neurosci. *27*, 1325–1333.

Page, K.M., Stephens, G.J., Berrow, N.S., and Dolphin, A.C. (1997). The intracellular loop between domains I and II of the B-type calcium channel confers aspects of G-protein sensitivity to the E-type calcium channel. J. Neurosci. *17*, 1330–1338.

Page, K.M., Cantí, C., Stephens, G.J., Berrow, N.S., and Dolphin, a C. (1998). Identification of the amino terminus of neuronal Ca2+ channel alpha1 subunits alpha1B and alpha1E as an essential determinant of G-protein modulation. J. Neurosci. *18*, 4815–4824.

Palay, S.L., and Chan-Palay, V. (1974). Cerebellar cortex: cytology and organization (Springer).

Pan, B., and Zucker, R.S. (2009). A general model of synaptic transmission and short-term plasticity. Neuron *62*, 539–554.

Pekhletski, R., Gerlai, R., Overstreet, L.S., Huang, X.P., Agopyan, N., Slater, N.T., Abramow-Newerly, W., Roder, J.C., and Hampson, D.R. (1996). Impaired cerebellar synaptic plasticity and motor performance in mice lacking the mGluR4 subtype of metabotropic glutamate receptor. J. Neurosci. *16*, 6364–6373.

Richards, D. a, Rizzoli, S.O., and Betz, W.J. (2004). Effects of wortmannin and latrunculin A on slow endocytosis at the frog neuromuscular junction. J. Physiol. *557*, 77–91.

Rizzoli, S.O., and Betz, W.J. (2005). Synaptic vesicle pools. Nat. Rev. Neurosci. *6*, 57–69.

Robitaille, R., and Charlton, P. (1992). Presynaptic Calcium Signals and Transmitter by Calcium-activated Potassium Channels. J. Neurosci. *12*, 297–305.

Rosenmund, C., and Stevens, C.F. (1996). Definition of the readily releasable pool of vesicles at hippocampal synapses. Neuron *16*, 1197–1207.

Rossi, D.J., Hamann, M., and Attwell, D. (2003). Multiple modes of GABAergic inhibition of rat cerebellar granule cells. J. Physiol. *548*, 97–110.

Ruigrok, T.J.H., Hensbroek, R.A., and Simpson, J.I. (2011). Spontaneous activity signatures of morphologically identified interneurons in the vestibulocerebellum. J. Neurosci. *31*, 712–724.

Ruiz-Velasco, V., and Ikeda, S.R. (2000). Multiple G-protein betagamma combinations produce voltage-dependent inhibition of N-type calcium channels in rat superior cervical ganglion neurons. J. Neurosci. *20*, 2183–2191.

Rusakov, D. a, Savtchenko, L.P., Zheng, K., and Henley, J.M. (2011). Shaping the synaptic signal: molecular mobility inside and outside the cleft. Trends Neurosci. *34*, 359–369.

Sabatini, B.L., and Regehr, W.G. (1997). Control of neurotransmitter release by presynaptic waveform at the granule cell to Purkinje cell synapse. J. Neurosci. *17*, 3425–3435.

Sakaba, T., and Neher, E. (2001a). Calmodulin mediates rapid recruitment of fast-releasing synaptic vesicles at a calyx-type synapse. Neuron *32*, 1119–1131.

Sakaba, T., and Neher, E. (2001b). Quantitative relationship between transmitter release and calcium current at the calyx of held synapse. J. Neurosci. *21*, 462–476.

Sakaba, T., and Neher, E. (2003). Involvement of actin polymerization in vesicle recruitment at the calyx of Held synapse. J. Neurosci. *23*, 837–846.

Schneggenburger, R., and Neher, E. (2000). Intracellular calcium dependence of transmitter release rates at a fast central synapse. Nature *406*, 889–893.

Schneggenburger, R., Meyer, a C., and Neher, E. (1999). Released fraction and total size of a pool of immediately available transmitter quanta at a calyx synapse. Neuron *23*, 399–409.

Schneggenburger, R., Sakaba, T., and Neher, E. (2002). Vesicle pools and short-term synaptic depression: lessons from a large synapse. Trends Neurosci. *25*, 206–212.

Schneggenburger, R., Han, Y., and Kochubey, O. (2012). Ca(2+) channels and transmitter release at the active zone. Cell Calcium *52*, 199–207.

Schneider, T., Wei, X., Olcese, R., Costantin, J., Neely, A., Palade, P., Perez-Reyes, E., Qin, N., Zhou, J., Crawford, G., et al. (1994). Molecular analysis and functional expression of the human type E neuronal Ca2+ channel alpha 1 subunit. Recept. Channels *2*, 255–270.

Schwaller, B., Meyer, M., and Schiffmann, S. (2002). "New" functions for "old" proteins: the role of the calcium-binding proteins calbindin D-28k, calretinin and parvalbumin, in cerebellar physiology. Studies with knockout mice. Cerebellum *1*, 241–258.

Seifert, R., and Wenzel-Seifert, K. (2002). Constitutive activity of G-protein-coupled receptors: cause of disease and common property of wild-type receptors. Naunyn. Schmiedebergs. Arch. Pharmacol. *366*, 381–416.

Shahrezaei, V., and Delaney, K.R. (2004). Consequences of molecular-level Ca2+ channel and synaptic vesicle colocalization for the Ca2+ microdomain and neurotransmitter exocytosis: a monte carlo study. Biophys. J. *87*, 2352–2364.

Shao, X., Davletov, B.A., Sutton, R.B., Südhof, T.C., and Rizo, J. (1996). Bipartite Ca2+-binding motif in C2 domains of synaptotagmin and protein kinase C. Science *273*, 248–251.

Sheng, J., He, L., Zheng, H., Xue, L., Luo, F., Shin, W., Sun, T., Kuner, T., Yue, D.T., and Wu, L.-G. (2012). Calcium-channel number critically influences synaptic strength and plasticity at the active zone. Nat. Neurosci. *15*, 998–1006.

Simon, S.M., and Llinás, R.R. (1985). Compartmentalization of the submembrane calcium activity during calcium influx and its significance in transmitter release. Biophys. J. *48*, 485–498.

Smith, S.J., Augustine, G.J., and Charlton, M.P. (1985). Transmission at voltage-clamped giant synapse of the squid: evidence for cooperativity of presynaptic calcium action. Proc. Natl. Acad. Sci. U. S. A. *82*, 622–625.

Sodickson, D.L., and Bean, B.P. (1998). Neurotransmitter activation of inwardly rectifying potassium current in dissociated hippocampal CA3 neurons: interactions among multiple receptors. J. Neurosci. *18*, 8153–8162.

Soong, T.W., Stea, A., Hodson, C.D., Dubel, S.J., Vincent, S.R., and Snutch, T.P. (1993). Structure and functional expression of a member of the low voltage-activated calcium channel family. Science *260*, 1133–1136.

Stephen, B.Y., Ii, J.S., Ii, J.B., Ossestll, L.R., Charltonti, M.P., and Augustine, G.J. (1993). Augustine§11t. 573–593.

Stephens, G.J. (2009). G-protein-coupled-receptor-mediated presynaptic inhibition in the cerebellum. Trends Pharmacol. Sci. *30*, 421–430.

Stevens, C.F., and Wesseling, J.F. (1998). Activity-dependent modulation of the rate at which synaptic vesicles become available to undergo exocytosis. Neuron *21*, 415–424.

Stevens, C.F., and Williams, J.H. (2007). Discharge of the Readily Releasable Pool With Action Potentials at Hippocampal Synapses. 3221–3229.

Straiker, A.J., Borden, C.R., and Sullivan, J.M. (2002). G-protein alpha subunit isoforms couple differentially to receptors that mediate presynaptic inhibition at rat hippocampal synapses. J. Neurosci. *22*, 2460–2468.

Sudhof, T., and Rizo, J. (1996). Synaptotagmins: C-Domain Proteins That Regulate Membrane Traffic. Neuron *17*, 379–388.

Südhof, T.C. (2013). Neurotransmitter release: the last millisecond in the life of a synaptic vesicle. Neuron *80*, 675–690.

Sun, J., Pang, Z.P., Qin, D., Fahim, A.T., Adachi, R., and Südhof, T.C. (2007). A dual-Ca2+-sensor model for neurotransmitter release in a central synapse. Nature *450*, 676–682.

Takahashi, K. a, and Linden, D.J. (2000). Cannabinoid receptor modulation of synapses received by cerebellar Purkinje cells. J. Neurophysiol. *83*, 1167–1180.

Takahashi, T., Kajikawa, Y., and Tsujimoto, T. (1998). G-Protein-Coupled Modulation of Presynaptic Calcium Currents and Transmitter Release by a GABA B Receptor. *18*, 3138–3146.

Taniyama, K., Niwa, M., Kataoka, Y., and Yamashita, K. (1992). Activation of Protein Kinase C Suppresses the y-Aminobutyric Acids Receptor-Mediated Inhibition of the Vesicular Release of Noradrenaline and Acetylcholine.

Taschenberger, H., and von Gersdorff, H. (2000). Fine-tuning an auditory synapse for speed and fidelity: developmental changes in presynaptic waveform, EPSC kinetics, and synaptic plasticity. J. Neurosci. *20*, 9162–9173.

Taschenberger, H., Leão, R.M., Rowland, K.C., Spirou, G.A., and von Gersdorff, H. (2002). Optimizing Synaptic Architecture and Efficiency for High-Frequency Transmission. Neuron *36*, 1127–1143.

Taschenberger, H., Scheuss, V., and Neher, E. (2005). Release kinetics, quantal parameters and their modulation during short-term depression at a developing synapse in the rat CNS. J. Physiol. *568*, 513–537.

Tedford, H.W., and Zamponi, G.W. (2006). Direct G Protein Modulation of Cav2 Calcium Channels. *58*, 837–862.

Trommershäuser, J., Schneggenburger, R., Zippelius, A., and Neher, E. (2003). Heterogeneous presynaptic release probabilities: functional relevance for short-term plasticity. Biophys. J. *84*, 1563–1579.

Tsodyks, M. V, and Markram, H. (1997). The neural code between neocortical pyramidal neurons depends on neurotransmitter release probability. Proc. Natl. Acad. Sci. U. S. A. *94*, 719–723.

Varela, J. a, Song, S., Turrigiano, G.G., and Nelson, S.B. (1999). Differential depression at excitatory and inhibitory synapses in visual cortex. J. Neurosci. *19*, 4293–4304.

Varela, J.A., Sen, K., Gibson, J., Fost, J., Abbott, L.F., and Nelson, S.B. (1997). A quantitative description of short-term plasticity at excitatory synapses in layer 2/3 of rat primary visual cortex. J. Neurosci. *17*, 7926–7940.

Vervaeke, K., Lorincz, A., Gleeson, P., Farinella, M., Nusser, Z., and Silver, R.A. (2010). Rapid desynchronization of an electrically coupled interneuron network with sparse excitatory synaptic input. Neuron *67*, 435–451.

Vyleta, N.P., and Jonas, P. (2014). Loose Coupling Between Ca2+ Channels and Release Sensors at a Plastic Hippocampal Synapse. Science (80-.). *343*, 665–670.

Wadel, K., Neher, E., and Sakaba, T. (2007). The coupling between synaptic vesicles and Ca2+ channels determines fast neurotransmitter release. Neuron *53*, 563–575.

Wagner, J., and Keizer, J. (1994). Effects of rapid buffers on Ca2+ diffusion and Ca2+ oscillations. Biophys. J. *67*, 447–456.

Walter, J.T., and Khodakhah, K. (2006). The linear computational algorithm of cerebellar Purkinje cells. J. Neurosci. *26*, 12861–12872.

Wang, L.Y., and Kaczmarek, L.K. (1998). High-frequency firing helps replenish the readily releasable pool of synaptic vesicles. Nature *394*, 384–388.

Watanabe, D., and Nakanishi, S. (2003). mGluR2 postsynaptically senses granule cell inputs at Golgi cell synapses. Neuron *39*, 821–829.

Van Welie, I., and du Lac, S. (2011). Bidirectional control of BK channel open probability by CAMKII and PKC in medial vestibular nucleus neurons. J. Neurophysiol. *105*, 1651–1659.

Wells, C.A., Zurawski, Z., Betke, K.M., Yim, Y.Y., Hyde, K., Rodriguez, S., Alford, S., and Hamm, H.E. (2012). Gβγ inhibits exocytosis via interaction with critical residues on soluble N-ethylmaleimide-sensitive factor attachment protein-25. Mol. Pharmacol. *82*, 1136–1149.

Wesseling, J.F., and Lo, D.C. (2002). Limit on the role of activity in controlling the release-ready supply of synaptic vesicles. J. Neurosci. *22*, 9708–9720.

Wölfel, M., Lou, X., and Schneggenburger, R. (2007). A mechanism intrinsic to the vesicle fusion machinery determines fast and slow transmitter release at a large CNS synapse. J. Neurosci. *27*, 3198–3210.

Wu, L.G., and Saggau, P. (1994). Pharmacological identification of two types of presynaptic voltage-dependent calcium channels at CA3-CA1 synapses of the hippocampus. J. Neurosci. *14*, 5613–5622.

Wu, L.G., Borst, J.G.G., and Sakmann, B. (1998). R-type Ca2+ currents evoke transmitter release at a rat. J. Neurosci. *95*, 4720–4725.

Wu, L.G., Westenbroek, R.E., Borst, J.G.G., Catterall, W.A., and Sakmann, B. (1999). Calcium channel types with distinct presynaptic localization couple differentially to transmitter release in single calyx-type synapses. J. Neurosci. *19*, 726–736.

Xu, W., and Edgley, S.A. (2010). Cerebellar Golgi cells in the rat receive convergent peripheral inputs via a lateral reticular nucleus relay. Eur. J. Neurosci. *32*, 591–597.

Xu-Friedman, M.A., Harris, K.M., and Regehr, W.G. (2001). Three-dimensional comparison of ultrastructural characteristics at depressing and facilitating synapses onto cerebellar Purkinje cells. J. Neurosci. *21*, 6666–6672.

Yoon, E., Gerachshenko, T., Spiegelberg, B.D., Alford, S., and Hamm, H.E. (2007). G □ Interferes with Ca 2 ∂ -Dependent Binding of Synaptotagmin to the Soluble N -Ethylmaleimide-Sensitive Factor Attachment. 1210–1219.

Yum, D.-S., Cho, J.-H., Choi, I.-S., Nakamura, M., Lee, J.-J., Lee, M.-G., Choi, B.-J., Choi, J.-K., and Jang, I.-S. (2008). Adenosine A1 receptors inhibit GABAergic transmission in rat tuberomammillary nucleus neurons. J. Neurochem. *106*, 361–371.

Zamponi, G.W., Bourinet, E., and Snutch, T.P. (1996). Nickel Block of a Family of Neuronal Calcium Channels: Subtype- and Subunit-Dependent Action at Multiple Sites. J. Membr. Biol. *151*, 77–90.

Zhang, W., and Linden, D.J. (2009). Neuromodulation at single presynaptic boutons of cerebellar parallel fibers is determined by bouton size and basal action potential-evoked Ca transient amplitude. J. Neurosci. *29*, 15586–15594.

Zhou, Z., and Neher, E. (1993). Mobile and immobile calcium buffers in bovine adrenal chromaffin cells. J. Physiol. *469*, 245–273.

Zhou, J.Y., Siderovski, D.P., and Miller, R.J. (2000). Selective regulation of N-type Ca channels by different combinations of G-protein beta/gamma subunits and RGS proteins. J. Neurosci. *20*, 7143–7148.

Zhu, P.J., and Lovinger, D.M. (2005). Retrograde endocannabinoid signaling in a postsynaptic neuron/synaptic bouton preparation from basolateral amygdala. J. Neurosci. *25*, 6199–6207.

Zucker, R.S., and Regehr, W.G. (2002). Short-term synaptic plasticity. Annu. Rev. Physiol. *64*, 355–405.